REACTOR MATERIALS

A Quarterly Technical Progress Review

Prepared for DIVISION OF TECHNICAL INFORMATION, USAEC, by
E. M. SIMONS, D.L. KELLER, and ASSOCIATES, BATTELLE MEMORIAL INSTITUTE

Spring 1967

● VOLUME 10

● NUMBER 1

TECHNICAL PROGRESS REVIEWS

To meet the needs of industry for concise summaries of current atomic developments, the Atomic Energy Commission is publishing this series, Technical Progress Reviews. Issued quarterly, each of the reviews digests and evaluates the latest findings in a specific area of nuclear technology and science.

The journals published in this series are:

Isotopes and Radiation Technology P. S. Baker, A. F. Rupp, and associates
Oak Ridge National Laboratory

Nuclear Safety Wm. B. Cottrell, W. H. Jordan, J. P. Blakely, and associates
Nuclear Safety Information Center, Oak Ridge National Laboratory

Power Reactor Technology
Argonne National Laboratory

Reactor Materials E. M. Simons and associates
Battelle Memorial Institute

See the back cover for availability information.

The views expressed in this publication do not necessarily represent those of the United States Atomic Energy Commission, its divisions or offices, or of any Commission advisory committee or contractor.

Availability of Reports Cited in This Review

U. S. Atomic Energy Commission (USAEC) reports are available for inspection at USAEC depository libraries and are sold by the Clearinghouse for Federal Scientific and Technical Information (CFSTI), National Bureau of Standards, U. S. Department of Commerce, 5285 Port Royal Road, Springfield, Va. 22151. [All reports sold by CFSTI are $3.00 per binding for eye-legible copy and $0.65 per binding for microfiche.] Some of the reports cited are not available owing to their preliminary nature; however, the information contained in them will eventually be made available in formal progress or topical reports.

Other U. S. Government agency reports identified in this journal generally are available from CFSTI.

Private organization reports should be requested from the originator.

United Kingdom Atomic Energy Authority (UKAEA) and *Atomic Energy of Canada Limited (AECL)* reports may be inspected at USAEC depository libraries. UKAEA reports are sold by Her Majesty's Stationery Office, London; AECL reports are sold by the Technical Information Officer, Atomic Energy of Canada Limited, Chalk River, Ontario, Canada. UKAEA and AECL reports issued after March 1, 1967, are sold by CFSTI to purchasers in the United States and its territories.

Contents

Reactor Materials

Vol. 10, No. 1

I Fuel and Fertile Materials

Uranium Metal and Alloys 1
Plutonium 4
Thorium 8
Metal–Ceramic Fuels 9
Coated-Particle Fuels 10
Uranium and Thorium Oxides 11
Carbide and Nitride Fuels 12
Fuel–Water Reactions 14
Mechanism of Corrosion of Fuel Alloys . . 15
Basic Studies of Irradiation Effects in Fuel Materials 15
References 17

II Moderator Materials

Graphite 20
Beryllium and Beryllium Alloys 20
Beryllium Oxide 22
Solid Hydrides 22
References 23

III Nuclear Poisons

Metallic Poison Materials 24
Dispersion and Nonmetallic Poison Materials 24
References 25

IV Cladding and Structural Materials

Corrosion 26
Metal–Water Reactions 32
Radiation Effects in Structural Materials . . 33
Selected Mechanical Properties of Cladding and Structural Materials 42
Selected Metallurgical Aspects of Cladding and Structural Materials 46
Diffusion Studies 54
Ceramic Technology 54
References 55

V Special Fabrication Techniques

Melting and Casting 59
Hot and Cold Working 60
Powder Processing 61
Pressure Bonding 62
Plating 62
High-Energy-Rate Processes 64
Nondestructive Testing 64
References 65

Issued quarterly by the U. S. Atomic Energy Commission. Use of funds for printing this publication approved by the Director of the Bureau of the Budget on July 8, 1966.

Reactor Materials

is one of a series of quarterly technical progress reviews broadly covering the field of nuclear science and technology. Under the auspices of the USAEC Division of Technical Information, *Reactor Materials* is prepared by Battelle personnel from worldwide literature. It covers properties, behavior, and fabrication processes of materials applicable to nuclear reactor components and associated equipment.

The reader will recognize that the scope of this Review is too broad to permit detailed coverage of every topic. Rather, the authors and editors attempt to combine the highlights of significant new developments into an information summary of current research for both management and the technical specialist. As a rule, enough of the results are presented to define the research and summarize the findings. For readers desiring more information on any particular topic, a complete set of references is provided at the end of each section.

Each quarter a number of bibliographies, monographs, and books appear on subjects within the scope of *Reactor Materials*. Although the main purpose of this Review is to call attention to findings that are new and significant, such publications are noted in the text because they often represent excellent compilations of available information on important materials topics.

E. M. SIMONS
S. W. POREMBKA, JR.
D. L. KELLER

Battelle Memorial Institute

Section

I

Reactor Materials

Fuel and Fertile Materials

Uranium Metal and Alloys

Unalloyed Uranium

The effects of high pressure and temperature on the microstructure of alpha uranium were studied at Argonne.[1] The pressure–temperature diagram for uranium was determined up to 57 kbars pressure and is presented in Fig. I-1 along with the data ob-

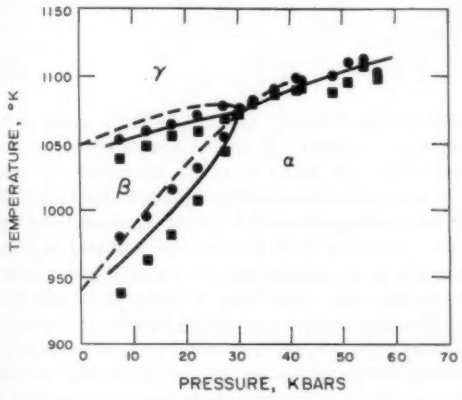

Fig. I-1 The phase diagram of uranium.[1] ●, *heating;* ■, *cooling;* —, *data of Klement et al.*

tained by other investigators.[2] It was also found that the temperature hysteresis for the alpha ⇌ beta transformation is decreased by increasing hydrostatic pressure. Metallographic observations have shown that subgrains and plastic deformation in the alpha structure can be eliminated by slowly cooling samples, immersed in liquid alkali metals, from the gamma-phase temperature range at a pressure of 40 kbars. It appears that good single crystals of alpha uranium can be grown by the phase-transformation technique at hydrostatic pressures greater than about 33 kbars.

A translation of Czechoslovakian work[3] on the interdiffusion of uranium and beryllium has been published. The experimental data and the calculated penetration coefficients and activation energies are given in Table I-1.

The National Lead Co. of Ohio[4] has reported that the identification of the inclusions in uranium which are rich in Fe, Si, C, or Al can be performed by heat-tinting techniques that cause the phases to assume characteristic colors.

Australian investigators[5] have reported observations on the creep fracture of reactor-grade uranium between 300 and 520°C at a stress of 2.8 kg/mm^2. It was found that creep ductility is high at 300°C, but at 420°C, a brittle intercrystalline fracture associated with the formation of wedge-shaped cavities at grain corners is exhibited. At 520°C, nonductile behavior is again observed: voids form at grain boundaries, but these grow in a direction parallel to the tensile axis rather than propagating transversely; failure then ensues by gradual cavity coalescence. The results are correlated with the swelling of uranium under reactor operating conditions.

The subject of grain-boundary cracking in irradiated uranium has been treated by the British.[6] Growth of grain-boundary gas bubbles as induced by severe thermal cycling during irradiation was shown to be responsible for the grain-boundary cavitation and cracking observed in some specimens of a U–$\frac{1}{2}$ at.% Cr alloy. The phenomenon provides one explanation of the pronounced tendency of irradiated alpha uranium to develop grain-boundary cracks, with an accompanying decrease in apparent density, in certain circumstances. The observations imply that similar intergranular cavitation and cracking, with accompanying changes in dimensions and density, can in principle be produced in irradiated uranium by any other conditions that cause intergranular tensile stresses. Irradiation growth, alpha–beta cycling, or external stressing as in a tensile or creep test can result in these intergranular stresses, which must then be maintained for sufficient time at temperature for vacancy diffusion to occur. The limited evidence available suggests that this type of structure may develop only under the conditions of thermal cycling at temperatures $\gtrsim$490°C for irradiation levels of ~2000 Mwd/ton. It is possible that this temperature limit may be somewhat lower for higher irradiations.

The results obtained from the irradiation of high-purity enriched (1.43% ^{235}U)-uranium specimens have been reported by Battelle–Northwest.[7] The uranium

was irradiated to 0.04 at.% burnup at a controlled temperature of 500°C. Table I-2 summarizes the irradiation history and volume-change results. Most of the specimens show no appreciable change in external appearance. The specimens that did show severe distortion had a large original grain size and operated at approximately 450°C. The measured swelling and the R values are significantly lower than those previously reported. Previous experiments indicated that the irradiation behavior of enriched material was similar to that of natural specimens and no significant difference due to the fission rate was evident. These data suggest that fission rate might influence swelling at this low burnup (0.04 at.%).

$$K = 0.0585 + 6.550 \times 10^{-5} T$$

where K is the conductivity in cal/(cm)(sec)(°C) and T is the temperature in °C. This equation gives a substantially higher conductivity above 300°C than that given by a previous equation for Springfields uranium, but it agrees well with U. S. data. The specimens were selected to cover a range of iron contents. No correlation was found between the conductivity and any one of the individual variables: iron, aluminum, or carbon content. However, a relation between the uranium conductivity and the ratio of the carbon-to-iron content was revealed. The significance of this relation is in doubt.

Table I-1 INTERDIFFUSION OF URANIUM AND BERYLLIUM[3]

Temp., °C	Time, days	Maximum thickness of diffusion zone, μ	Penetration coefficient* ($A = X^2/t$), cm²/sec	Activation energy (Q), kcal/mole	Applicable temperature range, °C
550	25	40	7.7×10^{-12}	21.7	550–600
600	7	10	1.65×10^{-11}	15.6	550–800
800	7	65	7.0×10^{-11}	13.5	600–800
				16.9	500–800

*$A_0 = 2.28 \times 10^{-7}$.

The low R values indicate the presence of a certain threshold exposure that must be exceeded before extreme swelling begins. This is consistent with the proposal that swelling in this temperature range is a mechanical process; i.e., the lattice must be damaged a certain amount by the fission events before extensive swelling begins. In conjunction with the low exposure, the short time at temperature, due to irradiating enriched specimens, may not provide sufficient time for recovery processes to induce swelling.

The latest addition to the bibliography, "Radiation Effects on Solid, Uranium-Based Nuclear Fuel Materials," has been published by Sweden.[8]

Recently published articles on uranium considered noteworthy are: "The Beta → Alpha Phase Change in Pure Uranium,"[9] "Density Changes Upon Heat-Treating Unirradiated Pure and Adjusted Uranium,"[10] "Some Metallographic Observations of Plastic Deformation in Thermally Cycled Uranium,"[11] "On the Question of the Grain Size Dependence of Flow and Fracture Stress in Alpha Uranium,"[12] and "Effect of Environmental Conditions on the Pitting of Uranium."[13]

Alpha-Phase Uranium Alloys

British investigators[14] have reported the results of thermal-conductivity measurements performed on 15 specimens of Springfields adjusted uranium (uranium containing small additions of iron, aluminum, and carbon). The determinations were made between 160 and 620°C, and the results fit the equation

Battelle–Northwest[15] has conducted a study of the irradiation stability of specimens of uranium containing different sizes of finely dispersed UC particles. One set of specimens had particles ($\sim 9 \times 10^{11}$ cm^3) with a diameter of 0.5 μ or less, whereas another set had particles with an average diameter of 2.5 μ. Both types of specimens had the same chemical composition and were clad with Zircaloy-2 by coextrusion. The fuel rods were irradiated to an exposure of 0.3 at.% (1.4×10^{20} fissions/cm^3). Maximum irradiation temperature at the center of the uranium rods was 500°C. The corresponding temperatures at the mid-radius and outer edge of the uranium were 425 and 325°C, respectively.

Examination of the irradiated fuel rods showed considerably greater volume increase in the uranium with the fine UC particles than in that with the larger UC particles. The cladding on all rods containing fine UC failed in a brittle manner, thus allowing unrestrained swelling, whereas the cladding on the two rods with larger UC particles remained intact, providing several thousand percent restraint. Brittle failure of Zircaloy-2 cladding has occurred during irradiation with other brittle materials and is not believed related to the irradiation behavior of these fuel rods containing fine uranium carbide particles. Results of density measurements on declad specimens from the irradiated rods are shown in Table I-3. Optical and electron metallographic examinations performed on specimens in the as-irradiated condition show that, in the uranium with the fine UC particles, extensive tearing porosity existed in the sector near the cladding split. The as-irradiated uranium

Table I-2 IRRADIATION HISTORY AND VOLUME CHANGE OF SPECIMENS* OF HIGH-PURITY URANIUM[7]

Specimen	Heat-treatment	Irradiation temp., °C		As-irradiated density (ρ_i), g/cm³	Swelling $(\Delta\rho/\rho_i) \times 100$, %	R, % swelling/ at. % burnup†
		Reactor up	Reactor down			
25-A-1	900°C for 15 min, oil quench	455	375	18.80	1.1	27
25-A-2	900°C for 15 min, furnace cool	455	375	18.81	1.0	25
25-B-1	As extruded	500	390	18.56	2.4	59
25-B-2	730°C for 15 min, oil quench	500	390	18.86	0.74	19
25-C-1	As extruded	485	405	18.35	3.5	88
25-C-2	730°C for 15 min, oil quench	485	405	18.78	1.2	29
25-D-1	730°C for 15 min, furnace cool	~450	~370	18.83	0.9	23
25-D-2	575°C for 4 days	~450	~370	18.73	1.4	36

*Specimens were half-tubular in geometry, ½ in. in outside diameter and ½ in. long with a 0.030-in. wall thickness. Composition (ppm): high-purity uranium (1.43% enriched) containing 110 Fe, 20 Al, 38 Si, 30 C, and 25 N.
†Burnup, 0.04 at. %.

Table I-3 CHANGES IN DENSITY OF IRRADIATED U–UC SPECIMENS[15]

Specimen	Density, g/cm³		Density change $(\Delta\rho = \rho_i - \rho_f)$	Swelling $(\Delta\rho/\rho_f \times 100)$, %	R, % swelling/ at. % burnup*
	Preirradiation (ρ_i)	Postirradiation (ρ_f)			
			Normal UC Size		
1	18.95	18.51	0.44	2.4	8.0
2	18.95	18.33	0.62	3.4	11.3
			Submicron UC Size		
31	18.85	17.66	1.19	6.7	22.3
32	18.85	16.62	2.23	13.4	44.5
41	18.85	17.15	1.70	9.9	33.0
42	18.85	17.33	1.52	8.8	29.3

*Burnup, 0.3 at. %.

containing the larger UC particles showed some tearing scattered throughout the uranium, but on a much smaller scale.

Electron microscopy was performed on two of the rods containing fine UC particles, in a region of the uranium where the irradiation temperature was approximately 450°C. The major structure features were oxide stringers resulting from the fabrication procedure, the submicron UC particles, very little porosity, and unidentified 0.1-μ inclusions present in much larger numbers than the UC. This type of inclusion was not observed in the unirradiated uranium. Near the colder 325°C edge of uranium, the electron photomicrographs show the tearing observed optically.

During subsequent alpha-, beta-, and gamma-phase postirradiation annealing, the "fine carbide" uranium swelled much less than did the "coarse carbide" uranium. Metallographic examination showed that the fine carbides inhibited recrystallization in the alpha phase and hence prevented fission-gas sweeping. This may have also influenced the subsequent beta- and gamma-phase annealing behavior, although at 800°C there appeared to be an additional pinning effect of the fine carbides. This suggests that, had the cladding remained intact on the fine carbide rods, the in-reactor behavior would have been at least as good as that of the coarse carbide rods and possibly better.

These results indicate that there was more fine (<1 μ) spherical-shaped porosity in the hotter region of the uranium in the rods containing normal-size UC particles than in those containing the fine UC particles. Near the colder edge of the uranium containing normal-size UC particles, there is essentially no porosity. The results of postirradiation annealing experiments on both types of materials showed that the uranium containing the submicron UC swelled much less in the high alpha, the beta, and the gamma temperature ranges than the uranium containing large UC particles.

The irradiation of uranium and dilute uranium alloys has been performed by investigators at Battelle–Northwest.[7] The composition, metallurgical condition, density, irradiation temperature, and swelling for two different irradiation capsules are given in Table I-4. Most of the specimens from both capsules appeared visually to be in excellent condition, with little or no warping, surface roughening, or cracking being observed. Only one specimen showed severe external cracks; these were probably caused by cycling through the alpha–beta transformation while the reactor was up. It should be noted that the measured swelling was very small in all instances and that the alloy specimens behaved in the same manner as the high-purity uranium. Swelling above 600°C is thought to be primarily due to fission-gas porosity. The low volume changes agree with previous observations that indicate decreasing swelling with increasing irradiation temperatures in the temperature range 450 to 700°C. Swelling should increase with temperature above 700°C. These ob-

Table I-4 IRRADIATION HISTORY AND VOLUME CHANGE OF SPECIMENS* OF URANIUM AND URANIUM ALLOYS†

Specimen	Type material†	Heat-treatment	Irradiation temp., °C		As-irradiated density (ρ_f), g/cm³	Swelling ($\Delta\rho/\rho_f \times 100$), %	R, % swelling/at. % burnup
			Reactor up	Reactor down			
		Irradiated to 0.3 at. % burnup					
33-A-1	U(T-3)	As extruded	660	460	18.71	1.5	15
33-A-2	U(T-3)	640°C for 4 days, furnace cool	660	460	18.22	4.4	44
33-B-1	U + Fe–Al–Si	As extruded	700	500	18.66	1.3	13
33-B-2	U + Fe–Al–Si	900°C for 1 hr, oil quench	700	500	18.58	1.6	16
33-C-1	U(PT3-NA)	As extruded	680	505	18.84	0.7	7
33-C-2	U(T-3)	730°C for 15 min, oil quench	680	505	18.78	1.1	11
33-D-1	U(PT3-NA)	As extruded	~640	~500	18.75	1.2	12
33-D-2	U(PT3-NA)	730°C for 15 min, oil quench	~640	~500	18.65	1.7	17
33-E-1	U + Fe–Si	As extruded	620	450	18.91	0.3	3
33-E-2	U + Fe–Si	900°C for 1 hr, oil quench	620	450	18.66	1.8	18
		Irradiated to 0.1 at. % burnup					
34-A-1	U(T-3)	As extruded	610	435	18.52	2.6	13
34-A-2	U(T-3)	640°C for 4 days, furnace cool	610	435	18.46	3.3	17
34-B-1	U + Fe–Al–Si	As extruded	700	500	18.30	3.1	16
34-B-2	U + Fe–Al–Si	900°C for 1 hr, oil quench	700	500	18.41	2.4	12
34-C-1	U(T-3)	As extruded	690	500	18.36	3.4	17
34-C-2	U(T-3)	730°C for 15 min, oil quench	690	500	18.37	3.7	18
34-D-1	U(PT3-NA)	As extruded	675	490	18.48	2.7	14
34-D-2	U(T-3)	730°C for 15 min, oil quench	675	490	18.46	2.9	15
34-E-1	U + Fe–Si	As extruded	630	460	18.41	3.1	15
34-E-2	U + Fe–Si	900°C for 1 hr, oil quench	630	460	18.54	2.5	12

*Specimens were half-tubular in geometry, ½ in. in outside diameter by ⅝ in. long, and 0.030 in. in wall thickness.
†Compositions (in ppm) are:
U(T-3): high-purity U containing 64 Fe, 5 Al, 25 Si, 6 C, and 8 N
U(PT3-NA): high-purity U containing 54 Fe, 10 Al, 34 Si, 480 C, and 24 N
U + Fe–Al–Si: U containing 400 Fe, 645 Al, 85 Si, 500 C, and 23 N
U + Fe–Si: U containing 140 Fe, 25 Al, 95 Si, 400 C, and 14 N

servations tend to enhance previous data which indicated that swelling in uranium is dependent on mechanical processes and is not simply related to the nucleation and growth of fission-gas pores.

Several papers concerned primarily with alpha-uranium alloys have been published which are of interest: "Pearlitic Reaction in Some Uranium-Chromium Alloys,"[16] "The Orientation Relationship Between Gamma and Alpha Structures in Uranium-Zirconium Alloys,"[17] "The Influence of Microstructure on the Behavior of Uranium Alloys During Temperature Cycling Creep Experiments,"[18] and "The Effect of Small Aluminum Additions on the Structure of Uranium-Molybdenum Alloys."[19] (M. S. Farkas)

Plutonium

Plutonium Metal and Alloys

Los Alamos investigators are conducting a continuing program to determine the solubilities of various selected elements in liquid plutonium. Solubility data[20,21] generated to date for C, Mo, Nb, Re, Ta, and W in the temperature range 700 to 950°C are summarized in Table I-5. The data fit the equation

$$\log N_x = A - 1000\ B/T$$

where N_x is the solubility expressed as atom fraction of solute, T is the temperature in °K, and A and B are constants whose values for each element are listed in Table I-6.

To help determine the feasibility of venting fission gases in a sodium-cooled liquid-plutonium-alloy-fueled fast-reactor system, open tantalum capsules containing Pu–Co–Ce fuel have been exposed to flowing sodium[22] at 650°C. The tendency of the fuel to climb up the walls of the tantalum capsules led to measurable fuel losses within 1000 to 3000 hr. Also, it was found that cobalt depletion in the fuel occurred

Table I-5 SOLUBILITIES OF SELECTED ELEMENTS IN LIQUID PLUTONIUM[20]

Temp., °C	Solubility, at. %					
	C[21a]	Mo[21b]	Nb[21c]	Re[21d]	Ta[21e]	W[21f]
700	1.36	1.57	1.10	1.57		0.0038
750	1.61	2.11	1.44	1.84	0.085	0.0072
800	2.26	2.65	1.69	2.35	0.119	0.0105
850	2.67	3.08	2.05	2.75	0.140	0.0159
900	3.57	3.64	2.68	3.27	0.267	0.0255
950	4.47	4.58	3.14	4.05	0.352	0.0379

Table I-6 VALUES[20] FOR THE CONSTANTS IN THE SOLUBILITY EQUATION LOG $N_x = A - 1000\ B/T$

Element	A	B
Carbon	0.50	2.30
Molybdenum	0.329	2.06
Niobium	0.277	2.18
Rhenium	0.195	1.96
Tantalum	0.769	3.94
Tungsten	0.352	4.64

through the formation of a Ta–Co intermetallic compound at the capsule walls. The resulting Pu–Ce residence was more corrosive to the tantalum than was the original fuel.

Two methods for measuring the quantity of alpha plutonium in nominally delta-stabilized plutonium alloys have recently been reported. The technique developed at Rocky Flats[23] is based on X-ray diffractometry, whereas Los Alamos researchers[24] used electrical-resistivity measurements.

Investigators at Nuclear Materials[25] have grown large grains of alpha plutonium by a pressure technique. Plutonium with an average grain size of 0.030 mm was subjected to a pressure of 25 kbars at 350°C for 8 hr followed by cooling to room temperature under pressure. Grains measuring 2.0 × 2.4 mm were produced by this method.

Argonne[26] has used an ultrasonic-pulse method to study the mechanism and kinetics of the beta → alpha transformation in high-purity plutonium. The behavior during transformation was consistent with a martensitic-type transition.

Work on the development of metallic U–Pu based alloys for fast breeder fuel applications is continuing.[27] Thermal conductivities of several U–Pu–Zr and U–Pu–Ti alloys were measured at temperatures up to 900°C, and the results are shown in Table I-7. Studies of phase equilibria in the U–Pu–Ti system indicate that the addition of plutonium to a U–33.3 at.% Ti alloy stabilizes the gamma phase to lower temperatures. In alloys containing 16.7 and 23.3 at.% plutonium, the gamma phase is stabilized to 817 and 782°C, respectively. The gamma to U_2Ti transformation occurs at 898°C in binary U–Ti alloys. A tentative isopleth of the U–Pu–Ti ternary diagram at 33.3 at.% titanium is shown in Fig. I-2.

An analysis of the solid-state reactions in the uranium corner of the U–Pu–Ti phase diagram is given in Fig. I-3. This analysis accounts for the six binary solid-state transformations in the U–Pu and U–Ti binary systems and is supported by dilatometric and DTA data for ternary alloys. Three major reactions at 655, 650, and 575°C were found to occur in alloys of interest as fast reactor fuels. The highest temperature isothermal reaction, a Class II reaction, involves the transformation beta + gamma → $(U,Pu)_2Ti$ + eta. The zeta phase forms peritectoidally by a Class III reaction at 650°C. The lowest temperature isothermal reaction occurs at 575°C, i.e., $(U,Pu)_2Ti$ + beta → alpha + zeta. After the reaction at 575°C occurs, the three-phase region $(U,Pu)_2Ti$ + alpha uranium + zeta is stable to room temperature. The two Class II reactions at 600 and 585°C are based on a limited amount of data and are subject to revision as additional alloys in this region are investigated.

Table I-7 THERMAL CONDUCTIVITIES OF U–Pu–Zr AND U–Pu–Ti ALLOYS[27]

	Composition*					
	Pu–Ti	Pu–Ti	Pu–Ti	Pu–Zr	Pu–Zr	Pu–Zr
At. %	10.0 13.3	15.1 23.9	11.4 29.8	14.7 15.0	12.7 21.9	15.5 25.3
Wt. %	11.4 3.0	18.6 5.9	15.0 7.8	16.2 6.2	14.7 9.7	18.4 11.5
Temp., °C	Thermal conductivity, watts/(cm)²(°C)					
100	0.105	0.095	0.087	0.109	0.100	0.092
200	0.139	0.125	0.117	0.142	0.132	0.117
300	0.171	0.155	0.142	0.177	0.164	0.144
400	0.201	0.185	0.163	0.210	0.196	0.171
500	0.228	0.216	0.184	0.241	0.225	0.197
600	0.254	0.245	0.201	0.264	0.253	0.219
700	0.278	0.275	0.216	0.280	0.278	0.234
800	0.302	0.306	~0.229	0.293	0.301	0.248
900	~0.326	~0.335		~0.301	~0.323	~0.260

*Balance uranium.

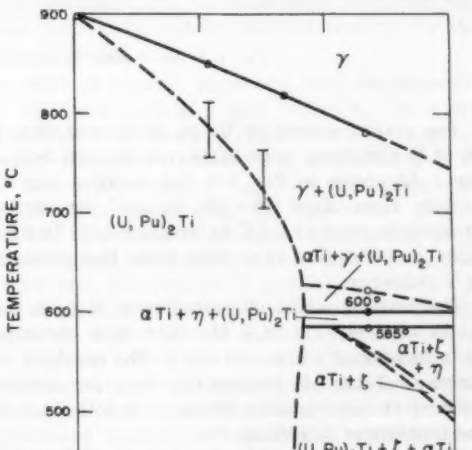

Fig. I-2 Section through U–Pu–Ti ternary system at 33.3 at.% titanium.[27]

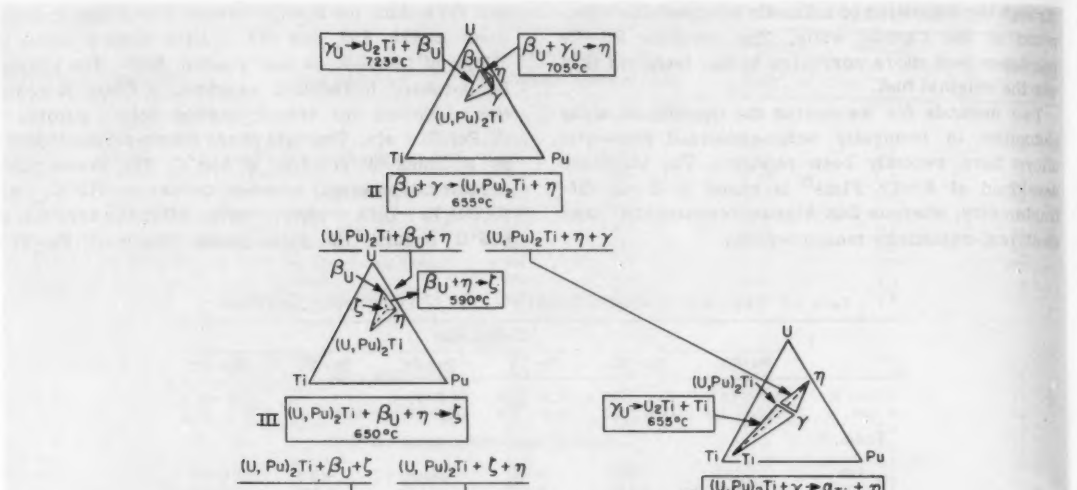

Fig. I-3 Solid-state reactions in uranium corner of the U–Pu–Ti system.[27]

The elastic moduli of U–Pu alloys containing 0 to 20 at.% plutonium were measured at room temperature. As shown in Fig. I-4, the modulus decreases rapidly from about 23×10^3 kg/mm^2 for unalloyed uranium to about 13×10^3 kg/mm^2 for a U–10 at.% Pu alloy and changes very little from that point to 20 at.% plutonium.

Thermal-expansion characteristics of a hot-rolled U–25 wt.% Pu–2.5 wt.% Mo alloy were investigated as a function of rolling direction. The resulting data, shown in Table I-8, indicate that the expansion characteristics are virtually the same in both the rolling and transverse directions.

The compatibility of U–25 wt.% Pu–2.5 wt.% Mo and U–28 wt.% Pu–2.5 wt.% Mo alloys with type 304L stainless steel has been tested at 600, 650, and 700°C. After 1 week at 600°C, only a minor reaction between the alloys and stainless steel was noted. At 650°C the reaction was much more severe, and at 700°C alloying and melting occurred.

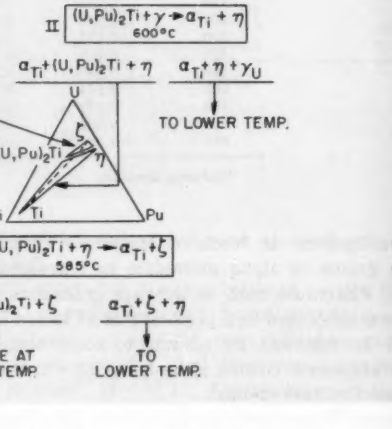

Fig. I-4 Variation of elastic modulus with plutonium in uranium.[27]

Table I-8 EXPANSION CHARACTERISTICS OF U–25 WT.% Pu–25 WT.% Mo ALLOY[27]

	As rolled		
	Rolling direction	Transverse direction	As cast
Mean coefficient of expansion, 10^{-6}/°C			
25 to 200°C	14.2	15.3	15.4
200°C to transformation temperature	25.5	24.8	26.2
Transformation to 780°C	23.7	24.2	25.3
Transformation range, °C	545–620	545–620	540–630
Expansion (Δl), %	0.41	0.41	0.46

The International Atomic Energy Agency (IAEA) has recently published a monograph "Plutonium: Physico-Chemical Properties of Its Compounds and Alloys."[28] Included in this special issue of the *Atomic Energy Review* are data pertaining to thermodynamic properties, structures, densities, equilibrium diagrams, and diffusion rates of plutonium and its compounds and alloys. (V. W. Storhok)

Plutonium Compounds

The oxidation in air at 750°C of solid solutions of $(Pu,U)O_2$ containing up to 80 mole % PuO_2 has been investigated at Harwell.[29] Variable solid-solution oxidation products are formed, either single phase (cubic or orthorhombic) or two phase (cubic + orthorhombic), according to the composition and physical state of the initial $(Pu,U)O_2$ solid solution. The cubic solid solutions are of the MO_{2+x} type of a wide composition range, 40 to 100 mole % PuO_2, whereas the orthorhombic solid solutions are of an M_3O_{8-x} type with a narrow composition range, 0 to 10 mole % PuO_2. No evidence is found for the formation of either pure PuO_2 or pure U_3O_8.

Oak Ridge[30] has successfully prepared microspheres of PuO_2 and mixed oxides of $(Pu,U)O_2$ and $(Pu,Th)O_2$ by the sol-gel process on a laboratory scale. Plutonium sols are prepared from $Pu(NO_3)_4$ solution by a precipitation–peptization technique. Densities of 95 to 99% of theoretical are reported for microspheres following an 1150°C calcining.

A method of chemically etching PuO_2 to reveal grain boundaries and twins and which distinguishes between PuO_2 and beta–Pu_2O_3 in a sintered compact has been reported by Los Alamos.[31] The etchant, equal proportions of concentrated HF and HNO_3, is placed on the polished surface and evaporated by heating the sample.

Battelle–Columbus has prepared tungsten-coated PuO_2 and $(Pu_{0.2}Ce_{0.8})O_2$ microspheres for the fabrication of intrinsic thermocouples for fast-flux measurement.[32] Microspheres 500 μ in diameter were prepared by mechanical spheroidizing and sintering and were coated in a fluidized bed by the hydrogen reduction of WF_6. Heat content vs. temperature data for these materials were estimated and reported.

Uranium–plutonium monoxide for possible application in water-cooled thermal reactors has been synthesized by United Nuclear[33] by two methods: (1) the carbon reduction of mixed dioxides and (2) the reduction of mixed dioxides with uranium metal. Both processing routes were evaluated in helium and vacuum at temperatures from 1450 to 1900°C. Pure (U,Pu)O could not be synthesized. Essentially single-phase $(U_{0.9}Pu_{0.1})(O_xC_{1-x})$ was synthesized by carbon reduction in helium and vacuum with a maximum attainable oxygen content of $x = 0.4$. Similar material was obtained by uranium-metal reduction of the oxides in helium, provided carbon was added to stabilize the monoxide structure. In vacuum this method led to an undesirable metal phase in the final product. Higher oxygen contents, approaching $x = 0.6$, were produced by carbon reduction; however, the monoxide weight fraction was limited to 60 wt.%. Efforts to increase oxygen content and monoxide weight fraction were unsuccessful. Synthesis of $(U,Pu)(O_xC_yN_z)$ by the uranium-metal reduction of mixed dioxides with UC and UN additions resulted in a monoxide weight fraction of 90 wt.% or greater, provided the oxygen content did not exceed $x = 0.3$ and the O/C ratio was less than 1.

$(U,Pu)(O_xC_{1-x})$ with an oxygen content of $x = 0.37$ disintegrated within 1 hr in boiling water. $(U,Pu)(O_xC_yN_z)$ with a carbon content of $y < 0.4$ survived the boiling-water corrosion test. All $(U,Pu)(O_xC_yN_z)$ compositions tested in 550°F (288°C) water disintegrated[33] within 1 hr. Thermal-diffusivity measurements indicated that monoxide-type materials have higher room-temperature thermal conductivity than UO_2 or $(U,Pu)O_2$.

In work at Nuclear Materials, both stoichiometric and substoichiometric 5 wt.% PuO_2–UO_2 fuels prepared from coprecipitated $(Pu,U)O_2$ and mechanically blended component powders were irradiated to 10,000 and 20,000 Mwd/metric ton.[34] An unidentified nonmetallic gray phase near the fuel center line and metallic spheroidal inclusions were noted in the substoichiometric coprecipitated and mechanically blended fuel. No evidence of cladding (type 316 stainless steel) corrosion was observed in the substoichiometric coprecipitated capsule, but evidence of a thin reaction zone at the fuel–cladding interface was noted in the case of mechanically blended substoichiometric oxides. All the stoichiometric material experienced central void formation with columnar grain growth. No gray phases or white inclusions were present in this material. The average fission-gas release of the substoichiometric materials was 21.5% for either powder preparation method. Stoichiometric mechanically blended oxide had a 35% higher average fission-gas release than the substoichiometric material. (W. M. Pardue)

Thorium

A tentative phase diagram was proposed for the Th–C system over the composition range 4 to 11 wt.% carbon.[35] The results of the investigations at Harwell show that ThC_2 undergoes two polymorphic transformations, changing from monoclinic to tetragonal at 1410 ± 20°C and from tetragonal to cubic at 1500 ± 20°C. When ThC is present, the lower allotropic temperature is reduced to 1290 ± 20°C. A solid solution is formed between ThC and cubic ThC_2 at temperatures higher than about 2100°C. Methods used to investigate phase equilibria were metallography, X-ray diffraction, and DTA techniques.

Workers at Oak Ridge are investigating the hot hardness of a Th–1.3 wt.% Be alloy prepared by the SLIS method.[36] A slight increase in hardness was obtained on this alloy over that of a Th–5 wt.% Zr alloy in the range 600 to 750°C. Metallographic studies revealed that the $ThBe_{13}$ precipitate coarsens when heat-treated at 600 to 800°C. Further investigation of this alloy system is being planned.

Postirradiation heat-treatments were performed on specimens of two Th–U alloys at Battelle–Northwest.[7] As seen in Table I-9, the Th–5.4 wt.% U alloy generally swelled more than the Th–1 wt.% U alloys.

Levinson[37] measured the heat contents of alpha- and beta-phase thorium between 1269 and 1650°K and between 1667 and 1991°K, respectively. Similar measurements of molten thorium at 2069 and 2100°K, using a drop calorimeter, were also made. Estimates of the heat of the beta → alpha transition were 857 ± 28 cal/mole, and the heat of fusion for thorium was determined as $3.3 \times 10^3 \pm 300$ cal/mole.

In phase studies of the Th–U–Pu system, Argonne workers[38] noted that the (U,Pu) phase of the Th–20 wt.% U–10 wt.%–Pu alloy undergoes two reversible transformations: $\gamma \rightleftharpoons \beta$ at 938°C and $\beta \rightleftharpoons \alpha$ at 590°C. Specimens of this alloy along with those of the Th–10 wt.% U–10 wt.% Pu alloy are undergoing irradiation tests and have reached burnups of 0.5% at 630°C and 0.34% at 600°C, respectively. A schematic diagram of the liquidus surface is shown in Fig. I-5. The miscibility gap of the binary Th–U system is probably closed in the ternary system at low plutonium concentrations as shown. A peritectic should extend across the system from the Th–U side to the Th–Pu side if the alpha-thorium phase forms from the beta-thorium phase by peritectic reaction. A eutectic valley extends from the Th–U side to the plutonium corner of the Th–Pu system where a four-phase reaction, alpha Th + liquid → Pu_7Th_3 + sigma, near 610°C is probable.

Perhaps one of the most up-to-date collections of recent work on thorium is contained in a single volume to be published by the IAEA.[39] This book contains 23 survey papers in addition to brief reviews on important aspects of thorium utilization.

(R. L. Martin)

Table I-9 DENSITY OF IRRADIATED Th–U ALLOYS[7]

Sample	Condition	Burnup, at.%	Density, g/cm³	Swelling $(\Delta\rho/\rho_f \times 100)$, %	R, % swelling/at.% burnup
T-123 (Th–1 wt.% U)	As irradiated	1.5	11.51		
	Annealed at 725°C* 100 hr	1.5	11.33	1.6	1.1
	Annealed at 825°C 100 hr	1.5	11.30	1.9	1.3
	Annealed at 900°C 100 hr	1.5	10.98	4.8	3.2
C-12 (Th–5.4 wt.% U)	As irradiated	1.3	11.67		
	Annealed at 725°C* 100 hr	1.3	11.58	0.8	0.6
	Annealed at 825°C 100 hr	1.3	11.32	3.1	2.4
	Annealed at 900°C 100 hr	1.3	10.45	11.7	9

*Both specimens experienced a brief temperature excursion to 800°C.

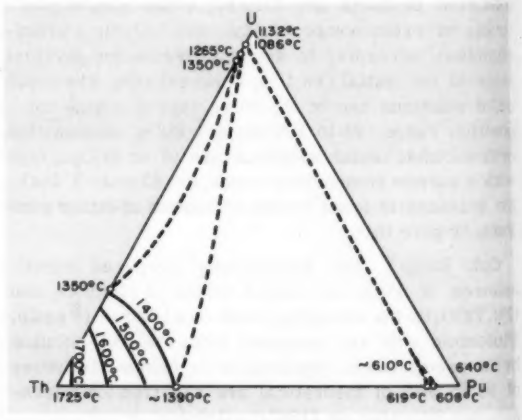

Fig. I-5 Schematic diagram for the liquidus surface in the Th–U–Pu system.[39]

Metal–Ceramic Fuels

Dispersion Fuels (Less Than 50 Vol.% Ceramic Phase)

Workers at Oak Ridge[40] have studied the influence of irradiation temperature and high burnups on the dimensional and chemical stability of both U_3O_8 and niobium-coated UO_2–15 wt.% ZrO_2 dispersed in a matrix of X8001 aluminum and clad with Alclad 6061 aluminum. Examination of the U_3O_8-bearing fuel specimens (reference HFIR and ATR fuel) showed reaction between the U_3O_8 and the aluminum matrix. The extent of this reaction appeared to be primarily a function of the irradiation temperature, not fuel burnup. A specimen irradiated to 6.3×10^{20} fissions/cm^3 at 110°C reacted less than an identical specimen irradiated to 3.9×10^{20} fissions/cm^3 at 165°C. Significantly greater reaction occurred in a specimen irradiated to 9.4×10^{20} fissions/cm^3 at 182°C, and complete reaction between the U_3O_8 and matrix occurred after 16.1×10^{20} fissions/cm^3 at 238°C. No evidence of gross failure was observed, although the irradiation conditions for the latter specimens were significantly higher than expected in the HFIR.

The niobium-coated UO_2–ZrO_2 fuel particles were found to swell at a rate of 1.3 vol.% change per at.% ^{235}U fissioned. The niobium coating prevented reaction between the fuel particles and the matrix, with the particles retaining their spherical shape and fission products. The fission-gas porosity in the fuel particles was found to be directly proportional to the fuel burnup.

Work at Battelle–Columbus[38] on UO_2–stainless-steel dispersions has involved studies of blending procedures, the effects of fuel thickness on fuel-particle distribution, and UO_2 behavior on rolling. It was found that homogeneity could be achieved in low inventory fuels (5 to 15 wt.% UO_2) by using blending procedures similar to those employed for a 37 wt.% UO_2–stainless-steel dispersion. Studies of various fuel concentrations and plate thicknesses (i.e., 6, 12, and 37 wt.% UO_2 in 0.030-, 0.015-, and 0.006-in.-thick dispersions, respectively) demonstrated that the best quality of fuel-particle spacing and overall uniformity of fuel dispersion was obtained with a 0.030-in.-thick dispersion. The UO_2 characterization and evaluations were made with 12 commercial and laboratory-produced oxides of 85 to 90% density. Examination after rolling showed that UO_2 with 2 to 3 wt.% CaO or ZrO_2 additions had higher crushing strengths than did UO_2 without additives when rolled at 1100°C. The oxide with additives resulted in 20 to 30% particle fracture, whereas the pure UO_2 displayed a ductility during rolling. Rolling to reductions of 6:1 produced high densification and deformation (footballing) of the pure UO_2 in 37 wt.% UO_2–stainless-steel dispersions.

Mechanical properties of UO_2–type 304 stainless-steel dispersions as related to different fabrication techniques have been evaluated at Battelle–Northwest.[7] Data were obtained for dispersion pins extruded in both mild-steel cans and copper cans. After swaging, extruded pins containing 0 to 30 vol.% UO_2 showed an increase in both yield and ultimate strengths when compared with the as-extruded material. The swaging operation fractured the UO_2 particles, and the severely fractured particles were found to behave more like voids in the matrix than a dispersed solid phase. Therefore the modulus of the dispersion was lowered by swaging. Fig. I-6 shows the decrease in yield stress as the volume loading of UO_2 is increased for the dispersions extruded in both types of jacket materials. Table I-10 shows the tensile properties at the various temperatures. The UO_2 particles in general exhibit less fracturing as the testing temperature is increased. It was also found that, at 1000°C, the yield stress is approximately the same for both pure stainless steel and the 20 vol.% UO_2 dispersion.

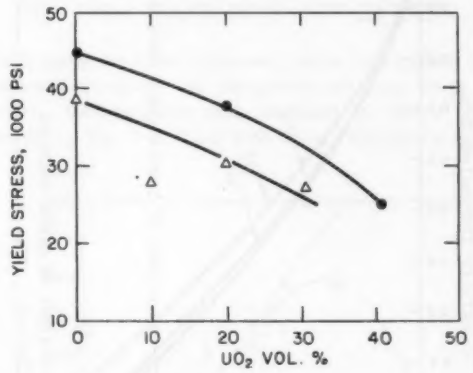

Fig. I-6 Dependence of yield stress on volume loading of UO_2 for type 304L stainless-steel–UO_2 cermets.[7] ●, current extrusion process with copper cans; △, former process with mild-steel cans.

Table I-10 TENSILE PROPERTIES OF A 20 VOL.% UO_2 TYPE 304 STAINLESS-STEEL CERMET[7]

Fuel pin	Test temp., °C	Yield strength, psi	Ultimate strength, psi	Elongation, %
18UL	22	38,200	54,500	10
18UL	400	24,500	37,000	9
2UH	720	16,500	23,000	8
15UL	800	16,500	18,700	8
2UH	940	6,500	7,300	8
4UL	1000	4,000	5,000	13
4UL	1100	3,000	3,200	11

(D. E. Lozier)

Cermet Fuels (Over 50 Vol.% Ceramic Phase)

Several attempts have been made to calculate the theoretical strength of cermet structures. The model used assumes no bonding between the dispersed ceramic and continuous metal-matrix phases; hence the tensile yield strength is dependent upon the minimum cross-sectional area of the matrix for various assumed types of spherical-particle packing. Figure I-7 shows various curves taken from an article by

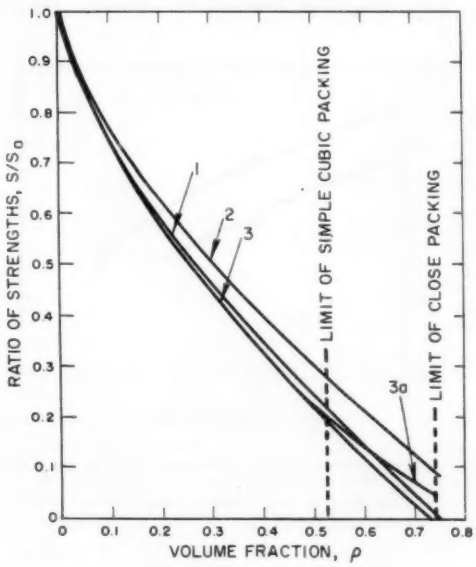

Fig. I-7 Effect of volume fraction on the ratio of the cermet strength to the strength of the matrix metal (Ref. 41). 1, simple cubic packing, $S/S_0 = 1 - 1.209\ P^{2/3}$; 2, single layer close packed, $S/S_0 = 1 - 1.109\ P^{2/3}$; 3, double layer close packed, $S/S_0 = 1 - 1.233\ P^{2/3}$; 3a, double layer close packed, corrected for overlap.

Butcher and Howlett[41] which express the ratio of cermet strength to strength of a similar cross-sectional area of matrix (S/S_0) as a function of the dispersed ceramic-phase volume fraction (ρ). Curve 1 was previously proposed by Eudier[42] and was shown in an article by Cope[43] to agree relatively well with available cermet-properties data. As shown in Fig. I-7, the calculated curves for the different types of spherical-ceramic-phase packing differ most at the higher fuel-volume fractions. (R. A. Smith)

Coated-Particle Fuels

Particle Coating

Oak Ridge has issued a report[44] that includes calculated curves for rapid estimation of density and surface area of pyrolytic carbon (PyC)-coated fuel particles. The curves are useful for overall particle diameters of 100 to 1400 μ, core diameters of 100 to 1200 μ, core densities of 8 to 14 g/cm^3, and coating densities of 0.6 to 2.2 g/cm^3. In other work on PyC, successful operation of a 5-in.-diameter fluidized-bed coater at temperatures up to 1500°C is described.[45,46] Measurements of the stress–strain relations for PyC coatings of different densities is reported.[47] The measurements revealed that low-density porous coatings (0.6 g/cm^3), in spite of significantly lower crushing strength, deformed elastically to a much higher degree before rupturing than did coatings of intermediate densities (1.5 g/cm^3).

The corrosive action of HCl on PyC-coated UC_2 particles was investigated at Los Alamos[48] over the range 1600 to 2100°C. The rate-determining step in the leaching process was the diffusion of uranium from the core through the PyC coating. Uranium chloride vapor evolved from the reaction chamber was condensed and measured spectrophotometrically. In the range 1800 to 2100°C, the relative standard deviations for median values of the amount of uranium leached varied from 4 to 21% for six or more determinations.

In work on PyC coatings in Great Britain, process parameters were studied[49] for the application of PyC on UC fuel to be used in advanced gas-cooled reactors (CO_2 cooled and graphite moderated). It is interesting to note that the PyC-coated UC could be fabricated in a SiC matrix more readily than could SiC-coated UC (Ref. 50). The key to the successful fabrication in this case is final bonding by impregnation of a loosely bonded mixture of the matrix and fuel with silicon at a high temperature and reduced pressure.

Workers at Union Carbide have applied nickel coatings to UO_2 particles by hydrogen reduction of nickel oxide.[51] The fuel particles are tumbled along with vacuum-dried, high-surface-area, nickel oxide which adheres to the UO_2 without the aid of a binder. The nickel-oxide-coated particles are hydrogen treated at 300°C to reduce the nickel oxide to metal and are annealed at 800 to 1000°C in hydrogen to densify the nickel coating. Coatings about 1 mil thick have been obtained. (N. D. Veigel)

Irradiation and Evaluation of Coated-Particle Fuels

Three irradiation experiments for the evaluation of 35 types of PyC-coated fuel particles were conducted by General Atomic.[52–54] Fuel particles of UC_2, UO_2, $(Th-U)C_2$, and $(Th-U)O_2$ with isotropic, buffer-isotropic, and triplex coatings were irradiated at temperatures to 1650°C over a burnup range of 9 to 24% of the fissionable atoms. From the results of these experiments it was concluded that: (1) high-density isotropic coatings have the greatest radia-

tion stability and their stability increases with increasing density, (2) a coating thickness-to-core diameter ratio (T/D) of 0.4 appears to be required for stability in high-temperature high-burnup irradiations (3) for a constant T/D ratio, small particles have greater radiation stability than large particles, (4) **Buffer-Isotropic** coatings appear equivalent to **Triplex** coatings (for equivalent T/D ratio), and (5) coated oxides appear equivalent in radiation stability to coated carbides.

An experiment at Oak Ridge[55] was conducted to evaluate three fuel spheres that had been fabricated by the mass-production techniques used for the first-core fuel of the AVR, the German Pebble Bed Reactor at Jülich. Each sphere contained 200-μ-diameter UC_2 particles with 106-μ-thick duplex PyC coatings. The 6-cm-diameter fuel spheres were formed by injection molding a fueled-graphite matrix material into 1-cm-thick unfueled graphite shells and were sealed with threaded graphite plugs. The spheres were irradiated with maximum center fuel temperatures of 690 to 850°C to burnups of 5.5 to 7.4% of the fissionable atoms. Throughout the experiment the release fraction (R/B) of ^{133}Xe remained in the order of 1×10^{-4}. Postirradiation metallographic examinations of the spheres showed that no coatings failed as a result of the irradiation, thus demonstrating the effectiveness of the duplex coatings on the fuel particles. Graphite powder surrounding each sphere during the irradiation was analyzed for fission products. For the three spheres the fraction of the calculated inventory of ^{140}Ba ranged from 7×10^{-8} to 3×10^{-7}, and that of ^{137}Cs ranged from 5.6×10^{-5} to 3.4×10^{-4}. The experiment showed that the spheres successfully met the irradiation-performance requirements for the AVR fuel.

The stable fission-gas release from fuel kernels in intact coated particles has been measured at Harwell[56] by cracking open the coatings after irradiation and counting the ^{85}Kr released. The results from UC_2 kernels showed a marked increase in the gas release (2 to 40%) between 4.3 and 6.6 at.% burnup. The release levels appeared relatively insensitive to irradiation temperature in the range 925 to 1275°C. These results show that at low burnup the fission-gas release from the kernel may be attributed to fission-product recoil rather than to a diffusion-type process.

(N. E. Miller)

Uranium and Thorium Oxides

Properties and Behavior

The mechanism and kinetics of nitrogen release from sintered UO_2 pellets have been studied by Ferrari.[57] X-ray and metallographic analysis showed that nitrogen present in UO_2 exists as a second phase in the form of uranium nitride. Release measurements at temperatures between 1000 and 1600°C indicate that the release is controlled by nitrogen diffusion through the UO_2 lattice. Diffusion coefficients for nitrogen in UO_2 were found to follow the relation

$$D = 2.25 \times 10^{-9} \exp(-33{,}400/RT) \text{ cm}^2/\text{sec}$$

Investigators at General Electric[58] have performed melting-point measurements on uranium oxides of different stoichiometries with oxygen-to-uranium ratios varying between 1.75 and 2.003. Over part of this range, the melting point can be expressed as

$$T_m = -9443 + 11{,}488\ (\text{O/U}) - 2665\ (\text{O/U})^2, \ ^\circ\text{C}$$

Care must be taken, however, not to extrapolate this expression above an oxygen-to-uranium ratio of 2.000. Melting-point data obtained by Bates[59] are shown in Fig. I-8, along with those reported by other

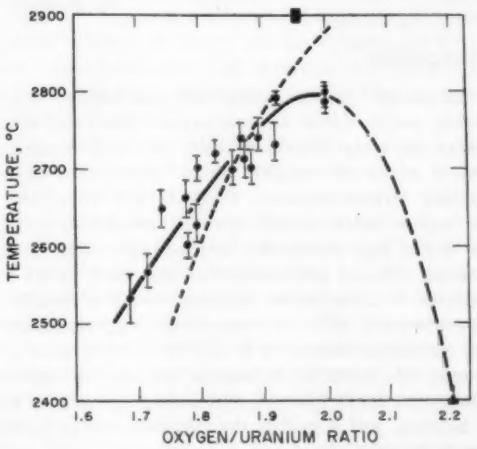

Fig. I-8 Melting points of hypostoichiometric uranium dioxide.[59] ▲, *Christiansen, HW-69234;* ■, *Duncan et al.,* Trans. Amer. Nucl. Soc., *6(1): 154 (1963);* ---, *Latta and Fryxell, Ref. 58;* Φ, *Bates, Ref. 59.*

investigators. The lack of agreement between values calculated from the above expression and measured values for oxygen-to-uranium ratios above 2.000 is illustrated in this comparison.

Heat-capacity data for UO_2 have been analyzed at Oak Ridge[47] over the temperature range 298 to 876°K. Values were found to follow the relation

$$C_p = 13.51 + 1.91 \times 10^{-2}T - 1.16 \times 10^{-5}T^2 - 8.54 \times 10^{2}T, \text{ cal/(mole)(°K)}$$

within 0.4%. Thermal-conductivity measurements performed on ThO_2–10% UO_2 at Babcock & Wilcox[60] are

summarized in Table I-11. The data are tabulated along with UO_2 data in terms of the mean thermal conductivity, k_{mean}, defined by the following equation

$$k_{mean} = \frac{\int_{T_1}^{T_2} k dt}{T_2 - T_1}$$

Table I-11 MEAN THERMAL CONDUCTIVITY OF UO_2 AND ThO_2–10% UO_2 (REF. 60)

Material	Temperature, °C		k_{mean}, watts/(cm)(°C)
	T_2	T_1	
UO_2	930	800	0.030
	1150	960	0.034
	1810	1560	0.036
ThO_2–10% UO_2	980	780	0.030
	1050	830	0.031
	1140	890	0.030
	1150	930	0.034
	1220	1010	0.038
	1370	1150	0.039

(R. H. Barnes)

Fabrication

Oak Ridge[61] has reported on a new method of preparing metal oxide microspheres. The process involves spraying nitride or chloride solutions or sols onto a layer of organic liquid floating on an ammonium nitrate solution. Droplets are dispersed in the organic layer and fall into the ammonium hydroxide where they hydrolyze to form hydroxide microspheres. These microspheres are then dried and sintered to form oxide spheres having a density of approximately 87% of theoretical. Microspheres of UO_2 having a density of 99% of theoretical were also formed by bubbling ammonia through an aqueous solution to form the gel, converting the gels to sols by heating, and adjusting the viscosity before formation of the droplets.

Since high-density pellets could not be directly fabricated from pot denitrated ThO_2 powder, Bettis[62] investigators have investigated methods of increasing the sinterability of such material. Basically, major milling and micronizing were utilized to reduce the particle size to such a point that pellets 95% dense could be fabricated. Because the pellets were extremely sensitive to thermal shock, special sintering rates were required to produce crack-free sintered bodies. Low-density pellets having a controlled porosity were also fabricated using sucrose as a pore-producing additive.

Using a technique similar to that discussed above, Battelle workers[63] have fabricated selected compositions of UO_2–ZrO_2 and UO_2–ZrO_2–CaO in rods having controlled densities of 95 and 85% of theoretical. These rods were used in determining the thermal conductivity of the compositions by the thermal-diffusivity technique. (T. R. Wright)

Carbide and Nitride Fuels

Properties and Behavior

It has long been known that UC, or rather U(C,O), forms a quasi-binary system with UO_2 under moderate pressures of CO. Morlevat[64] has discovered that the system is of the eutectic type with the eutectic near 45 to 50 vol.% U(C,O) and at a temperature above 2200°C. Microstructures accompanying an article by Ervin and Miller[65] suggest that the oxidation of UC in low-pressure oxygen at 900 to 950°C proceeds in three distinct steps corresponding to three distinct two-phase layers formed on the surface of the UC:

$$2UC + O_2 = UC_2 + UO_2 \text{ (inner layer)}$$

$$UC_2 + O_2 = UO_2 + 2C \text{ (middle layer)}$$

$$UO_2 + 2C + O_2 = UO_2 + 2CO \text{ (outer layer)}$$

These reactions are consistent with a ternary diagram of the U–C–O system which shows quasi-binary ties radiating from UO_2 to U, UC, UC_2, graphite, and CO.

It is suggested that UN can exhibit congruent sublimation under certain conditions.[66] The implication is that, at temperatures "below 1800°C, pure solid UN can be vaporized *in vacuo* indefinitely without appearance of liquid uranium." This suggestion would require that the vapor pressure of uranium over UN be approximately six times that of nitrogen at these temperatures.

Battelle–Columbus[67] has found that UN is compatible with type 304 stainless steel from 1000 to 1350°C, with iron from 700 to 1000°C, and with chromium from 800 to 1000°C. Extensive reactions were observed between UN and zirconium at 600 to 700°C, with Zircaloy-2 at 600 to 900°C, with nickel at 800 to 1200°C, and with aluminum at 500 to 600°C.

Argonne reports[68] no reaction between Haynes 56 (Fe + 12 wt.% Ni + 12 wt.% Co + 21 wt.% Cr + 4 wt.% Mo + 1 wt.% W) and stoichiometric or hypostoichiometric $U_{0.8}Pu_{0.2}C$ in 42 days at 800°C. Likewise, there was no reaction between stoichiometric $U_{0.8}Pu_{0.2}C$ and 304 stainless steel. However, reaction zones up to 43 μ thick were observed between stoichiometric and hypostoichiometric $U_{0.8}Pu_{0.2}C$ and other austenitic alloys under these conditions.

Brookhaven workers[69] have determined the relative integral molar free energy of formation of U_2C_3 and UC_2 over the temperature range from 700 to 900°C. These results plus data for UC from the literature are shown in Fig. I-9. This figure shows that, at these temperatures, U_2C_3 is the stable phase in equilibrium with graphite, UC is the stable phase in equilibrium with uranium, and UC_2 is only slightly unstable with respect to U_2C_3 and graphite. These

results are in agreement with the known behavior of these carbides.

Thermal-expansion coefficients of U_2C_3 and UC_2 have been determined at temperatures[70] over 1000°C. Because these compounds show an increasing rate of expansion with increasing temperature, the coefficients reported are significantly larger than would be obtained using a reference temperature near room temperature. The reaction UC_2 (tetragonal) = UC_2 (cubic) proceeds to the right with a volume increase of about 2½%. The reaction $2UC_2$ (tetragonal) = U_2C_3 + C proceeds to the right with a volume decrease of about 1½%.

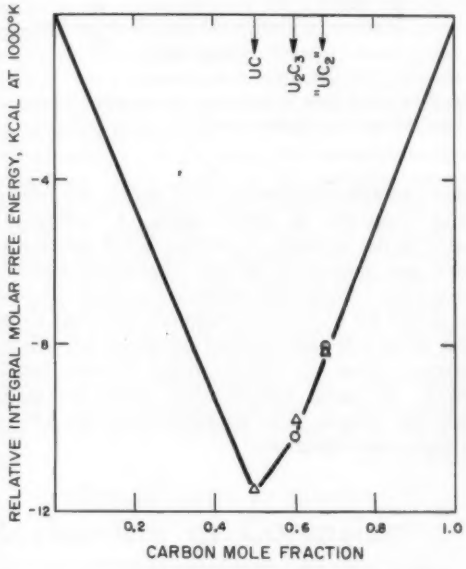

Fig. I-9 Relative integral molar free energy in the system U–C.[72]

The modulus of elasticity of UP is 18,000 kg/mm² at 20°C, 10,500 kg/mm² at 1000°C, and 5500 kg/mm² at 1500°C (Ref. 71).

Argonne has commenced a series of irradiations of vibratorily compacted UC–20 wt.% PuC powders. Surface temperatures to 1000°C and burnups to 10 at.% of the metal atoms are expected. Some initial results are available. When unenriched UC powder was mixed with PuC powder and irradiated to 6.8 at.% burnup at maximum surface temperatures of about 700°C, the PuC particles showed a tendency to swell, with appreciable bubble formation, and fill the void spaces between relatively inert UC particles.[72] In agreement with previous findings, hypostoichiometric fuel released 20 to 40% of its fission gas, whereas hyperstoichiometric fuel released less than 1%. The claddings of niobium and stainless steel on these specimens did not fail; however, the niobium claddings of two alloyed $(U_{0.8}Pu_{0.2})C$ specimens in another capsule[68] failed by cracking at about half the above burnup and at temperatures up to 1260 and 1350°C. The niobium cladding of one of four US specimens also cracked under similar conditions.

Characterization of the pore size and distribution in a sample of UC that had swelled about 3% during irradiation showed that the total pore volume could account for between ⅕ and ⅓ of the total swelling.[73] Over 80% of the total pore volume was found to reside within the UC grains and less than 20% in the grain boundaries. All the gas in the UC could be accommodated in the observed pores at a relatively modest pressure. (W. Chubb)

Fabrication

A technique for producing spherical UN particles was developed and tested in Germany.[74] Seed particles of crystalline uranium nitride are fluidized in a quartz chamber by a gaseous mixture at high temperature. Uranium nitride produced by the reaction of UCl_4, steam, and ammonia in the chamber precipitates on the seed particles, which grow into smooth-surfaced spherical particles.

High-purity (U,Zr) carbide, suitable for use as the cathode in a diode for the direct conversion of fission heat to electric power, is produced by a technique patented in Great Britain.[75] A mixture of 67 wt.% UC and 33 wt.% ZrC is ground for 7 to 20 hr until the particle sizes are less than 5 μ. The powder is compacted at a pressure in excess of 5 tsi and then heated in one or more stages *in vacuo* to a temperature in excess of 1800°C. During all operations the concentrations of oxygen and moisture in the atmosphere must be kept below 30 and 150 ppm, respectively.

For laboratory use, UN has been prepared from metallic uranium. However, for industrial production, uranium dioxide would be a more suitable starting material, in accordance with the equation

$$UO_2 + 2C + \frac{1}{2}N_2 = UN + 2CO$$

Unfortunately, the hypothetical uranium monoxide (UO) shows an appreciable solubility in both UN and UC, and one obtains not the pure mononitride but a solid solution of the composition $UN_{1-x-y}C_xO_y$. Thermodynamic calculations have been made to define the single-phase region as functions of temperature and partial pressures of CO and nitrogen, as well as the maximum obtainable purity of UN under different conditions.[76] Similar calculations have been carried out for the solid solutions $UN_{1-x}C_x$, giving the stability range and expected purities. Experimental results are in good agreement with these calculated values. (D. S. Acuncius)

Fuel–Water Reactions

Argonne[77–79] reports studies on the kinetics of the reaction between metallic uranium with steam and water:

$$U + 2H_2O \rightarrow UO_2 + 2H_2$$

Three experimental methods were employed in an attempt to observe the reaction under the widest possible range of conditions: (1) isothermal studies[77] of the reaction of relatively large samples with flowing steam, (2) a laboratory study[78] of the reaction of fine particles of molten uranium with water under nonisothermal conditions, and (3) in-pile studies of the reaction of representative fuel specimens with water in TREAT.[79]

In the isothermal studies the kinetics of the reaction was determined using uranium sample cubes having known surface areas. Each cube was mounted on the end of a thermocouple and heated to the desired temperature by an induction coil. The steam was produced by pumping water through heated tubing and then passing the steam over the cube. The hydrogen generated by the reaction was collected and employed to determine the extent of the reaction. Typical results of an experiment at each of the temperatures employed in the study are shown in Fig. I-10. The following rate equations summarize the results of the 600 to 1200°C and the 1200 to 1600°C studies:

$$600 \leq T < 1200^\circ C \qquad V^2 = (1.95 \pm 0.8) \times 10^5 \times t[\exp(-18{,}600 \pm 750)/RT]$$

$$1200 \leq T \leq 1600^\circ C \qquad V^2 = (1.59 \pm 0.5) \times 10^6 \times t[\exp(-25{,}000 \pm 1000)/RT]$$

where V = volume of hydrogen evolved, ml(STP)/cm^2
t = time, min
R = gas constant, 1.987 kcal/(mole)(°K)
T = absolute temperature, °K

These equations are shown in Fig. I-11.

The condenser discharge method, developed to study the zirconium–water reaction,[80] was used to investigate the reaction of solid wires and molten particles of uranium with water.[78] Initial metal temperatures were from 600 to 4000°C, wires were 30 and 60 mils in diameter, and water temperatures were 25 and 100°C. Wires heated to the melting point of uranium (1133°C) reacted to a maximum of about 4% in 25°C water and 7% in 100°C water. Wires heated above the melting point formed molten particles whose mean diameter decreased continuously with increasing metal temperature. At initial metal temperatures approaching 4000°C, 45% uranium–water reaction occurred in 25°C water, and 100% reaction occurred in 100°C water. A mathematical model of the reaction of molten-metal spheres with water was applied to the data. Good agreement between experimental and calculated extents of reaction was found for metal temperatures below the melting point using the experimental parabolic rate equation reported above for temperatures between 600 and 1200°C. At metal temperatures above the melting point, the results were correlated with the following parabolic rate equation:

$$V^2 = 8.69 \times 10^6 \times t \times [\exp(-30{,}000/RT)]$$

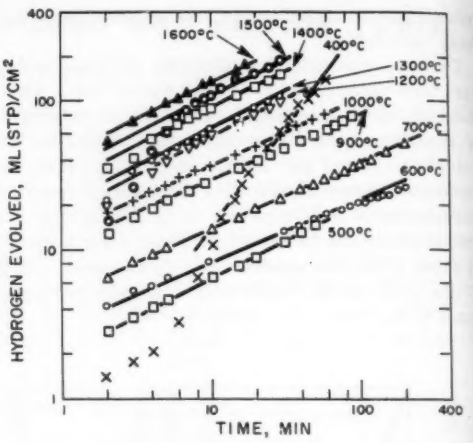

Fig. I-10 Hydrogen evolution in the reaction of steam at 1 atm with uranium-representative experiments.[77]

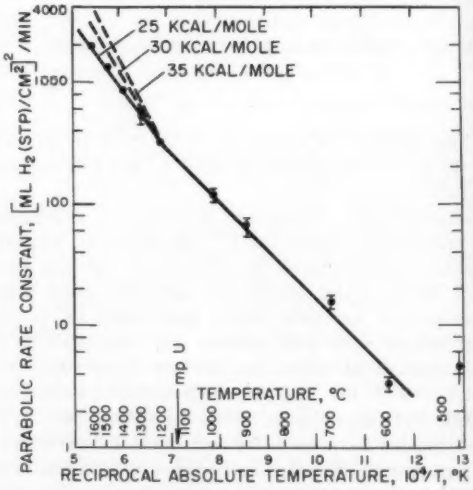

Fig. I-11 Parabolic rate constant for the uranium–steam reaction as a function of temperature.[77]

The extent of reaction with water of fuel materials having uranium metal as the major constituent is reported.[79] This chemical reaction occurs as a result of the fission heating and meltdown of these materials during a nuclear transient. Observations of the physical changes that occur are also noted. The technique involves the transient irradiation of fuel samples immersed in water in stainless-steel capsules in the TREAT facility. Uranium wires 64 mil in diameter by 1 in. long and U–5 wt.% Zr–1.5 wt.% Nb alloy pins 0.2 in. in diameter by $5\frac{5}{8}$ in. long were heated under water by the transient neutron pulse of the TREAT reactor. Subsequent measurement of the hydrogen evolved was used to determine the extent of reaction. The extent of reaction was correlated as a function of the fission energy developed in the fuel samples. Fission energies ranging from 37 to 394 cal/g and reactor periods from 63 to 515 msec were investigated. With reactor periods of the order of 100 msec, melting of fuel samples began at a fission-energy input of 40 cal/g, and complete melting occurred at 95 cal/g. The extent of reaction varied from a few tenths of 1% for those samples which had not melted appreciably to 4% for those which were completely melted in the experiments conducted in 25°C water (20-psia helium overpressure). Above 95 cal/g, the samples fragmented, and the extent of reaction increased with increasing fission energy to 50% at the highest energy of 384 cal/g. Three experiments were performed in 285°C water (1000-psi steam overpressure). The three samples in 285°C water reacted from two to three times as much as those in the 25°C water at the same energies. (J. M. Genco)

Mechanism of Corrosion of Fuel Alloys

The kinetics and morphology of the oxidation in CO_2 of two grades of uranium containing small amounts of impurities have been studied in Great Britain.[81] The shapes of weight-gain curves for these materials were found to be similar to those for pure uranium. The early acceleration observed in oxidation rates at 450°C was believed to be the result of localized oxidation at carbide inclusions. At higher temperatures, localized oxidation apparently became less important. Aluminum and iron impurities lowered the oxidation rate, presumably by their incorporation as ions in the oxide lattice where they reduced the number of interstitial oxygen ions and hence the diffusion rate.

The oxidation and ignition of uranium alloys have been studied at Argonne.[82–84] Isothermal oxidation at 300 to 625°C revealed almost identical self-accelerating reaction rates up to 400°C for unalloyed uranium and a U–1 at.% Cu alloy. Both exhibited transition to slower reaction rates above 500°C, with the copper alloy being more resistant. The ignition temperature of unalloyed uranium varied from 315 to 640°C and was found to be dependent upon specimen size. A simple mathematical model based upon isothermal-reaction-rate laws and simple heat-transfer laws yielded an ignition temperature–specific area relation which agreed well with the experimental results and which predicted the irregularity. Binary additions of up to 2 at.% of 24 different elements also affected ignition temperatures. Additions of Al, Be, Bi, C, Cu, Pb, Mo, Nb, Pd, Pt, Ru, Si, Ti, or V inhibited the transition of the oxide from an autocatalytic to a protective form, and thereby lowered the ignition temperature. Additions of Ce, Cr, H, Fe, Ni, Rh, Ag, Ta, or Zr had no significant effect on the ignition temperature. (W. E. Berry)

Basic Studies of Irradiation Effects in Fuel Materials

Metals

As a result of theoretical studies, the growth of gas bubbles in a solid under the influence of internal stress gradients and the application of theory to the swelling of alpha uranium under irradiation are discussed by the British.[85] In assessing the growth rates of bubbles in alpha uranium, it is shown that the irradiation processes themselves produce the internal stresses necessary for bubble growth and this process is both temperature and rate dependent. It is demonstrated that, because of the existence of a critical radius for bubble growth, there is an incubation period beyond which bubble growth can quite rapidly lead to a breakaway swelling. A maximum in the stress-enhanced swelling is predicted in the temperature range 400 to 500°C and is shown to be due to the temperature dependence of the internal stresses. Quantitative agreement is found between theory and experiment over a range of temperature and burnup rates.

The production of irradiation damage in alpha uranium has been investigated at Harwell[86] by observing the ejection of atoms from single-crystal and polycrystalline specimens during irradiation with 80-kev Kr^+ ions. Ejection from the single crystals was found to occur preferentially near to the [1 0 0], [1 1 0], and [4 8 7] type directions. This is interpreted in terms of focused-collision sequences traveling along these directions which, on intersecting the surface, cause ejection in the same direction. The possible focusing mechanisms are discussed for each sequence, and an estimate is made of their focusing energies.

Atomic ejection from the polycrystals was measured as a function of temperature. The sputtering

ratio (the average number of atoms ejected per ion) remained effectively constant from room temperature up to about 400°C; however, between 400 and 600°C, an approximately exponential increase was observed. The increase is explained in terms of evaporation from thermal spikes created by the individual bombarding ions, and analysis of the results has provided information as to the spike's size, lifetime, and temperature. In the light of the present results, the spatial distribution of interstitials and vacancies produced in alpha uranium as a result of recoils from direct collisions with fast neutrons is discussed qualitatively. Some of the main conclusions are also appropriate to a better understanding of the damage produced by fission fragments.

In France[87] the thin-layer technique was used to study U–Mo alloys irradiated in the reactor for periods from 3 months to 3 years and cooled for a period of 1 to 2 years after discharge. The experimental techniques and conditions used for following the evolution of the structure of the strongly irradiated materials are described. The results showed that the irradiation of U–Mo alloys in the temperature range from 300 to 450°C leads first of all to the distortion of the gamma lamellae caused by the growth of pseudo-alpha grain. Above an irradiation exposure of 2500 Mwd/ton, all lamellar morphology had disappeared and the material had a new structural state. The mechanisms leading to this state have not been defined.

It has been deduced that the torsion observed in fuel elements irradiated in current United Kingdom power-producing reactors develops from irradiation-induced effects occurring within the uranium bar.[88] The observed rates of torsion can most satisfactorily be accounted for by postulating a slight preferred crystallographic orientation which takes the form of a helix, so that torsion results as a consequence of irradiation growth. The nature and extent of this texture are assessed.

In France[89] measurements of the diffusion coefficients of rare gases in metals, performed either on irradiated materials or on models in which the rare gas was introduced by electric discharge, showed that precipitation of the rare gas during thermal-diffusion treatment interferes considerably with the measurements, producing values of D which are either too high or too low. Models were used to study the different factors affecting the generation and growth of bubbles, i.e., temperature, gas concentration, and number and distribution of crystal defects. The study was carried out by transmission electron microscopy on neutron-irradiated Al–^{6}Li alloys. The diffusion coefficients of ^{133}Xe in irradiated uranium were precisely measured with respect to radiation rates giving rise to very low gas contents. The results show that there is a discontinuity in the diffusion coefficient as the uranium passes from the beta phase to 98 kcal/atom for the gamma phase. Various interpretations of the phenomenon in relation to the mechanisms of rare-gas diffusion are considered.

At Bettis[90] a numerical solution was obtained which gives the morphological changes and kinetics during the coalescence of two spheres by surface diffusion. The solution may be used to determine surface diffusion coefficients by observing the coalescence of two gas bubbles within a solid or to determine interfacial diffusivities by observing the same phenomenon involving spherical precipitates in a solid matrix. The former parameters are of great interest in the fission-gas swelling of nuclear fuels, whereas the latter figure prominently in various transformations in the solid state. The present analysis provides a theoretical framework by which these parameters may be determined under conditions of minimal absorption difficulties, as well as guidelines for applicability of the results.

The equilibrium configuration of inert-gas bubbles attached to precipitates has been discussed by the British.[91] It is shown that the energy gained on attachment in enveloping the interface is exactly equal and opposite to that necessary to create the new equilibrium surface area. The binding energy between the two, therefore, depends only on the work done by the gas on expansion to its new equilibrium volume. The retaining force of precipitates is compared with various bubble driving forces expected to occur in nuclear fuels in an attempt to evaluate the effectiveness of precipitates in controlling swelling and gas release by restricting the motion of bubbles. It is concluded that the precipitate must have a high interfacial tension in order to give adequate control at high burnup.

At Brookhaven[92] the current understanding of the formation of fission-fragment tracks in solids as influenced mainly by electron-microscopic studies is reviewed. The predictions of radiation-damage theories are compared with experimental observations, and certain conclusions are drawn about the permanent effects of fission-fragment interactions with various kinds of solids.

Ceramics

The Germans[93] have measured the diffusion of ^{88}Kr in UO_2 and UC single crystals at integrated irradiation doses of 5×10^{13} neutrons/cm^2. In the case of UO_2, no difference was observed in comparison with ^{133}Xe measurements at integrated fluxes of 2 to 10×10^{16} neutrons/cm^2. UC showed slightly higher D values.

In Japan[94] electron-microscope observations of irradiated epitaxial uranium dioxide films were made in order to examine the effects of factors such as the crystallography and film thickness on fission-fragment-track registration. A transmission electron micrograph of an epitaxial film after irradiation

is shown. The mosaic or island structure of the epitaxial film is considered significant in the registration of the fission-fragment tracks.

(F. A. Rough)

References

1. L. T. Lloyd, R. G. Liptai, and R. J. Friddle, The Effects of High Pressure and Temperature on the Microstructure of Alpha Uranium, *J. Nucl. Mater.*, 19: 173-180 (1966).
2. W. Klement, Jr., A. Jayaraman, and G. C. Kennedy, Phase Transformations in Uranium at High Pressures, *Phys. Rev.*, 129: 1971 (1963).
3. E. Karnikova, M. Holinka, and V. Masarik, Compatibility of Uranium and Beryllium, USAEC Report UCRL-Trans-1303(L) [from *Jad. Energ.*, 9: 277-280 (1963)].
4. E. L. Schaich, The Identification of Inclusions in Uranium Metal by Color Metallography, USAEC Report NLCO-977, National Lead Co. of Ohio, May 1, 1966.
5. D. M. R. Taplin, Preliminary Observations on the Creep Fracture of Alpha Uranium, *J. Brit. Nucl. Energy Soc.*, 5: 153-155 (April 1966).
6. W. H. Chatwin and E. D. Hyam, Grain-Boundary Holes in Irradiated Uranium, British Report TRG-Report-325, May 1, 1962.
7. F. W. Albaugh, S. H. Bash, J. J. Caldwell, D. R. deHalas, and D. C. Worlton, Reactor Fuels and Materials Development Programs for Fuels and Materials Branch of USAEC Division of Reactor Development and Technology, Quarterly Progress Report, April-June 1966, USAEC Report BNWL-CC-761, Battelle-Northwest, August 1966.
8. W. Uhlmann, Radiation Effects on Solid, Uranium-Based Nuclear Fuel Materials. A Bibliography. Vol. 6, No. 1, Swedish Report FTI-16(6.1), May 1966.
9. K. M. Pickwick and W. J. Kitchingham, The $\beta \rightarrow \alpha$ Phase Change in Pure Uranium, *J. Nucl. Mater.*, 19: 109-110 (1966).
10. R. C. Lobb, Density Changes Upon Heat-Treating Unirradiated "Pure" and "Adjusted" Uranium, *J. Nucl. Mater.*, 20: 104-107 (1966).
11. R. Somasundaram and J. Premand, Some Metallographic Observations of Plastic Deformation in Thermally Cycled Uranium, *J. Nucl. Mater.*, 19: 283-289 (1966).
12. D. M. R. Taplin, On the Question of the Grain Size Dependence of the Flow and Fracture Stress in Alpha Uranium, *J. Nucl. Mater.*, 19: 208-209 (1966).
13. R. T. Kato and D. H. Price, Effect of Environmental Conditions on the Pitting of Uranium, USAEC Report NLCO-957, National Lead Co. of Ohio, December 1965.
14. D. A. Howl, The Thermal Conductivity of Springfields Adjusted Uranium in the Temperature Range 160-620°C, *J. Nucl. Mater.*, 19: 9-14 (1966).
15. F. W. Albaugh, S. H. Bush, J. J. Caldwell, D. R. deHalas, and D. C. Worlton, Reactor Fuels and Materials Development Programs for Fuels and Materials Branch of USAEC Division of Reactor Development and Technology, Quarterly Progress Report, January-March 1966, USAEC Report BNWL-CC-694, Battelle-Northwest, May 1966.
16. A. Bar-Or, Pearlitic Reaction in Some Uranium-Chromium Alloys, *J. Inst. Metals*, 94: 214-217 (June 1966).
17. B. A. Hatt, The Orientation Relationships Between Gamma and Alpha Structures in Uranium-Zirconium Alloys, *J. Nucl. Mater.*, 19: 133-141 (1966).
18. J. Chamberlain, M. P. Johnson, J. R. Kench, and A. G. Young, The Influence of Microstructure on the Behavior of Uranium Alloys During Temperature Cycling Creep Experiments, *J. Nucl. Mater.*, 19: 121-132 (1966).
19. D. Lazarevic, The Effect of Small Aluminum Additions on the Structure of Uranium-Molybdenum Alloys, *Tehnika (Belgrade)*, No. 3: 515-519 (1966).
20. D. F. Bowersox, Los Alamos Scientific Laboratory, personal communication, Oct. 12, 1966.
21. D. F. Bowersox and J. A. Leary, The Solubilities of Selected Elements in Liquid Plutonium, Los Alamos Scientific Laboratory:
    a. I. Carbon, USAEC Report LAMS-2832, Dec. 18, 1962.
    b. VIII. Molybdenum, USAEC Report LA-3523, May 24, 1966.
    c. VII. Niobium, USAEC Report LA-3436, Nov. 1, 1965.
    d. VI. Rhenium, USAEC Report LA-3359, June 30, 1965.
    e. V. Revisions to the Tantalum Study, USAEC Report LA-3338, June 7, 1965.
    f. III. Tungsten, USAEC Report LA-3252, Dec. 1, 1964.
22. J. C. Clifford, Behavior of Liquid Pu-Co-Ce Alloys in Contact with Sodium. I. Out-of-Pile Fuel Pin Venting Experiments, USAEC Report LA-3495, Los Alamos Scientific Laboratory, Mar. 15, 1966.
23. R. J. Jackson, R. J. Pinkney, and R. R. McDonald, Measuring Percent Alpha in Delta-Stabilized Plutonium Alloys by X-Ray Techniques, USAEC Report RFP-708, Rocky Flats Division, Dow Chemical Co., June 15, 1966.
24. J. W. Anderson, and R. R. Gilmore, Measurement of Alpha-Phase Plutonium in Plutonium-1 Wt.% Gallium Alloy by Electrical Resistivity, USAEC Report LA-3332, Los Alamos Scientific Laboratory, January 1965.
25. Nuclear Materials and Equipment Corp., Growth of Single Crystals of Plutonium, Progress Report, April 1-June 30, 1966, USAEC Report NUMEC-3428-23, July 20, 1966.
26. M. Rosen, R. G. Peterson, and L. T. Lloyd, The Beta Yields Alpha Transformation in High-Purity Plutonium, USAEC Report ANL-7135, Argonne National Laboratory, February 1966.
27. Argonne National Laboratory, Reactor Development Program Progress Report, June 1966, USAEC Report ANL-7230, p. 10, July 27, 1966.
28. M. H. Rand, D. T. Livey, P. Freschotte, H. Nowotny, K. Seifert, and R. Ferro, Plutonium: Physico-Chemical Properties of Its Compounds and Alloys, *At. Energy Rev.*, 4 (Special Issue 1): 112 pp. (June 1966).
29. N. H. Brett and A. C. Fox, Oxidation Products of Plutonium Dioxide-Uranium Dioxide Solid Solutions in Air at 750°C, *J. Inorg. Nucl. Chem.*, 28: 1191-1203 (May 1966).
30. P. A. Haas, M. H. Lloyd, W. D. Bond, and J. P. McBride, Sol-Gel Process Development and Microsphere Preparation, USAEC Report ORNL-P-2159, Oak Ridge National Laboratory, May 1966.
31. V. Shadden, Chemical Etchant for PuO_2, *J. Nucl. Mater.*, 10: 215 (May 1966).
32. M. S. Farkas, The Preparation and Heat Content of Uranium-, Plutonium-, Neptunium-Containing Microspheres for Use as Intrinsic Thermocouple Flux Probes, USAEC Report BMI-X-10175, Battelle Memorial Institute, July 21, 1966.
33. R. L. Forbes, N. Fuhrman, J. Andersen, and K. Taylor, Study of Uranium-Plutonium Monoxides, USAEC Report UNC-5144 (EURAEC-1566), United Nuclear Corp. and Carborundum Co., Jan. 31, 1966.
34. W. J. Ross, K. N. Puechl, C. S. Caldwell, J. Miles, F. Shipko, and W. C. Judd, Postirradiation Examination of 5 Wt.% PuO_2-UO_2 Fuels, *Trans. Amer. Nucl. Soc.*, 9(1): 40-41 (1966).
35. J. Henney and J. W. S. Jones, Phase Equilibria in the Thorium-Carbon System, *Trans. Brit. Ceram. Soc.*, 65: 207-217 (April 1966).
36. P. Patriarca (Comp.), Oak Ridge National Laboratory, unpublished, February 1966.
37. L. S. Levinson, The Heat Content of Crystal-Bar Thorium, *J. Nucl. Mater.*, 19: 50-52 (1966).
38. Argonne National Laboratory, Reactor Development Program Progress Report, June 1966, USAEC Report ANL-7230, pp. 12-13, July 27, 1966.
39. *Proceedings of the Panel on the Utilization of Thorium*

in Power Reactors, held in Vienna, June 14 to June 18, 1965, International Atomic Energy Agency, Vienna, 1966. Copies are obtainable from the National Agency for International Publications, Inc., 319 E. 34th St., New York 10016.

40. S. Peterson (Comp.), Metals and Ceramics Division Annual Progress Report for Period Ending June 30, 1966, USAEC Report ORNL-3970, pp. 109-111, Oak Ridge National Laboratory, October 1966.
41. B. R. Butcher and B. W. Howlett, The Theoretical Strength of Cermets Containing Spheroidal Ceramic Particles, British Report AERE-M-1728, March 1966.
42. M. Eudier, The Mechanical Properties of Sintered Low-Alloy Steels, *Powder Met.*, No. 9: 278 (1962).
43. L. H. Cope, The Mechanical Properties of Nuclear Cermets, *Metallurgia*, 72: 165-177 (October 1965).
44. R. L. Pilloton, Calculated Densities of Coated Nuclear Fuel Particles, USAEC Report ORNL-TM-1513, Oak Ridge National Laboratory, July 1966.
45. Oak Ridge National Laboratory, unpublished, Aug. 4, 1966.
46. Oak Ridge National Laboratory, unpublished, Sept. 7, 1966.
47. Oak Ridge National Laboratory, Gas-Cooled Reactor Program Semiannual Progress Report for the Period Ending March 31, 1966, USAEC Report ORNL-3951, July 1966.
48. M. E. Smith, J. H. Cappis, and G. R. Waterbury, Leaching of Uranium by Hydrogen Chloride from Pyrolytic-Carbon-Coated Uranium Dicarbide Beads, USAEC Report LA-3488, Los Alamos Scientific Laboratory, Feb. 1, 1966.
49. L. H. Ford, B. E. Ingleby, and N. S. Hibbert, Pyrolytic-Carbon-Coated Uranium Carbide Particles. The Effect of Deposition Conditions on Coating Efficiency, Structure, and Density, British Report TRG-Report-1180, Jan. 24, 1966.
50. R. W. M. D'Eye, Dispersed Ceramic Fuels and the Advanced Gas-Cooled Reactor, British Report TRG-Report-1210, Jan. 5, 1966.
51. F. Lambdin, Nickel Coating of Ceramic Spheroids Using Fine Nickel Powder and Oxide, USAEC Report Y-1538, Union Carbide Corp., Nuclear Division, Y-12 Plant, July 6, 1966.
52. C. S. Luby, Description and Results of the Target P7 Coated Particle Irradiation Capsule, USAEC Report GA-6356, General Atomic Division, General Dynamics Corp., June 22, 1966.
53. C. S. Luby, Description and Results of the Target P8 Coated Particle Irradiation Capsule, USAEC Report GA-6493, General Atomic Division, General Dynamics Corp., June 22, 1966.
54. C. S. Luby, Description and Results of the Target P10 Coated Particle Irradiation Experiment, USAEC Report GA-7171, General Atomic Division, General Dynamics Corp., July 21, 1966.
55. F. R. McQuilkin, J. W. Prados, D. R. Cuneo, E. L. Long, Jr., and J. H. Coobs, An Irradiation Test of AVR Production Fuel Spheres in the Oak Ridge Research Reactor, USAEC Report ORNL-TM-1512, Oak Ridge National Laboratory, June 1966.
56. K. S. B. Rose and D. J. Clough, Fission Gas Release from High Burnup Carbide Fuel Kernels, British Report DP-Report-413, March 1966.
57. H. M. Ferrari, Mechanism and Kinetics of Nitrogen Release from UO_2 at Elevated Temperatures, USAEC Report WCAP-2098, Westinghouse Electric Corp., Atomic Power Division, 1961.
58. R. E. Latta and R. E. Fryxell, Determination of the Melting Point of UO_{2+X}, USAEC Report GE-TM-65-11-8, General Electric Company, Nuclear Materials and Propulsion Operation, Nov. 16, 1965.
59. J. L. Bates, Melting Points of Hypostoichiometric Uranium Dioxide, USAEC Report BNWL-224, Battelle-Northwest, June 1966.
60. E. N. Harbinson and R. J. Walker, Thermal Conductance of ThO_2-10% UO_2 Under Simulated Operating Conditions, *Trans. Amer. Nucl. Soc.*, 9: 26-27 (June 1966).
61. T. A. Gens, Formation of Uranium, Zirconium, and Thorium Oxide Microspheres by Hydrolysis of Droplets, USAEC Report ORNL-TM-1508, Oak Ridge National Laboratory, July 10, 1966.
62. R. G. R. Johnson, Fabrication of Fuel Pellets from Pot-Process Denitrated ThO_2 Powder, USAEC Report WAPD-TM-577, Westinghouse Electric Corp., Bettis Atomic Power Laboratory, July 1966.
63. H. W. Deem (Comp.), Fabrication, Characterization, and Thermal-Property Measurements of ZrO_2-Base Fuels, USAEC Report BMI-1775, Battelle Memorial Institute, June 7, 1966.
64. J. P. Morlevat, Contribution to the Study of the System Uranium-Carbon-Oxygen (Thesis), French Report CEA-R-2857, May 10, 1966.
65. G. Ervin and K. T. Miller, Oriented Growth of Oxidation Products on Single Crystals of Uranium Monocarbide, *Acta Met.*, 14: 222-228 (February 1966).
66. R. Benz and M. G. Bowman, Some Phase Equilibria in the Uranium-Nitrogen System, *J. Amer. Chem. Soc.*, 88: 264-268 (Jan. 20, 1966).
67. D. E. Price, D. P. Moak, W. Chubb, and D. L. Keller, The Compatibility of Uranium Nitride With Potential Cladding Metals, USAEC-Euratom Report BMI-1760 (EURAEC-1591), Battelle Memorial Institute, Feb. 8, 1966.
68. Argonne National Laboratory, Reactor Development Program Progress Report, April 1966, USAEC Report ANL-7204, May 31, 1966.
69. Brookhaven National Laboratory, Nuclear Engineering Department Annual Report, December 31, 1965, USAEC Report BNL-954.
70. A. L. Bowman, Thermal Expansion of UC_2 and U_2C_3, *J. Nucl. Mater.*, 19: 111-112 (1966).
71. C. R. Tottle, Mechanical Properties of Uranium Compounds, USAEC Report ANL-7070, Argonne National Laboratory, November 1965.
72. Argonne National Laboratory, Reactor Development Program Progress Report, March 1966, USAEC Report ANL-7193, Apr. 22, 1966.
73. A. M. Ross and D. H. Rose, Replica Electron Microscopy of Irradiated UC Fuel from Phase 1 of X-721 Experiment, to be published as an AECL report.
74. D. Naumann, W. Heyne, and W. Burk, Production of Spherical Uranium Nitride Particles Using the Fluidized-Bed Technique (in German), *Kernenergie*, 9: 50-54.
75. C. C. H. Wheatley and T. Thorpe, Improvements in or Relating to the Manufacture of Uranium/Zirconium Carbide, British Patent No. 1,023,157, Mar. 23, 1966.
76. S. Imoto and H. J. Stoecker, Preparation of Uranium Mononitride by the Reaction of Uranium Oxide with Carbon and Nitrogen, in Report STI-PUB-109(Vol. 2), pp. 533-545, 1966.
77. R. E. Wilson, C. Barnes, Jr., R. Koonz, and L. Baker, Jr., Isothermal Reaction of Uranium with Steam Between 400 and 1600°C, *Nucl. Sci. Eng.*, 25: 109-115 (1966).
78. L. Baker, Jr., Nonisothermal Reaction of Uranium with Water by the Condenser Discharge Method, *Nucl. Sci. Eng.*, 25: 116-130 (1966).
79. R. O. Ivins, R. C. Liimatainen, and F. J. Testa, Reaction of Uranium with Water as Initiated by a Power Excursion in a Nuclear Reactor (TREAT), *Nucl. Sci. Eng.*, 25: 131-140 (1966).
80. L. Baker, Jr., R. L. Warchal, R. C. Vogel, and M. Kilpatrick, Studies of Metal-Water Reactions at High Temperatures: I. The Condenser Discharge Experiment: Preliminary Results with Zirconium, USAEC Report ANL-6257, Argonne National Laboratory, May 1961.
81. J. J. Stobbs and I. Whittle, The Influence of Impurities on the Oxidation of Uranium in Carbon Dioxide Be-

tween 450 and 650°C, *J. Nucl. Mater.*, 19 (2): 160-168 (May 1966).
82. L. Baker, Jr., and J. D. Bingle, The Kinetics of Oxidation of Uranium Between 300 and 625°C, *J. Nucl. Mater.*, 20 (1): 11-21 (July 1966).
83. L. Baker, Jr., J. G. Schnizlein, and J. D. Bingle, The Ignition of Uranium, *J. Nucl. Mater.*, 20 (1): 22-38 (July 1966).
84. J. G. Schnizlein, L. Baker, Jr., and J. D. Bingle, The Ignition of Binary Alloys of Uranium, *J. Nucl. Mater.*, 20 (1): 39-47 (July 1966).
85. J. W. Harrison, The Growth of Gas Bubbles in a Stressed Medium and the Application to Stress Enhanced Swelling in Alpha Uranium, British Report AERE-R-5229, July 1966.
86. R. S. Nelson, An Investigation of Atomic Collision Sequences and Thermal Spikes in Alpha Uranium, *J. Nucl. Mater.*, 18: 348 (1966).
87. G. Colombe, N. Azam, and J. Lehmann, Observation of Thin Layers of Uranium-Molybdenum Alloys from Irradiated Fuel Element, *J. Nucl. Mater.*, 18: 66-69 (January 1966).
88. M. V. Speight, G. F. Hines, and G. W. Greenwood, On the Origin of Torsional Deformation in Irradiated Uranium-Magnox Fuel Elements, *J. Nucl. Mater.*, 2: 126-129 (April 1966).
89. V. Levy, M. Gerl, B. Perraillon, and Y. Adda, Study of the Diffusion and Precipitation of Rare Gases in Metals, in Report STI-PUB-109 (Vol. 2), pp. 115-132, 1966.
90. F. A. Nichols, Coalescence of Two Spheres by Surface Diffusion, *J. Appl. Phys.*, 37: 2805-2808 (June 1966).
91. R. S. Nelson, On the Binding of Inert Gas Bubbles to Precipitates, *J. Nucl. Mater.*, 19: 149-154 (December 1965); also British Report AERE-R-5056.
92. A. N. Goland, Microscopic Observations of Fission-Fragment Tracks in Solids, USAEC Report BNL-9169, Brookhaven National Laboratory, 1965.
93. Hahn-Meitner-Institut fuer Kernforschung, Diffusion of Rare Gases in Solids, Quarterly Report No. 22, October–December 1965, USAEC–Euratom Report EURAEC-1573, January 1966.
94. S. Nasu, K. Shiozawa, and T. Kikuchi, Fission-Fragment Damage in Epitaxial Film of Uranium Dioxide, *Jap. J. Appl. Phys.*, 5: 248 (March 1966).

Section II

Reactor Materials

Moderator Materials

Graphite

A review has been issued which describes analytical methods that have been adapted or developed by the British[1] primarily for the inspection of nuclear-grade graphite and associated carbon products. The report covers sampling procedure, pitch-testing methods, petroleum–coke testing methods, chemical analytical methods, emission–spectrographic analytical methods, and miscellaneous methods.

Battelle–Northwest[2] has reported a new theoretical approach to the calculation of thermal-expansion coefficients of polycrystalline graphites. Previous analyses of the polycrystalline-expansion behavior have first involved a theoretical calculation of the coefficients of expansion based on crystallite orientation and single-crystal expansion, and then added accommodation factors to account for discrepancies between predicted and experimental expansions. In Battelle's analysis, accommodation is introduced in the initial stages of the theoretical calculations. The resulting good agreement of predicted with experimental expansion coefficients (at 400°C) is illustrated in Fig. II-1. The orientation parameter R corresponds to the effective fraction of crystallites having their c-axes oriented at right angles to the calculated or measured polycrystalline expansion.

The results of an exploratory program on hot-pressing metal–graphite composites at 2800 to 3000°C have been reported by Harada.[3] Ten metal additions were studied: Nb, Hf, Mo, Ta, Zr, Ti, B, Be, U, and Th. Observed bonding was explained by liquid-phase sintering through formation and diffusion of a carbide–carbon eutectic under the hot-pressing conditions and subsequent recrystallization of this phase. The strongest composites produced were in the systems Nb–C, Hf–C, and Mo–C. Compositions containing 50 wt. % (or 6 to 11 at. %) metal exhibited flexural strengths in excess of 10,000 psi, the highest being 16,000 psi for the 50 wt. % Nb–C material processed at 3000°C. This system and a 50 wt. % Hf–C material also processed at 3000°C displayed increases in strength at 2000°C. Intermediate strengths (~5000 psi) were obtained for most of the other systems. Composites incorporating tantalum carbide or thorium carbide had low strengths. The former system did not form liquid at the processing temperature used, and the latter system was subject to failure on cooling owing to dimensional changes accompanying a phase transformation for ThC_2.

(M. C. Brockway)

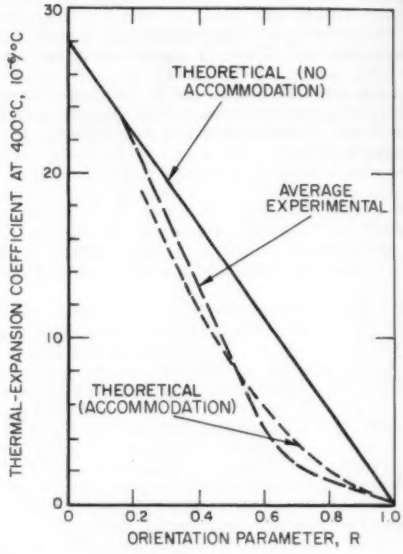

Fig. II-1 Comparison of the theoretical coefficients of thermal expansion at 400°C with average experimental values.[2]

Beryllium and Beryllium Alloys

Test Procedures

The Materials Advisory Board (MAB) Committee on Beryllium Metallurgy has issued a much-needed report[4] to establish standardized methods and procedures for conducting mechanical-property tests on beryllium. Such methods are required because of the characteristics of beryllium that make conventional test procedures difficult. Beryllium generally lacks three-dimensional ductility in sheet, extrusions, and forgings as a result of its extreme plastic anisotropy that develops highly preferred textures. The low ductility of beryllium can lead to premature and

catastrophic failure if it is not recognized and accommodated in design features. Also, surface defects and irregularities that may have little effect on more ductile materials are known to play a definite role in beryllium failures. The contributors to the MAB report have attempted to standardize only the most basic tests where a measure of procedural agreement exists and to present information on the usefulness and limitations of the various tests for the designer, fabricator, and quality inspector.

Specimen preparation and test techniques including alignment procedure and gripping in tension are described. Procedures for tension and three- and four-point bending tests and for measurement of precision elastic limit are presented in detail. Appendixes to the report also provide a good summary of recommended safety practices for handling beryllium.

Beryllium Joining

Brazing beryllium is difficult because of the presence of oxide that inhibits braze-alloy flow. Solar, Division of International Harvester Co., is studying the effect of oxide content of beryllium on flow and wetting of brazing alloys in an argon atmosphere.[5] Preliminary results show that copper and phosphorus are strong flow promoters whereas Cu–Bi, Ta, Li, and Ti promote the usefulness of the Ag–7.5 wt. % Cu braze alloy in a wider range of flow conditions. Titanium appears to be the most powerful promoter of usefulness because it forms a protective beryllide and can counteract the negative effects exerted by germanium, manganese, and indium additions which do not form protective compounds. Beryllium, phosphorus, and lithium appear to reinforce the effect of copper in forming a protective beryllide.

A report containing unclassified information on joining beryllium presented during a meeting held Nov. 30 to Dec. 1, 1965, has now been released.[6] Some of the topics covered were mechanical fastening, diffusion bonding, brazing, and electron-beam welding. Information on mechanical fastening presented by The Brush Beryllium Co. at this meeting emphasizes the sensitivity of beryllium to failure from stress concentrations that are inherent in mechanical joints.

Beryllium Machining

Gun drilling of long precision holes in beryllium was discussed by Dabringhaus.[7] In the case of beryllium, the chip produced is very abrasive and, if recycled through the coolant, can wear the tool unevenly. Thus the feed of the tool per revolution must remain constant so that the chip produced is of a constant size. To accomplish this, the feed is mechanically linked to the machine spindle so that accurate control of the feed is possible. Because of the fineness of the beryllium chip produced, it is necessary to use a special filter in the coolant system. Settling tanks cannot be used since the chips float on the coolant. Two types of parts were machined in this process: (1) a cylindrical part approximately 47 in. long with several longitudinal channels and (2) a part that was a sector of a hollow cylinder. Holes only $^5/_{16}$ in. in diameter were drilled through the entire length of the first part and were accurately sunk through the 51-in. length of the second.

Sandia Corp. reported on investigations conducted to minimize machining damage and thereby provide a process that would allow finishing to close tolerances.[8] It was found that machining conventional beryllium of 30-μ grain size caused surface deformation and twinning, necessitating close control on both the quality of the tools and the rate of metal removal. However, the author notes that control within practical limits is possible by appropriate selection of depths of cut. High-strength fine-grained beryllium did not exhibit as much damage because of the smaller grain size. Therefore etching of only 1 to 2 mils was required to remove the damage; consequently closer tolerances could be held on a finished part.

Powder Metallurgy

Butcher and Lowe reported on the effects of particle-size distribution and chemical composition on the compaction characteristics of three different commercial beryllium powders.[9] It was difficult to vary particle size without affecting purity, but it was found that hot pressability of a powder was a function of chemical composition. Silicon additions markedly increased hot pressability of high-purity powders. Additions of 500 to 750 ppm silicon increased the pressable length-to-diameter ratio from less than 1 to greater than 2. The beneficial effects of silicon additions were restricted to vacuum pressing at temperatures greater than 1050°C.

Physical Metallurgy

The Ti–Be phase diagram up to 10 wt. % beryllium was determined by Hunter using metallographic techniques.[10] Beryllium forms a beta-eutectoid type of diagram with titanium. This occurs at 0.5 wt. % beryllium at 1500°F (816°C). A eutectic is formed at 1887°F (1030°C) which contains between 5 and 7.5 wt. % beryllium. The solubility of beryllium in alpha titanium is less than 0.05 wt. %, whereas the solubility in beta titanium is 1 wt. %.

The Defense Metals Information Center (DMIC) has published a review of the physical metallurgy of beryllium.[11] Work on purification that yielded high-quality single crystals was reported. Basic deformation properties of beryllium have been more clearly defined, and the effects of alloying elements and impurities were discussed. Deformation modes in polycrystalline beryllium were reviewed, on the basis of the results of studies on single crystals. Texture

developed in polycrystalline beryllium by fabrication and the resulting effects on mechanical properties were summarized, as well as fracture modes in single-crystal and polycrystalline beryllium. Bend-plane splitting is the method suggested for initiation of fracture in beryllium. Effects of the distribution of impurities as a result of thermal treatment on the mechanical properties were also cited. Since grain size is an important factor in determining properties, recrystallization and grain-growth phenomena for the different types of beryllium are presented. Commercial products are discussed in terms of physical–metallurgical phenomena that contribute to their observed properties and fabricability.

Irradiation Damage

Fracture surfaces on beryllium, irradiated to integrated exposures in the range of 2.2 to 5.0×10^{21} neutrons/cm^2 (>1 Mev), were examined after rupturing specimens by compression impact testing and by Izod impact testing.[12] Specimens were tested as irradiated and after annealing 2 hr at 600°C. It was concluded that the manner of impact testing had little effect on the fracture surfaces after similar neutron exposures. Helium produced during irradiation migrates to the second-phase inclusions, regardless of the type of inclusion, during postirradiation pretest annealing and, to a lesser extent, during low-temperature irradiation. Annealing caused agglomeration of gas on the grain faces.

General

The MAB has issued a report covering the behavior of beryllium under ballistic impact.[13] Technical presentations centered around the mechanisms of impact fracture in metals. Suggestions for improving the impact behavior included effecting significant decreases in grain size. It was also suggested that the tendency for crack propagation might be reduced by orienting weak fracture-plane poles away from the shock direction. Also considered were the possibilities of turning cracks out of the tensile direction by microstructural barriers and of increasing spall strength by solid-solution alloying. The report, in addition, presents tests currently used for measuring impact properties and summarizes government programs on beryllium.

The DMIC is preparing a special collection of data on the mechanical properties of beryllium. Interested persons can obtain preliminary copies by request.

(H. D. Hanes)

Beryllium Oxide

The practical significance of impurities as they affect sinterability and other properties of beryllia is reviewed by Reeve.[14] The author's observations in regard to sinterability are presented below.

1. Impurity effects—if major cationic impurities are some or all of the elements Na, Si, Al, Mg, Ca, and Fe, the following rules can be of limited use in determining sinterability:
   a. Sodium content is of little importance
   b. Silicon and aluminum contents should be as low as possible
   c. Silicon + aluminum expressed in parts per million should be no higher than (calcium + magnesium + iron)
2. For a powder to be sinterable, it must
   a. Have a surface area of 10 m^2/g or higher
   b. Contain no residual hydroxide
   c. Contain no dense or highly structured aggregates
   d. Be capable of being pressed to ≥1.5 g/cm^3
   e. Have small spread of crystallite sizes

The above observations are particularly applicable to BeO powders similar to commercial-grade UOX.

Solid Hydrides

Lanthanum Hydride

In a study of the La–H system at Ames Laboratory,[15] it was found that the melting point of lanthanum increased with the addition of hydrogen. The addition of hydrogen also decreased the fcc-to-bcc transformation temperature of the metal to a eutectoid at 773°C at a composition of 23.5 at. % hydrogen. The solubility of LaH_2 in the fcc lanthanum metal ranged from 2.83 at. % at 375°C to 21.3 at. % at 773°C. Above 773°C the solubility of LaH_2 in bcc lanthanum was found to increase rapidly, and complete solubility occurred at temperatures above 960°C. The LaH_2 had no appreciable effect on the low-temperature transformation of hcp to fcc lanthanum.

Hydrided U–Zr Alloys

Data on SNAP-4 fuels which were originally compiled in 1961 have now been made generally available. A summary of the physical and mechanical properties of the U–Zr hydrides prepared by Atomics International[16] covers research carried out at several laboratories in addition to their own.

Miscellaneous Alloy Hydrides

The Zr–2.5 wt. % Nb–H system at temperatures below 550°C was studied at Chalk River[17] by measurement of the hydrogen equilibrium pressures as a function of temperature and concentration. The delta + epsilon hydride regions were found to be located at the same H/Zr ratios as in the Zr–H system. The terminal solubility appeared to be af-

fected by supersaturation in the alpha-zirconium phase. It was demonstrated that a metastable state of supersaturation can exist at more than 40 °C below the solubility limit.

The several ways in which hydrogen reacts with alloys and intermetallic compounds were reviewed by Westinghouse Electric Corporation.[18] The thermochemical stability of the alloy relative to that of either zirconium hydride or a new intermetallic hydride was the important factor in analyzing the hydrogen reaction. Thermochemical functions were derived to describe the solid solubility of hydrogen and the first hydrides formed in the individual intermetallic compounds. (H. H. Krause)

References

1. Manual of Analytical Methods for Graphite and Associated Carbonaceous Materials, British Report PG-Report-177(Rev.), 1966.
2. F. W. Albaugh, S. H. Bush, J. J. Caldwell, D. R. DeHalas, and D. C. Worlton, Reactor Fuels and Materials Development Programs for Fuels and Materials Branch of USAEC Division of Reactor Development and Technology, USAEC Report BNWL-CC-694, Battelle–Northwest, May 1966.
3. Y. Harada, Graphite-Metal Carbide Composites, Report NASA-CR-507, Illinois Institute of Technology Research Institute, June 1966.
4. Materials Advisory Board, National Academy of Sciences–National Research Council, Evaluation Test Methods for Beryllium, Report MAB-205-M, March 1966.
5. R. G. Bogowitz and A. G. Metcalf, Beryllium Brazing by Capillary Flow, Progress Report No. 4, April 1–June 30, 1966, Solar, Division of International Harvester Co., July 1966.
6. Materials Advisory Board, National Academy of Sciences–National Research Council, Report of the Committee on Beryllium Metallurgy, Sixth Progress Report, Report MAB-199-M(6), April 1966.
7. G. Dabringhaus, Gun Drilling Long Precision Holes in Beryllium, Paper MR66-185, presented at ASTME 1966 Engineering Conference and Tool Exposition, Detroit, Mich., Apr. 18–22, 1966.
8. D. M. Johnson, Finishing High-Strength Beryllium Pressings, USAEC Report SCL-DC-66-52, Sandia Corp., 1965.
9. J. W. Butcher and J. N. Lowe, Characterization of Beryllium Powder, in *Symposium on Powder Metallurgy*, Paris, June 1964.
10. D. B. Hunter, Titanium–Beryllium Phase Diagram Up to 10 Wt. % Beryllium, *Trans. Met. Soc. AIME*, 236: 900-902 (June 1966).
11. H. D. Hanes, S. W. Porembka, J. B. Melehan, and P. J. Gripshover, Physical Metallurgy of Beryllium, Report DMIC-230, Battelle Memorial Institute, Defense Metals Information Center, June 24, 1966.
12. Phillips Petroleum Company, Nuclear Technology Branches Quarterly Report, October 1–December 31, 1965, USAEC Report IDO-17191, June 1966.
13. Materials Advisory Board, National Academy of Sciences–National Research Council, Report of the Committee on Beryllium Metallurgy, Seventh Progress Report, Report MAB-199-M(7), June 1966.
14. K. D. Reeve, Impurities and Their Effects in Nuclear-Grade Beryllia Powders, Australian Report AAEC-TM-311, January 1966.
15. J. A. Straatmann, Lanthanum-Lanthanum Hydride Phase System, Thesis, Iowa State University of Science and Technology, Ames Laboratory, February 1966.
16. J. D. Watrous, Properties of SNAP-4 Materials, USAEC Report NAA-SR-Memo-6532, Atomics International, June 26, 1961.
17. W. H. Erickson, Hydrogen Solubility in Zirconium Alloys, *Electrochem. Tech.*, 4: 205-211 (May–June 1966).
18. A. Pebler and E. A. Gulbransen, Thermochemical and Structural Aspects of the Reaction of Hydrogen with Alloys and Intermetallic Compounds of Zirconium, *Electrochem. Technol.*, 4: 211-215 (May–June 1966).

Section

III

Reactor Materials

Nuclear Poisons

Metallic Poison Materials

Young's modulus (E) and shear modulus (G) of forged and rolled 0.220-in.-thick hafnium plate, in which the basal planes are strongly oriented parallel to the rolling direction, were found[1] to have the following temperature dependence:

$$E \text{ (long.)} = 20.8 \times 10^6 - 4.5 \times 10^3\, t, \text{ psi}$$

$$E \text{ (trans.)} = 21.4 \times 10^6 - 4.0 \times 10^3\, t, \text{ psi}$$

$$G \text{ (long.)} = 7.7 \times 10^6 - 1.7 \times 10^3\, t, \text{ psi}$$

$$G \text{ (trans.)} = 7.7 \times 10^6 - 1.4 \times 10^3\, t, \text{ psi}$$

where t is in °F. The measurements were carried out between room temperature and 900°F (482°C). Thermal expansions of the rolled hafnium plate from room temperature to 1400°F (760°C) are

$$\Delta L/L \text{ (long.)} = 3.62\ (t - 77) \times 10^{-6}$$

$$\Delta L/L \text{ (trans.)} = 4.20\ (t - 77) \times 10^{-6}$$

$$\Delta L/L \text{ (thickness)} = 4.32\ (t - 77) \times 10^{-6}$$

A Hf–Cr equilibrium phase diagram developed at Ames Laboratory[2] is shown in Fig. III-1. The solubility of chromium in alpha hafnium increases from 0.5 wt.% at room temperature to 3 wt.% at 1340°C. The Fe–Nd equilibrium phase diagram as determined by the Russians[3] is given in Fig. III-2.

Postirradiation examination of the Yankee reactor control rods during the first core life revealed that nickel plating was not effective in preventing oxidation of Ag–15 wt.% In–5 wt.% Cd control rods during reactor operation.[4] However, the oxidation of the control rods was only minor. The control rods operated in 540°F (282°C) water for 13,000 hr with fast-neutron (>0.82 Mev) exposures up to 11×10^{21} neutrons/cm^2. The room-temperature and 600°F (316°C) tensile properties of the control rods were not changed by the irradiation, except that the ductility was reduced somewhat.

A Canadian patent has been issued on a method of fabricating Ag–In–Cd control rods clad with stainless steel.[5] A good core-to-cladding bond is secured by applying a thin coat of copper and a subsequent layer of nickel on the inside of the cladding, and the composite is then heat-treated. (M. Kangilaski)

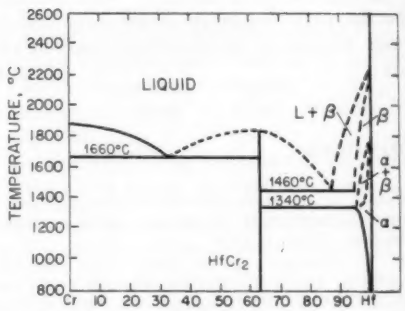

Fig. III-1 Proposed Cr–Hf equilibrium phase diagram.[2]

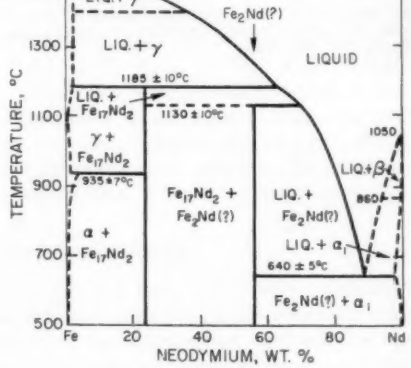

Fig. III-2 Equilibrium phase diagram of the Nd–Fe system.[3]

Dispersion and Nonmetallic Poison Materials

Boron and Boron Compounds

Control plates and end poison plates for the Phoebus II reactor have been developed by workers at Los Alamos[6] from Cu–20, 40, and 50 vol.% normal

B_4C. In a feasibility study the procedure was developed for producing the material in a uniform, dense, stable sheet from which the control and poison plates can be made. Neutron-absorption data show that the Cu–50 vol.% B_4C is equivalent to the Al–20 wt.% ^{10}B control blades previously used.

A Soviet sintering study[7] conducted on ZrB_2 has indicated that grain growth during the early stages of sintering is related to surface-tension forces. When the sintering time exceeds 30 min, subsequent grain growth is due to the diffusion mechanism. The activation energy for grain growth equals 29 ± 10 kcal/mole.

Rare Earths

Dispersions of Dy_2O_3 in nickel have been investigated at General Electric[8] and found to be chemically and metallurgically stable for 8000 hr in an inert atmosphere at 1000 to 1040°C. Dispersions of this type, when clad with Inconel 600, are also stable for periods up to 10,000 hr at 1040°C in contact with reactor-grade graphite in an inert atmosphere. Cladding of Ni–40 wt.% Dy_2O_3 dispersions with Inconel 600 by the high-temperature (1090°C) coextrusion technique was shown to be feasible.

In a study by Hittman Associates[9] on Eu_2O_3: TiO_2 compositions having molar ratios ranging from 1:3 to 1:0.6, it was found that all bodies containing more than 50 mole % TiO_2 have excellent corrosion resistance to water at 596°F (314°C) and 1500 psi. It was also noted that Eu_2O_3–TiO_2 blends are compatible with silicon-bearing stainless steel when sintered as stainless-steel cermets at 1250°C. The cermets also show good corrosion resistance to high-temperature water. Although blends containing less than 2:1 (molar) TiO_2: Eu_2O_3 show decreasing corrosion resistance with decreasing TiO_2 content, all the cermets containing the Eu_2O_3–TiO_2 are superior to high-fired Eu_2O_3–stainless-steel cermets without TiO_2.

(D. E. Lozier)

References

1. D. F. Washburn and F. K. Blechinger, Thermal Expansion and Temperature Dependence of the Elastic Moduli of Polycrystalline Hafnium, USAEC Report KAPL-3112, Knolls Atomic Power Laboratory, Apr. 15, 1966.
2. Ames Laboratory, Annual Summary Research Report of Chemistry, Engineering, Metallurgy, Physics, and Reactor Divisions, July 1, 1965–June 30, 1966, USAEC Report IS-1500, July 1966.
3. V. F. Terekhova, E. V. Maslova, and Y. M. Savitskiy, Iron–Neodymium Equilibrium Diagram, *Izv. Akad. Nauk SSSR, Metal.*, No. 3: 128-130 (May–June 1965).
4. W. R. Smalley and E. Paxson, Engineering and Metallurgical Evaluation of an Irradiated Yankee Core I Control Rod, USAEC Report WCAP-6074, Westinghouse Electric Corporation, Atomic Power Division, July 1966.
5. B. E. Mills, Method of Manufacturing Control Rods for Nuclear Reactors, Canadian Patent 725,771, Jan. 11, 1966.
6. H. Sheinberg and R. W. Keil, Fabrication and Properties of Copper-Boron Carbide Control Material for Phoebus II Reactor, USAEC Report LA-DC-7745, Los Alamos Scientific Laboratory, Mar. 17, 1966.
7. M. A. Kuzenkova and P. S. Kislyi, Increase in ZrB_2 Grains During Sintering, *Porosh. Met., Akad. Nauk Ukr. SSR*, No. 1: 12-16 (January 1966).
8. W. G. Baxter and J. W. Tenhundfeld, A Materials, Fabrication, and Design Feasibility Study for a High-Temperature, Uncooled, Articulating Control Rod, *Trans. Amer. Nucl. Soc.*, 9(1): 12-13 (1966).
9. Hittman Associates, Inc., Low-Enriched PM Replacement Core, Control Materials Metallurgical Evaluation, USAEC Report HIT-3583-24, Apr. 26, 1966.

Section

IV

Reactor Materials

Cladding and Structural Materials

Corrosion

Corrosion of Zirconium Alloys

Nineteen papers on the corrosion of zirconium alloys presented at the October 1965 meeting of the Electrochemical Society have been published in *Electrochemical Technology*.[1] Subject matter covered includes oxidation kinetics, mechanism of film growth, mechanism of breakaway, properties of oxide films, influence of zirconium oxide on hydrogen uptake in the metal, solute distribution in the oxide, transport of oxygen in the oxide film, influence of interstitial impurities on aqueous corrosion, nitriding kinetics, reactions with iodine, corrosion in fused KNO_3–$NaNO_2$–$NaNO_3$, and effects of irradiation on oxidation and hydrogen uptake.

The relation of proof testing of Zircaloy-2 in 400°C steam to long-term corrosion behavior in 400°C steam and in 316°C water has been studied by the British.[2] In 400°C steam it was found that oxidation rates and hydrogen uptake were greater if the specimens were initially covered with water during startup than if they were continuously exposed to steam. It was also found that "poor" quality Zircaloy-2 corroded at higher rates in 100-psi steam at 400°C than in 1500-psi steam at the same temperature.

The contamination by fluorine of pickled and electropolished Zircaloy-2 has been studied in Sweden[3] by radiotracer techniques. The amount of fluorine found on the surface was 0.56 $\mu g/cm^2$ after pickling and 0.26 $\mu g/cm^2$ after electropolishing. After $\frac{1}{2}$ to 1 year of exposure to water at 25 to 350°C, the fluorine content was 0.23 $\mu g/cm^2$ for pickled material and 0.16 $\mu g/cm^2$ for polished material. Most of the fluorine was found in a thin layer near the outer surface of the oxide.

Studies on the air oxidation at 360 to 400°C of single-crystal spheres of zirconium at Oak Ridge National Laboratory[4] have shown that the regions of greatest oxidation can be described as bands connecting (0 0 0 1) with (1 1 $\bar{2}$ 2), (1 1 $\bar{2}$ 2) with (3 1 $\bar{4}$ 4), and (3 1 $\bar{4}$ 4) with (1 0 $\bar{1}$ 0) planes. Similar behavior was observed in steam at 500°C. The oxide pustules that were observed during the steam oxidation were roughly hexagonal columns near (0 0 0 1), were square or rectangular near (1 1 $\bar{2}$ 0), and were first trapezoidal and then kidney shaped in cross section going from (1 1 $\bar{2}$ 0) toward (0 0 0 1).

The measurement of oxide-film thickness by color comparison (visible light) or spectrophotometric techniques (ultraviolet and infrared wavelengths) has recently been reviewed by the British.[5] The theory, practical applications, techniques of measuring, and apparatus were discussed. Also included were plots of the average thickness vs. the wavelength of reflectivity minimums for films on Zircaloy-2 and an appendix on the measurement of films by multiple-beam interference techniques. (W. E. Berry)

Corrosion of Aluminum Alloys

The Defense Metals Information Center (DMIC) has published a report[6] on the stress-corrosion cracking of aluminum alloys. The review includes descriptions of (1) the historical development and growth in awareness of the problem, (2) experimental techniques and test methods, (3) the mechanisms involved, (4) the theory of stress-corrosion cracking, and (5) preventive measures. (W. E. Berry)

Corrosion of Stainless Steels

The stress-corrosion cracking of austenitic stainless steel has been related to dislocation substructure as the result of laboratory studies conducted at Savannah River.[7] The results indicated that dislocations provided a continuous supply of localized anodic regions for selective electrochemical attack; that cracking occurred preferentially on the {1 1 1} family of planes; and that dislocation movement and therefore deformation were required in the cracking process. Suggested methods for reducing stress-corrosion cracking included any process or alloy change that inhibits dislocation movement, promotes cross slip, or reduces the tendency for corrosion.

Oxidation studies on the Fe–Cr–Al–Y alloy system are continuing at General Electric Company.[8] An Fe–25 wt.% Cr–4 wt.% Al–1 wt.% Y alloy has been found to exhibit optimum high-temperature (1100°C) oxidation resistance. However, at temperatures below 520°C, hardening and loss of ductility occur as a result of precipitation of a chromium-rich ferrite phase. When this alloy aged to equilibrium at 450°C, the DBTT (in bending) increased to approximately 110°C. Low-temperature embrittlement was reduced by lowering the chromium content and raising the

aluminum content (optimum composition: Fe–5 wt.% Cr–6 wt.% Al–1 wt.% Y). The lower chromium alloys oxidized more rapidly in steam. However, preoxidation of these alloys in air provided suitable corrosion resistance in steam.

Studies on the corrosion of stainless steels and crud formation in high-temperature water and steam are being continued by the French.[9] A maximum in corrosion and crud-formation rate has been observed between 200 and 250°C in high-temperature water. The oxidation mechanism in this temperature range was shown to consist of two diffusion processes—the migration of anions (oxygen) inward to form a continuous oxide film and the migration of iron ions outward to form ferrous hydroxide.

The structure of oxide films formed on 304 stainless steel in high-temperature water has been studied in Great Britain.[10] Transmission electron microscopy and X-ray diffraction of films after 750 hr of exposure revealed the following:

Water pH	Water temperature, °C	Inner scale (metal oxide)	Outer scale (oxide water)
7	300	Gamma Fe_3O_3	Alpha FeOOH
7	350	Fe_3O_4 + Fe_2SiO_4	(One layer only)
10	300	Fe_3O_4 + Fe_2SiO_4	Alpha FeOOH
10	350	Fe_3O_4	Alpha Fe_2O_3

There were variations in oxide thickness from grain to grain, in addition to localized attack at grain boundaries. (W. E. Berry)

Base Metals and Other Alloys

Intergranular modifications observed in unalloyed nickel in the fluidized-bed-volatility fuel-recovery process have been attributed to contamination from the alumina-bed material, in research performed at Battelle–Columbus.[11] The intergranular modification was found to cause a marked reduction in the ductility and ultimate tensile strength of Nickel 201. Penetrations of 20 mils (from both sides) on 55-mil-thick flat tensile specimens resulted in lowering the room-temperature elongation from 38% to 4% and the ultimate tensile strength from 57,000 psi to 25,000 psi (compared with as-received material).

The oxidation characteristics of 15 lanthanide metals (atomic numbers 57 to 71) have been examined in detail in dry and moist air at 100 to 800°C in studies conducted at Rensselaer Polytechnic Institute.[12] It was found that oxidation in dry air generally proceeded according to linear or parabolic oxidation kinetics. Cerium, erbium, and terbium oxidized catastrophically at high temperatures. Water vapor in the air generally increased the oxidation rates because of the formation of less protective hydroxide films. This effect was less pronounced at high temperatures where water adsorption was retarded.

The corrosion of mild steel in heavy water has been studied at Savannah River.[13] After 3 years in the Heavy Water Components Test Reactor, the steel surfaces were covered uniformly with adherent black oxide, and no significant pitting was observed. The total corrosion of mild-steel test coupons was 5500 mg/dm^2 after 33 months. Iron release to the D_2O moderator was 16 mg/(dm^2)(month) during the first 6 months and 4 mg/(dm^2)(month) thereafter. Particulate matter in the D_2O was about 80 ppb during the first 2 years of operation and about 6 ppb during the last year. (W. E. Berry)

Corrosion of Refractory Metals

UNCOATED REFRACTORY METALS

The Soviets[14] measured the rate of corrosion of rhenium in solutions of sulfuric, hydrochloric, phosphoric, and nitric acids, sodium chloride, potassium hydroxide, hydrogen peroxide, and distilled water at 25 and 100°C. In inorganic acids in the presence of air, the rate of corrosion was less than 0.1 mg/(m^2)(hr) at 25°C, increasing to about 16 mg/(m^2)(hr) at 100°C. In distilled water the corrosion rate was again small at 25°C, increasing to about 50 mg/(m^2)(hr) at 100°C.

The behavior of pure tantalum in a simulated reentry environment was studied by Sandia Corp.[15] The rate of reaction and mass loss was found to be a function of oxygen content of the gas and the square root of the reentry-model stagnation pressure. The reaction products melted at about 1800°C. The test results showed that Ta_2O_5 is not the only reaction product, but rather that tantalum and Ta_2O_5 are melted together to form a composition near "TaO."

COATED REFRACTORY METALS

Gradated intermetallic compound–refractory oxide coatings 4 to 8 mils thick have been used to protect Ta–10 wt.% W from oxidation at temperatures up to 3500°F for 15 min.[16] These coatings were applied with electrophoretic deposition equipment under development at Vitro Laboratories. The best protection was obtained by first applying base coats of $TaSi_2$, WSi_2, and $MoSi_2$. Gradated coatings such as WSi_2/ZrO_2 or WSi_2/Al_2O_3 were then applied and sintered. The density of the sintered coatings was found to be improved by adding a second phase to the oxide component. Typical oxide systems of this type included ZrO_2–2% TiO_2 and Al_2O_3–4% MgO (source does not indicate whether mole % or wt.%). Most coating failures that occurred in these gradated coatings were due to edge or corner defects, and none was observed to occur catastrophically. Studies for further improvement in the density of oxide gradated coatings are in progress.

Sylcor Division, Sylvania Electric Products Inc., described in detail the methods used to scale up

their Sn–Al coating process used for protecting tantalum-base alloys.[17] Tantalum structures 2 by 2 by 3 ft can be processed in Sylcor's specially designed vacuum-diffusion furnace. Improved lacquer-base slurries were developed with excellent stability and low settling characteristics. Parts could be coated by dipping, spraying, or brushing. Runoff of the tin-rich layer during the diffusion step of the coating process, an earlier problem, was effectively eliminated for large part sizes through the use of a single-cycle coating of Sn–27.5 Al–6.9 Mo (presumably by weight). Preliminary results indicate that this particular coating composition has improved resistance to oxidation under high mass-flow conditions. Progress was also made in the area of coating repair. Techniques were developed for stripping and recoating defective or oxidized parts. The effects of coating and processing on distortion were found to be minor.

Solar Division, International Harvester Co., has been able to protect the tantalum-base alloy T-222 from oxidation for up to 600 hr in air at 2400°F (1316°C), using a modified disilicide coating.[18] The coating modifiers, such as titanium and molybdenum, are applied to the surface of the alloy by a slurry coating technique. The slurry is dried and sintered in vacuum. This is followed by a pack-cementation siliconizing operation to produce the desired oxidation-resistant coating.

The results of an evaluation at the University of Dayton of six protective coatings for niobium-base alloys are reported.[19] The six coatings include Pfaudler PFR-32, Boeing Disil, Chromizing Durak KA, LTV Cr–B–Si, TRW Cr–Ti–Si, and Sylcor Ag–Si–Al. These coatings were evaluated on two niobium-base alloys, D43 and C129Y. Methods of evaluation included metallographic analysis, room-temperature tensile tests, bend transition-temperature measurements, cyclic oxidation tests from 1600 to 3000°F (871 to 1649°C), and creep-rupture tests at 2400 to 2800°F (1316 to 1538°C) at stress levels of 6000 to 9000 psi. None of the coating systems could be singled out as being superior to the others in every area of evaluation. Each coating was reported to have one or more serious deficiencies that could restrict its use in particular applications. (J. J. English)

Corrosion by Liquid Metals, Fused Salts, and Organics

CORROSION BY SODIUM

Several years ago at San Jose, it was reported that localized intergranular penetration to a maximum depth of 7 mils was found in one of General Electric's type 316 stainless-steel sodium mass-transfer test loops, after about 25,000 hr of operation at a peak temperature of 1200°F (650°C). Since then similar cases of localized grain-boundary penetration superimposed on general corrosion effects have been encountered. To explain this phenomenon[20] the General Electric workers made a thorough review of published data on basic liquid-metal corrosion and failure analysis, and presented their findings at a conference on large fast power reactors in October 1965.

These data showed that intergranular attack can occur in unstressed metal beneath a layer of Na_2O at room temperature and also in dilute to medium-strength solutions of NaOH at 250 to 300°C in stressed coupons. It was concluded that appropriate conditions existed in the General Electric loops. When a loop was shut down between runs, the internal piping surfaces were subjected to limited atmospheric contamination that resulted in the formation of Na_2O and NaOH. The combination of this highly corrosive film, the high stresses, and increasing temperature during the ensuing preheat cycle caused grain-boundary penetration. However, as soon as the flowing sodium was introduced to equalize temperatures and dissolve or wash away the Na_2O–NaOH film, the attack ceased. Thus the observed penetration must have occurred in steps, increasing slightly at each successive startup.

In the course of a continuing compatibility program, workers at MSA Research Corp. noted[21] that 1200°F (650°C) high-carbon sodium carburized the surfaces of types 304 and 316 stainless steels, producing structural changes and drastic losses in ductility. Subsequent examinations[22] of thin exposed specimens revealed ferrite at the austenitic grain boundaries and coarse carbides within the ferrite phase. These changes occurred in both type 316 and type 304 stainless steel, but were more extensive in the latter. In fact, in the type 304 specimens, ferrite formation and coalescence of carbides continued even after the source of carbon was removed. Application of stresses in the range 8000 to 12,000 psi during the exposures to high-carbon sodium was found to increase the rate of ferrite formation.

In another phase of this program,[23] the effects on type 316 stainless steel of up to 4000 hr of exposure to 1200°F flowing sodium, contaminated with 300 ppm oxygen, were assessed. Mechanical properties of high-oxygen-sodium-exposed specimens were compared with those of similar specimens exposed to air, helium, and low-oxygen sodium. In general, the high-oxygen sodium environment produces more deterioration than the helium environment, but not so much as air. On the basis of tensile, creep, creep-rupture, and impact tests, the most noticeable effect of exposure to a high-oxygen sodium environment is a marked decrease in ductility (though a high-carbon sodium environment is considerably more deleterious in this respect). The ductility of ferritic steels (e.g., 2.25 wt.% Cr–1 wt.% Mo) exposed to high-oxygen sodium is affected in exactly the opposite fashion. Such steels are softened through decarburization and undergo substantial improvements in impact strength.

At Battelle–Northwest[24] parallel and transverse (to the extrusion direction) samples of TSX and TSGBF graphite were heated in sodium-filled stainless-steel capsules for 96 hr at 1000°F (538°C). The temporary violet coloration observed after the samples were removed was postulated to come from a lamellar compound of graphite with sodium. Expansions ranging from 0.44 to 1.02% were measured, the largest expansion occurring in the transverse samples. The surface area of one of the transverse TSX samples was measured after removal of the residual sodium by vacuum distillation and found to be essentially unchanged from the pretest surface area, indicating that the small cracks noted after sodium exposure were not causing much increase in available surface area.

A paper study was carried out at Los Alamos Scientific Laboratory[25] to evaluate the possibility of destructive hydriding of tantalum capsules in the sodium coolant of a fast reactor test facility operating at 500 to 600°C. Problems with hydriding of the zirconium cladding on the original fuel elements in the Enrico Fermi Fast Breeder Reactor demonstrated that hydrogen can find its way into large sodium systems, in spite of precautions to avoid contamination. In fact, the Los Alamos study indicated that there may be up to 40 ppm of dissolved hydrogen in equilibrium with tantalum when operating with sodium cold trapped at 125°C and over 1000 ppm when the cold-trap temperature is 300°C. The hydrogen could stem from accidental entry of moisture, air, or hydrocarbons. It would take only 180 g of hydrogen in the whole reactor to contaminate all the tantalum to 1000 ppm hydrogen. This much would certainly embrittle the tantalum at room temperature, though its effect at 500 to 600°C is not known. In spite of the extrapolations and assumptions made in arriving at the above, it appears that continuous cold trapping at 150°C or lower is desirable to minimize hydriding in the Los Alamos facility.

The seriousness of "sodium logging" of oxide fuels (ingress into the hot fuel matrix through cladding defects or vents) is being investigated by General Electric at San Jose.[26] To determine whether vaporization of the sodium would cause damaging pressure transients, "sodium-logged" urania and urania–plutonia specimens were cycled in-pile up to eight times from 0 to 125% of full power in less than 3 sec without catastrophic results. In fact, the presence of the sodium caused a marked reduction in fuel temperatures. The mixed-oxide specimens showed evidence of incipient interaction with the sodium after these short in-pile tests, whereas the urania specimens were unaffected.

Out-of-pile capsule exposures of $(Pu,U)O_{2+x}$ specimens to sodium and NaK-78 (78 wt.% potassium) at 750°C for 150 hr, gave the following indications:

1. Sodium and NaK have a very similar effect on fuel.

2. Hyperstoichiometric fuel (O/M = 2.04) was chemically reduced by the coolant. The pellets were disintegrated into powder after coolant extraction.

3. Stoichiometric and hypostoichiometric fuels (O/M = 1.97) are not reduced chemically by the coolant. However, some swelling and surface cracking occurred, particularly in fuel pellets with low density.

CORROSION BY POTASSIUM

The effect of oxygen on corrosion in the Nb–K system was studied at Oak Ridge[27] by analyzing oxygen-doped niobium specimens after various periods of exposure in potassium at 1000 and 1250°C, with the following results:

Exposure, hr	0	0.5	1	2	5	16	100
Oxygen, ppm (1000°C)	2600		500	250	150	160	140
Oxygen, ppm (1250°C)	3300	230	190		180	170	180

Apparent steady state was reached more rapidly at the higher temperature. The niobium specimens lost about twice the weight of the oxygen transferred, indicating that niobium was being absorbed by the potassium along with the oxygen. Pre-steady-state hardness gradients in the 1000°C specimens indicate that the oxygen migration is controlled by solid-state diffusion.

In some contemplated applications of potassium as a heat-transfer medium or working fluid, it is desired to use type 316 stainless steel as the containment material and to have a Nb–1 wt.% Zr alloy also present in the system. Workers at the Allison Division of General Motors Corp. have been conducting bimetallic loop experiments in the 1200 to 1500°F (650 to 815°C) range for times up to 8000 hr to define design limits for these materials. The following observations were made:[28]

1. Type 316 stainless-steel samples obtained from 1200°F regions of loops after 2013, 3016, and 8006 hr contained predominantly $Cr_{23}C_6$ phase and some chi phase; in material exposed to 1500°F potassium, the amount of $Cr_{23}C_6$ decreased with respect to chi phase as exposure time increased.

2. The rupture life of type 316 stainless steel at 4750-psi stress is reduced by a factor of about 2 (from ~1000 to ~500 hr) by 8006 hr of exposure at 1500°F in a dynamic potassium system containing Nb–1 wt.% Zr inserts.

3. Nitrogen diffuses inward from the air through the type 316 stainless-steel heat-exchanger tubing and produces a continuously increasing nitrogen content in the niobium alloy, its diffusion rate into the latter being high enough to cause the whole cross section to be affected at 6000 hr.

4. Carbon migrates from the stainless steel, but its low diffusion rate into Nb–1 wt.% Zr inhibits

carburization of the latter beyond a protective reaction layer on the surface.

5. Inserts of Nb–1 wt.% Zr lose weight in accordance with the temperature and oxygen level in the potassium.

6. The oxygen pickup in the Nb–1 wt.% Zr inserts is continuous, being still measurable after 8006 hr; the rate of pickup as a function of time suggests that the oxygen stems from a large source that is being slowly exhausted.

In a basic study related to compatibility, the Soviets[29] measured the diffusion of potassium in molybdenum at 800 to 1100°C by traverses of the ^{42}K radioactivity in samples sectioned after exposure. Diffusion coefficients followed the Arrhenius equation

$$D = D_0 \exp\ (-Q/RT)$$

with the following constants:

Type of molybdenum	Single crystal	Polycrystalline
D_0, cm²/sec	9.34×10^{-3}	2.86×10^{-10}
Activation energy (Q), cal/mole	26,500	14,600

In the range of test temperatures, the D values for potassium in polycrystalline molybdenum were substantially higher than in monocrystalline material, the difference decreasing with increasing temperature.

CORROSION BY LITHIUM

Capsule studies at Argonne National Laboratory of tantalum in 1200°C lithium showed that tantalum specimens resist attack much better in molybdenum capsules than they do in tantalum capsules. Further improvement is effected by the addition of 1.6 at.% silicon to the lithium, presumably through the formation of $MoSiO_2$ as an oxidation barrier.[30] A 2.5 at.% yttrium addition, on the other hand, accelerates the corrosive attack of the tantalum, as does a 3.4 at.% sodium addition (eutectic composition) to the lithium in a tantalum capsule.[31]

Because of the strong tendency for lithium to form carbides, unclad graphite is not considered suitable for use in contact with lithium liquid or vapor. Along these lines, French investigators[32] used X-ray diffraction to identify the compounds LiC_6 (yellow), LiC_{18} (purple), LiC_{28} (blue), LiC_{36} (blue-black), and LiC_{72} (black), which formed when graphite was exposed to an atmosphere of lithium vapor.

CORROSION AND EROSION BY Pb–Bi ALLOY

A low-carbon-steel thermal-convection loop containing Pb–Bi with no additives was operated by the Canadians[33] at a maximum temperature of 450°C and a differential of at least 125°C for 1688 hr before the flow was halted by mass-transfer deposits on the walls in the cold leg. In spinner tests to study velocity effects, a Zircaloy-2 disk was seriously damaged after spinning in liquid lead–bismuth for 7 hr, whereas a similar disk protected by a layer of zirconium oxide showed no damage after 64 hr (presumably at 450°C).

At the University of Michigan, a program is under way to study cavitation in a Pb–30 wt.% Bi alloy at 500 and 1500°F (260 and 816°C) in mercury at 70 and 500°F (21 and 260°C) and in water at 70°F (21°C) with a variety of containment materials.[34,35] Ultrasonic-induced cavitation produced penetration that increased linearly with time, the slope depending on both temperature and material. Figure IV-1 shows a typical set of curves for various alloys in lead–bismuth under cavitating conditions at 1500°F. Some conclusions from this study are:

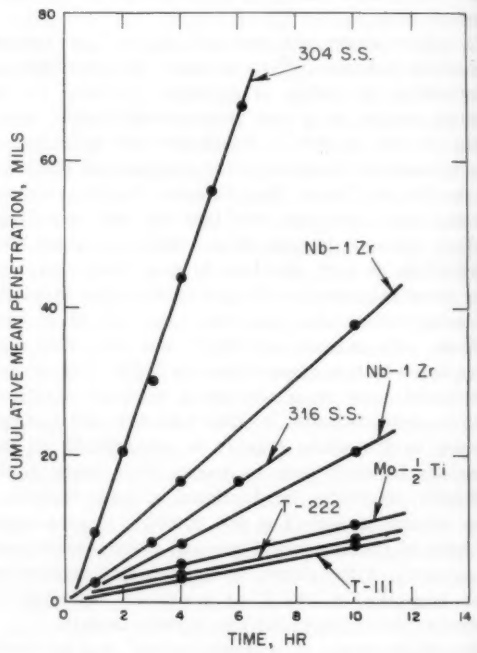

Fig. IV-1 Cavitation damage to various alloys at 1500°F (816°C) in Pb–Bi alloy.[34]

1. The tantalum-base alloys tested were the most cavitation resistant in all tests except in mercury at 70°F, where the stainless steels were the most resistant.

2. All materials tested in lead–bismuth and mercury sustained greater damage at the higher temperature, with the exception of carbon steel.

3. Corrosion effects were essentially nil in these short-duration (10 hr, maximum) cavitation tests.

4. Damage rates in mercury were 3 to 20 times those in water, depending on the material.

5. Good correlations of the Pb–Bi cavitation data were obtained for relating the average rate of penetration to the strength and energy properties of the materials, though more data are needed to ascertain the optimum predicting equation.

CORROSION BY ORGANIC COOLANTS

The WR-1 reactor in Canada is a heavy-water-moderated pressure-tube type, fueled with UO_2 clad in Zr–2.5 wt.% Nb alloy and cooled with HB-40, a partially hydrogenated terphenyl. The choice of fuel cladding and pressure-tube material is interesting, in view of the fact that early U. S. experiments showed that zirconium alloys hydrided, embrittled, and disintegrated in a matter of hours in a high-temperature organic-liquid environment. The secret, according to the Canadians,[36] lies in stringent control of the chlorine and water contents of the organic coolant.

Chlorine, which forms HCl and causes severe hydriding of zirconium, must be held to below 2 ppm (in WR-1 it has been maintained consistently below 0.5 ppm). Water (about 100 ppm in the coolant) has been found essential for the retention of the protective action of the ZrO_2 film against the ingress of hydrogen. It is not known whether the beneficial effects of water stem from replenishment of ZrO_2 lost by dissolution in the metal or from healing of cracks in the ZrO_2 film.

The most effective alloys to date are Zircaloy-4 and Zr–2.5 wt.% Nb. Data on hydriding rates are shown in Fig. IV-2. It is expected that low-temperature (below about 400 °C) hydriding would be increased by a factor of 2 or 3 in the presence of radiation, whereas annealing prevents the irradiation from having much effect at 480 °C.

CORROSION BY MOLTEN FUELS

Refractory alloys are being tested at Los Alamos[37] as possible container materials for molten plutonium-alloy fuels. Although the service temperatures will be below 750 °C, some capsules were tested at 900 to 1200 °C to obtain accelerated corrosion data on various fuel–container combinations. For example, four tantalum capsules containing 6.2 g/cm^3 Pu–Co–Ce alloy showed no evidence of penetration by the plutonium component after 1420 hr at 1100 °C, including four melt–freeze cycles. On the other hand, plutonium was detected on the external surfaces of three plutonium-filled internally carburized Ta–5 wt.% W alloy capsules after 288, 465, and 460 hr at 1000 °C. The purpose of the carburization was to block plutonium migration by precipitating carbides in the grain boundaries. On the basis of similar capsule tests, carburized Nb–10 wt.% W offers promise as a container for Pu–Co–Ce fuels with low plutonium concentrations.

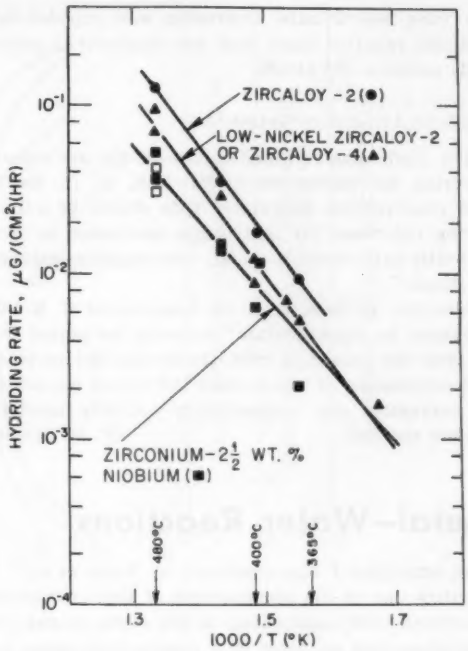

Fig. IV-2 Hydriding of zirconium alloys in organic coolant.[36] Open points are irradiation data; others are data from ex-pile tests.

Capsule experiments up to 10,500-hr duration at 750 and 850 °C led to the following conclusions:

1. Tantalum is more resistant to penetration by molten Pu–Co–Ce fuels than is Ta–10 wt.% W, though Ta–5 wt.% W has mechanical properties that are superior to those of tantalum.

2. Carburized containers are superior to uncarburized containers.

3. Yttrium additions to the container alloy are beneficial.

4. Corrosion is only slightly worse at 850 than at 750 °C.

5. There is little difference between the corrosiveness of a Pu–Co–Ce fuel containing 6 g/cm^3 of plutonium and that of an 8 g/cm^3 plutonium fuel.

Los Alamos investigators[37] are having little success in their search for a container material that will be inert to molten uranium at 2000 °C to enable them to study the effects of oxygen on vapor pressure of uranium. Thoria reacts extensively at 2000 °C, and ZrB_2 reacts at 1800 °C. The best material found so far is metallic tungsten, although its solubility is high in 2000 °C uranium.

Static, isothermal exposures for up to 84 days were performed at Los Alamos[38] with molten UCl_3–KCl eutectic in containers of Hastelloy N, Inconel 600, and HYMU-80 at 900 °C. The maximum penetration in

any case was 2 mils. Corrosion was impeded by a metallic reaction layer that was analyzed as principally uranium and nickel.

REVIEWS AND BIBLIOGRAPHIES

The DMIC has released a state-of-the-art report[39] covering the interaction of Na, NaK, K, Li, and Cs with construction materials. This should be a time-saving reference for individuals interested in compatibility data on alkali-metal–structural-metal combinations.

Attention is directed to an unannotated U. K. bibliography on liquid metals[40] covering the period 1958 to 1963 and issued in 1966. It contains 884 unclassified references, of which about 150 are on the subject of corrosion and compatibility — mostly involving sodium and NaK. (E. M. Simons)

Metal–Water Reactions

An experiment was conducted by Kubit et al.[41] to simulate one of the combinations of physicochemical conditions that could occur in the early stages of a loss-of-coolant accident in a pressurized-water reactor. The tests were conducted in an autoclave in 150-psi, 600°F (316°C) steam by internally heating 0.43-in.-diameter Zircaloy tubular specimens using Pt–Rh alloy resistance windings. The experimental assembly simulates the effect of thermal radiation from adjoining fuel elements in an actual reactor by means of two concentric, slotted, gold-plated reflecting shields surrounding each test specimen. The temperature transient at various positions on each specimen was followed by means of thermocouples tack-welded to the outer cladding surface. The results of this investigation indicate that the extent of the reaction is very small, about 0.03% at 1550°F (843°C) and 0.2 to 0.3% in a transient reaching a cladding temperature of 1750°F (954°C). The data also show that the heat-transfer conditions were adequate to dissipate a large portion of the heat of reaction, thus avoiding an autocatalytic effect that would otherwise lead to a very rapid temperature increase and acceleration of the metal–water reactions.

Battelle–Columbus researchers[42] report the development of a model for describing analytically the extent of a metal–water reaction that would occur during a loss-of-coolant accident. This technique was applied specifically to the zirconium–steam reaction and constitutes an extension of the work of previous investigators.[43] This model may be applied to any fuel-cladding material, provided the appropriate oxidation kinetics are available. The model is predicated upon the assumption that two broad types of rate-limiting phenomena can represent the mechanism for the oxidation of zirconium under accident conditions: (1) the gas-phase diffusion of steam from the bulk stream toward the cladding surface and (2) the solid-state diffusion of various ionic species through the zirconium dioxide product into the base metal, quantitatively expressed as the parabolic rate law. The core is segregated into 10 equal volume regions or radial core zones. Within each region one representative pin is selected, and a detailed analysis of the ensuing metal–water reaction is performed.

Figure IV-3 demonstrates the applicability of the model when applied to the LOFT reactor. Figure IV-3 presents a plot of the cladding surface temperature as a function of accident time at the core midplane for the "hottest" and "coldest" pins of the 10-pin representation. For comparison purposes, curves are also presented showing the thermal behavior under the same conditions, but with no metal–water reaction, and with an unlimited quantity of steam available for reaction (dashed curve). The model indicates two definite regimes of behavior, reflected by the curvature reversal at 75 sec for the hottest pin and at 315 sec for the coldest pin (the times are marked by vertical bars). Figure IV-4 illustrates that the reaction rate is controlled by the cladding surface temperature at times up to 145 sec since it rises exponentially with the cladding temperature and is inversely proportional to the thickness of cladding reacted. However, at 145 sec the steam in the channel is depleted such that the reaction rate is limited by the quantity of steam that can be transported to the surface. This amount is proportional to the steam concentration that continues to decrease, but at a slower rate. It is important to note that, even though the point considered was at the midplane of the

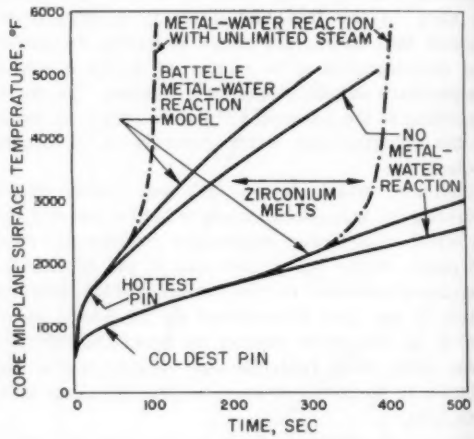

Fig. IV-3 Temperature histories that illustrate the effects of metal–water reactions (LOFT top-break accident with 2000 lb of water remaining).[42] Thermal radiation and meltdown are not considered.

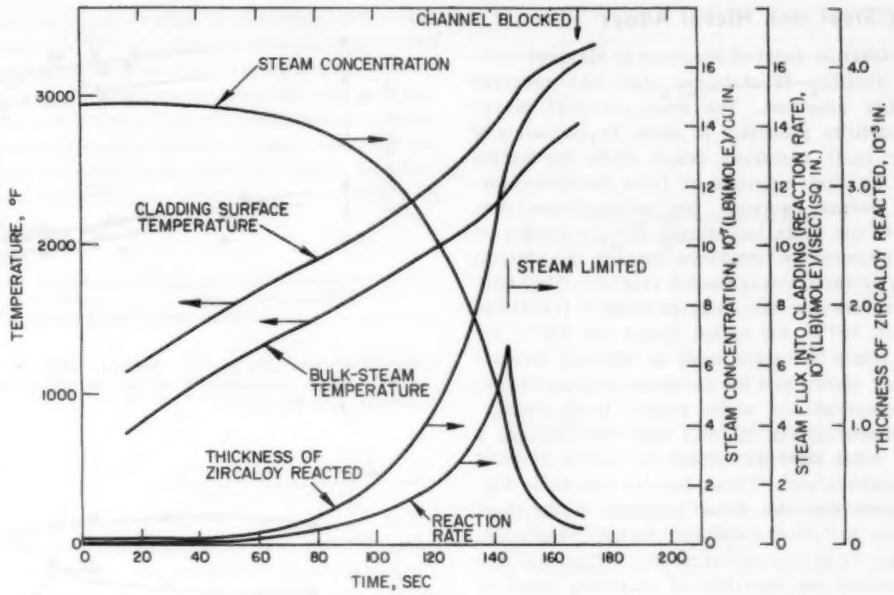

Fig. IV-4 History of metal–water reaction variables in LOFT central core zone near midplane.[42]

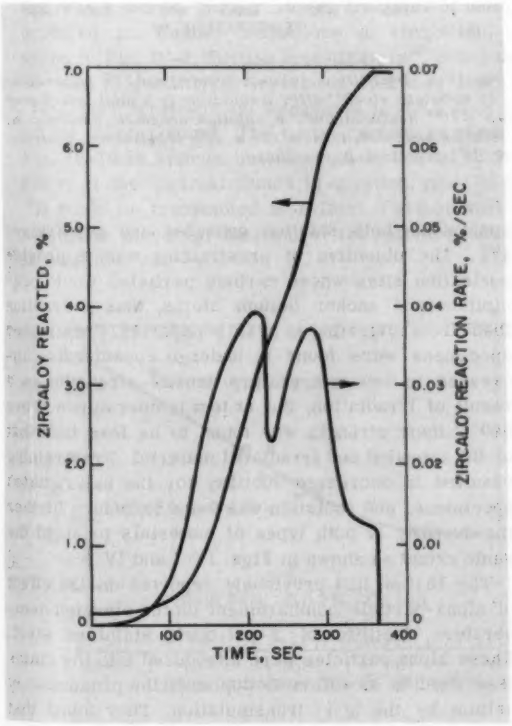

Fig. IV-5 Fraction of cladding reacted and reaction rate for LOFT.[42]

central core zone, i.e., the hottest regions, the additional temperature rise resulting from the metal–water reaction is only of the order of 400 °F (204 °C). Figure IV-5 shows the overall rate of metal–water reaction for the entire core and the accumulation of reacted material. The maximum rate of reaction predicted by this model is 0.04%/sec, or approximately 0.008 (lb)(mole)/sec of hydrogen evolved. This corresponds to a 48% hydrogen–52% steam mixture leaving the core. At approximately 360 sec the final radial core zone is blocked because of cladding melting and fuel displacement, and the total quantity of Zircaloy reacted reaches a plateau, namely, 6.9%.

(J. M. Genco)

Radiation Effects in Structural Materials

A number of excellent papers on irradiation effects in structural materials were presented at the 69th annual meeting of the American Society for Testing and Materials (ASTM) in Atlantic City, N. J., June 27 to July 1, 1966. These papers will be published in a book form as an ASTM Special Technical Publication in early 1967. These papers summarize most of the work which has been performed during the past year and much of the information presented has already been reviewed in previous issues of this Review. However, the new developments that were presented are discussed below.

Stainless Steel and Nickel Alloys

The irradiation-induced decrease in elevated-temperature ductility of stainless steel has received considerable attention. The most accepted theory for this ductility reduction is based on formation of helium by (n,α) reactions either from the matrix materials by fast neutrons or from the boron impurity by thermal neutrons. The helium formed then migrates to the grain boundaries and, on testing at elevated temperature, produces bubbles of a critical size which promote intergranular fracture. The critical temperature for this embrittlement in irradiated material is 550°C for nickel alloys and 600°C for stainless steels.[44] Recent work by German investigators[45] has shown that the decrease in elongation at elevated temperatures, which results from irradiation, is dependent on thermal flux and reaches a saturation value after integrated exposures of about 3×10^{20} neutrons/cm^2. These results (shown in Fig. IV-6) suggest that the boron impurity is the main cause of the irradiation-induced ductility decrease. Data in Fig. IV-6 also illustrate that epithermal flux also decreases the ductility of stainless steel at 750°C, although the effect is not so pronounced as that of thermal flux.

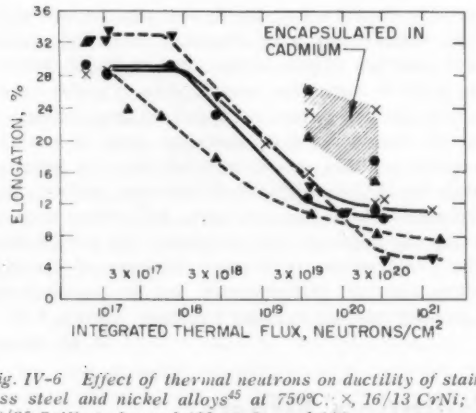

Fig. IV-6 Effect of thermal neutrons on ductility of stainless steel and nickel alloys[45] at 750°C. ×, 16/13 CrNi; ●, 20/25 CrNi; ▲, Inconel 625; ▼, Inconel 600.

British investigators have shown that the elongation at elevated temperatures is also reduced by a purely fast-neutron flux[46a] but that the reduction is not so severe as that caused by thermal flux. The effect of fast flux on elongation is shown in Fig. IV-7, and Fig. IV-8 illustrates the loss of ductility with increasing test temperature. Addition of 1 wt% niobium to type 316 stainless steel improved the ductility of the irradiated material at elevated temperatures. This is attributed to a fine NbC phase at the grain boundaries which acts as a barrier in preventing the migration of helium and subsequent bubble formation at grain boundaries. Tensile tests were performed on

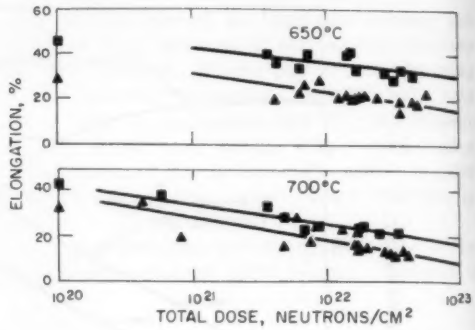

Fig. IV-7 Ductility of 316 stainless steel at 650°C and 700°C after irradiation[46a] at 250 to 350°C. ■, solution treated; ▲, prestrained.

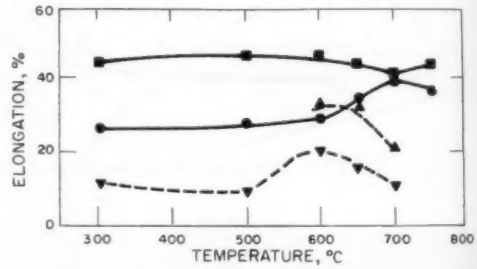

Fig. IV-8 Ductility of solution-treated and 17% prestrained 316 stainless steel[46a] after irradiation to a total fast flux of 3.6×10^{22} neutrons/cm^2. ■, solution annealed, controls; ▲, solution annealed, irradiated; ●, 17% prestrained, controls; ▼, 17% prestrained, irradiated.

specimens both solution annealed and prestrained 17%. The objective of prestraining was to provide nucleation sites where carbide particles would precipitate and anchor helium atoms, thus preventing them from migrating to grain boundaries. Prestrained specimens were found to undergo considerable increases in low-temperature tensile strengths as a result of irradiation, but at test temperatures above 600°C their strength was found to be less than that of the annealed and irradiated material. Prestraining resulted in decreased ductility for the unirradiated specimens, and radiation was found to reduce further the ductility of both types of materials to about the same extent as shown in Figs. IV-7 and IV-8.

The British had previously reported on the effect of alpha-particle bombardment on the elevated-temperature ductility of 2-mil-thick stainless steel. These alpha particles were introduced into the stainless steel in an effort to duplicate the production of helium by the (n,α) transmutation. They found that ductility was reduced as a function of helium concentration. However, they had used monoenergetic alpha particles which resulted in the helium being

distributed in a narrow band, thus setting up possible stress raisers. Further studies have been conducted by using alpha particles with varying energies which have resulted in a relatively even helium distribution.[47] The latter studies show a reduction in ductility, although the reduction is not so severe as that reported for monoenergetic alpha particles. Results[47] of both alpha-particle irradiations are shown in Table IV-1.

Table IV-1 EFFECT OF ALPHA-PARTICLE IRRADIATION ON THE DUCTILITY AT 750°C OF AN AUSTENITIC STEEL[47]

Calculated helium concentration, at.%	Elongation, %	
	Earlier irradiations (Cast N158)	Present irradiations (Cast N348)
	54.5	62.3
10^{-5}	26.1	59.5
10^{-4}		40.5
10^{-3}	14.8	21.8

In other studies attempts have been made to equate helium production with decreases in elevated-temperature ductility in irradiated materials. Workers at Oak Ridge[46b] found that significant reductions in elongation were caused by increases in helium concentration until a concentration of 10^{-7} atomic fraction was reached. Higher atomic fractions of helium produced no further reductions in elongation, as shown in Fig. IV-9. British investigators[46c] noted that the loss of ductility in irradiated stainless steel at 750°C was dependent on integrated neutron flux but not on boron content. The boron content as given in Fig. IV-10 is approximately equal to helium content since, at the thermal fluxes in question, most of the ^{10}B would be transmuted to helium. Further work to determine the exact location of the helium produced is needed.

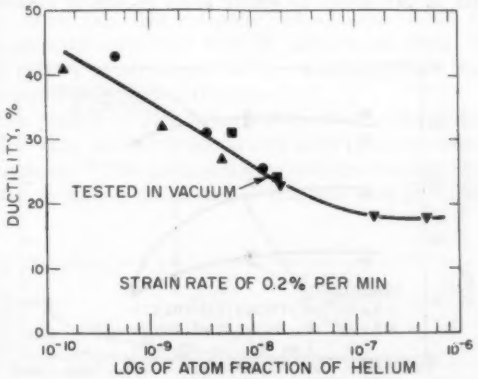

Fig. IV-9 Irradiation embrittlement of boron stainless steels at 700°C as a function of total helium content.[46b] Boron content: ▲, 15 ppb; ●, 110 ppb; ■, 150 ppb; ▼, 3900 ppb.

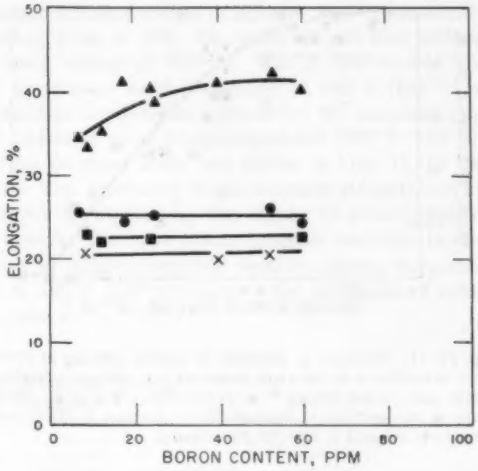

Fig. IV-10 Effects of thermal-neutron irradiation at 45°C on the elongation to fracture at 750°C of solution-treated 18-10-Nb austenitic steel as a function of boron content.[46c] ▲, unirradiated; ●, 1.5×10^{20} neutrons/cm²; ■, 5.0×10^{20} neutrons/cm²; ×, 1.4×10^{20} neutrons/cm².

The mechanism of helium-bubble formation in irradiated stainless steel has been described.[46d] This theory states that a critical helium-bubble size, stress, and elevated temperature are necessary for a helium bubble to grow and migrate to grain boundaries. The stress and strain rates are the most important factors in governing the helium movement. Results of electron-microscopy studies on the size and distribution of helium bubbles after various radiation exposures and postirradiation anneals are discussed. German investigators have developed a mathematical relation that enables one to predict the irradiation-induced decrease in elongation at elevated temperatures as a function of helium-bubble distribution.[48] The theoretical curve has been found to apply to all irradiated stainless steels and nickel alloys as shown in Fig. IV-11. The relative elongation in Fig. IV-11 is defined as

(Unirradiated elongation − irradiated elongation) × (unirradiated elongation − minimum elongation at saturation as illustrated in Fig. IV-6)$^{-1}$ × 100

Workers at Oak Ridge have attempted to improve the elevated-temperature ductility of irradiated stainless steel.[4] Stress-rupture tests were performed on specimens of 304 stainless steel which represented three different microstructures. One set of specimens had a fine grain size (ASTM-9), and the two other sets had coarse grain sizes (ASTM-5). Some of the coarse-grain-sized specimens had been heat-treated (1 hr at 1036°C and 100 hr at 800°C) to promote spheroidization of the carbide particles at the

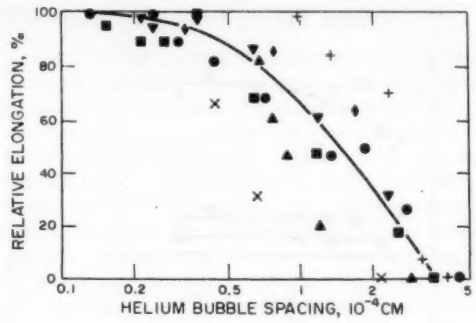

Fig. IV-11 Relation of ductility to bubble spacing at 750°C after irradiation by thermal neutrons for various stainless steels and nickel alloys.[48] ■, 16/13 NiCr; ▼ and ▲, 20/25 CrNi; ●, Inconel 600; ×, Inconel 625; +, Inconel X 750 (2 ppm boron); ♦, Inconel X 750 (50 ppm boron).

grain boundaries. Results of the 650°C stress-rupture tests on irradiated specimens (given in Table IV-2) illustrate the better properties of the fine-grained material and the improvement in ductility imparted by the spheroidizing treatment on the coarse-grained material. The improvement in ductility is attributed to: (1) high adherence between the matrix and the carbide particles and (2) suppression of crack formation by grain-boundary migration.

Table IV-2 VARIATION OF STRESS RUPTURE AND DUCTILITY OF IRRADIATED* 304 STAINLESS STEEL AT 650°C WITH GRAIN SIZE AND PRETEST HEAT-TREATMENT[4]

Stress, 1000 psi	Time to rupture, hr			Total elongation at fracture, %		
	Fine grain	Coarse grain	Aged, coarse grain	Fine grain	Coarse grain	Aged, coarse grain
30	11.3	1.5	14.8	44.0	11.4	24.2
25	79.0	5.5	50.8	29.5	9.0	25.1
20	191.0	109.5	664.1	17.2	3.8	14.3
15	514.4	194.4	3638.0	9.2	3.5	7.8

*Irradiated to exposure of 9×10^{20} neutrons/cm^2 (>1 Mev) and 7×10^{20} neutrons/cm^2 (thermal).

Further research at Oak Ridge shows that the maximum amount of irradiation hardening in 304 stainless steel occurs when the material is irradiated at 100 to 300°C.[49] The maximum increase in room-temperature ultimate and yield strength was found to occur at an irradiation temperature of 150°C, whereas the minimum ductility occurred at an irradiation temperature of 300°C (Fig. IV-12). Irradiation above 343°C resulted in considerable decrease in yield strength and increase in ductility when compared with values for these properties for material irradiated at lower temperatures. These results are explained in terms of defect clusters that were not observed at irradiation temperatures of 371°C and higher. The maximum strengthening caused by irradiation at 150°C is attributed to the critical size and distribution of these defect clusters.

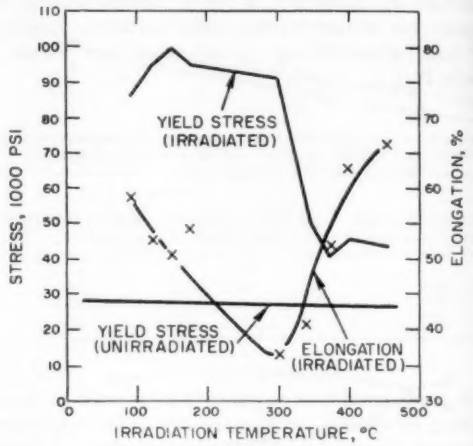

Fig. IV-12 Room-temperature tensile properties of 304 stainless steel as a function of irradiation temperature. Specimens were irradiated to a fast-neutron exposure of 7×10^{20} neutrons/cm^2.

It had previously been shown[50] that the elevated-temperature tensile properties of irradiated stainless steel were not dependent on irradiation temperatures up to 700°C. Further studies have been performed on specimens irradiated at 700, 800, and 900°C. Another variable in these tests was the carbon content which was 0.02 wt.% in one set of specimens and 0.06 wt.% in the other. The tensile-test results at 650°C (Fig. IV-13) show that the ductility decreases with increasing irradiation temperature. This is attributed to either grain growth or possible

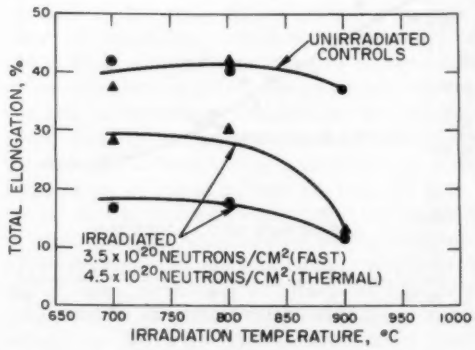

Fig. IV-13 Effect of irradiation temperature[50] on ductility of low- and high-carbon steels tested at 650°C. ▲, 0.06 wt.% carbon; ●, 0.02 wt.% carbon.

redistribution of carbon. The better ductility of the steel that contains higher carbon is believed to be due to the anchoring of helium atoms by carbide particles.

Tensile tests have been performed on irradiated Fe–15 wt.% Cr–4.5 wt.% Al–0.5 wt.% Y and Fe–24 wt.% Cr–4.5 wt.% Al–0.5 wt.% Y alloys.[47] These specimens were irradiated at 40°C to 2.4×10^{20} neutrons/cm^2 (thermal) and 7×10^{19} neutrons/cm^2 (fast) and then were tested at 650, 750, and 850°C. Results of the tests (shown in Table IV-3) indicate that irradiation does not affect the mechanical properties of the alloys at the temperatures of testing.

Table IV-3 EFFECT OF IRRADIATION ON THE MECHANICAL PROPERTIES OF Fe–Cr–Al–Y ALLOYS[47]

Alloy, wt.%	Condition	Yield strength (0.2% offset), psi	Ultimate tensile strength, psi	Elongation, %	Test temp., °C
15 Cr–4.5 Al–0.4 Y	Irradiated	11,860	15,840	57.6	650
	Irradiated	7,950	8,340	109.0	750
	Irradiated	4,440	4,540	108.0	850
	Unirradiated	12,900	15,800	71.4	650
	Unirradiated	8,490	8,490	108.8	750
	Unirradiated	4,560	4,560	116.8	850
24 Cr–4.5 Al–0.5 Y	Irradiated	16,160	18,660	73.6	650
	Irradiated	8,640	9,750	89.5	750
	Irradiated	5,180	5,370	131.7	850
	Unirradiated	16,550	20,000	70.0	650
	Unirradiated	9,630	9,630	110.7	750
	Unirradiated	5,050	5,150	150.0	850

The unattractive feature of these precipitation-hardened Fe–Cr alloys is their low strength at elevated temperatures.

Irradiation of Nimonic PE16 (age-hardenable nickel alloy) to large doses of fast flux in the Dounreay Fast Reactor resulted in considerable losses of elevated-temperature ductility.[46a] The strength properties at elevated temperatures showed a minor decrease with increasing fast flux but were not so pronounced as the ductility loss. The loss of ductility as shown in Fig. IV-14 is attributed to the helium bubbles that promote intergranular fracture.

The postirradiation tensile properties of Hastelloy X-280 were improved by various preirradiation heat-treatments.[51] The preirradiation heat-treatments consisted in taking the material that had been given the standard solution anneal at 2150°F (1177°C) and cold-working it up to 20%; the material was then further annealed either at 1000 or 1500°F (538 or 816°C). The specimens were irradiated at 540°F (282°C) to a total fast-neutron exposure of 1×10^{20} neutrons/cm^2 and tested at room temperature and 1350°F (732°C). Results of these tests are shown in Figs. IV-15 and IV-16. The increased postirradiation strength can be obtained by increasing the degree of preirradiation cold work. The best postirradiation ductility is obtained by eliminating cold work and giving the material a 100°F (538°C) anneal after the standard solution anneal.

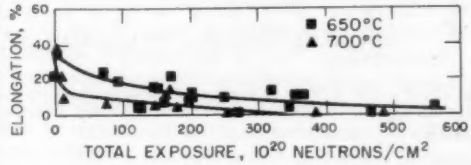

Fig. IV-14 Ductility[46a] of fully heat-treated Nimonic PE16 at 650 and 700°C after irradiation at 250 to 350°C.

The time to rupture of irradiated Hastelloy X-280 at 1350°F (732°C) was increased by preirradiation heat-treatments.[52] The preirradiation heat-treatments and irradiation conditions were the same as those for the tensile specimens discussed above. Results of these tests (shown in Fig. IV-17) indicate that the best results were obtained by annealing at 1500°F (816°C) after cold working. The observed improvement in rupture life is attributed to the following mechanism: Cold work provides dislocations where carbides precipitate when the material is annealed at 1500°F (816°C), resulting in a finely dispersed second phase. The presence of this fine second phase reduces the primary creep time but increases the secondary- and ternary-creep times. Since secondary- and ternary-creep times are considerably longer than the time for primary creep, the overall time to rupture is significantly increased.

Zirconium Alloys

Postirradiation tensile tests[53] at room temperature and 300°C have been performed on Zircaloy-2 specimens irradiated at 60 and 290°C to a maximum total fast flux of 2.36×10^{21} neutrons/cm^2. Results of these tensile tests are shown in Figs. IV-18 and IV-19. The greatest property changes were found in material that

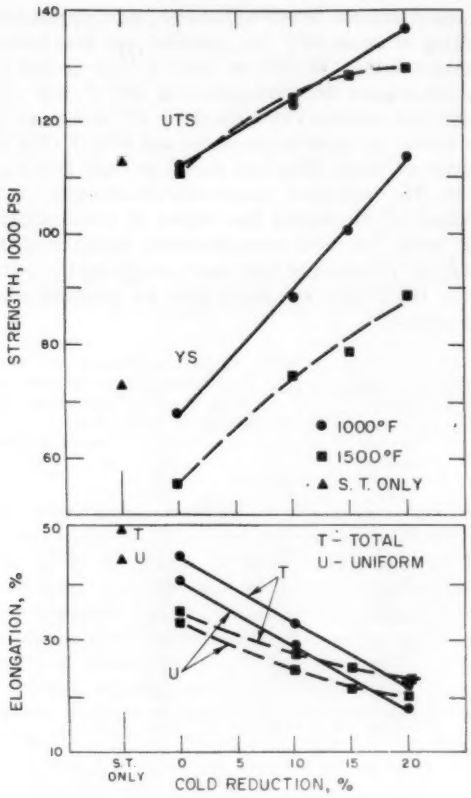

Fig. IV-15 Room-temperature tensile properties of Hastelloy X-280 irradiated to 1×10^{20} neutrons/cm² at 540°F (282°C).[51] Standard treatment: 2150°F for 1 hr, air cool. Experimental treatment: 2150°F for 1 hr, air cool; cold roll; anneal 24 hr, air cool.

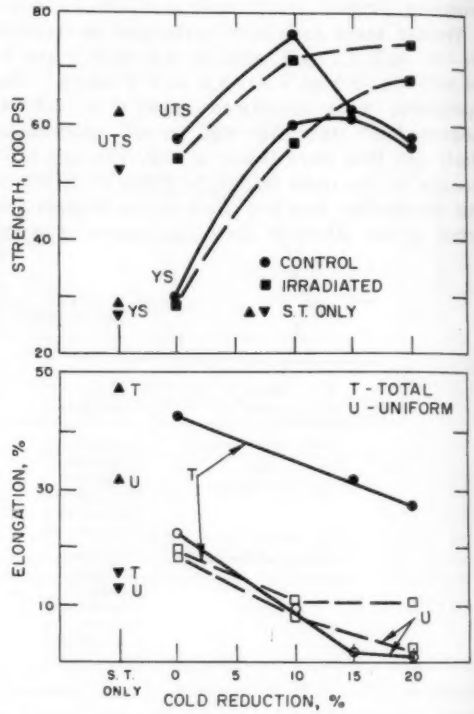

Fig. IV-16 The 1350°F tensile properties[51] of Hastelloy X-280 irradiated to 1×10^{20} neutrons/cm² at 540°F (282°C). Standard treatment: 2150°F for 1 hr, air cool. Experimental treatment: 2150°F for 1 hr, air cool; cold roll; 1000°F for 24 hr, air cool.

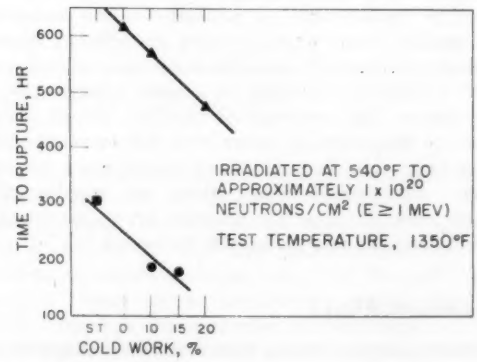

Fig. IV-17 Effect of preirradiation treatments[52] on post-irradiation time-to-rupture for Hastelloy X-280. ■, 2150°F for 1 hr, air cool (S. T.); ●, 2150°F for 1 hr, air cool; cold work; 1000°F for 24 hr, air cool; ▲, 2150°F for 1 hr, air cool; cold work; 1500°F for 24 hr, air cool.

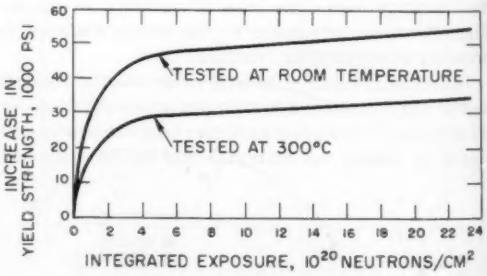

Fig. IV-18 The effects of neutron irradiation[53] on the 0.2% yield strength of NPR Zircaloy-2 tube material irradiated at 282°C.

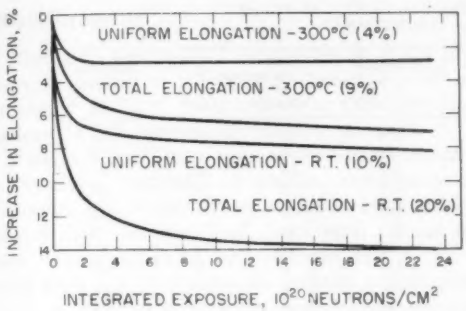
UNIFORM ELONGATION - 300°C (4%)
TOTAL ELONGATION - 300°C (9%)
UNIFORM ELONGATION - R.T. (10%)
TOTAL ELONGATION - R.T. (20%)
INCREASE IN ELONGATION, %
INTEGRATED EXPOSURE, 10^{20} NEUTRONS/CM^2

Fig. IV-19 The effects of neutron irradiation[53] on the ductility of NPR Zircaloy-2 tube material irradiated at 282°C. The preirradiation elongation is given in parentheses.

had been irradiated at 290°C and then tested at room temperature. In another investigation,[54] tensile and rupture tests were performed on Zircaloy-2 specimens that had been irradiated at 370°C to fast-neutron exposure of 1.5×10^{21} neutrons/cm^2. The tensile and burst strength increased as a function of fast-flux exposure, and the increase can be given by the following relation:

$$\text{Log } y = 3.62 + 0.39 \log (x/10^{19})$$

y = change in tensile strength, psi

x = fast-neutron exposure (>1 Mev)

Most of the in-pile creep results obtained at Chalk River and Battelle–Northwest on Zircaloy-2 and Zr–2.5 wt.% Nb alloys are summarized[55] in Fig. IV-20. These results indicate that the best in-pile creep performance is exhibited by Zr–2.5 wt.% Nb alloys that have been quenched and tempered. The degree of improvement imparted by cold-working the material between quenching and tempering has not been definitely established by the limited number of in-pile tests which have been performed. Irradiation does not cause any significant change in in-pile creep behavior during the early stages of creep.[56] However, the in-pile creep rate remains steady, whereas the out-of-pile creep rate on similar material decreases with time. For example, the in-pile and out-of-pile creep rates differ by a factor of 10 after 4000 hr at 300°C with a 20,000-psi load.

In a controlled experiment,[57] Zircaloy-2 and Zr–2.5 wt.% Nb-alloy specimens were impregnated with 120, 300, and 500 ppm hydrogen and irradiated to a fast-neutron exposure of 5×10^{20} neutrons/cm^2. It was concluded from postirradiation impact tests that the shifts in the transition temperature, which are caused by irradiation and increased hydrogen content, are not additive. The specimens having low hydrogen contents underwent larger irradiation-induced shifts in transition temperature than did specimens with high hydrogen content. In specimens containing 200 ppm hydrogen, irradiation increased the transition temperature 100 to 200°C, whereas the increase was only 50°C for specimens containing 300 ppm hydrogen.

Specimens[58] of Zr–2.5 wt.% Nb were given different heat-treatments before being irradiated at 50 to 375°C to a fast-neutron exposure of 3×10^{20} neutrons/cm^2. Material in the following heat-treated conditions was irradiated:

1. Slow cooled from beta phase
2. Slow cooled from alpha + beta phase
3. Quenched from beta phase and aged at 500°C
4. Quenched from alpha + beta phase and aged at 500°C
5. Slow cooled from alpha + beta phase and cold drawn 40%

The test results are summarized in Table IV-4. The alloy, quenched from the alpha + beta phase and aged at 500°C, loses only a small amount of its ductility owing to neutron irradiation. When its higher strength is taken into account, it becomes more attractive than the material that is cooled slowly from the alpha + beta phase, although their ductility after irradiation is about the same. The large ductility loss in the beta-quenched and tempered alloy is attributed to the low work-hardening ability of this material.

Tensile tests were performed on irradiated tabular specimens that contained a welded transition of Zircaloy-2 to Inconel 600 in the gauge section.[60]

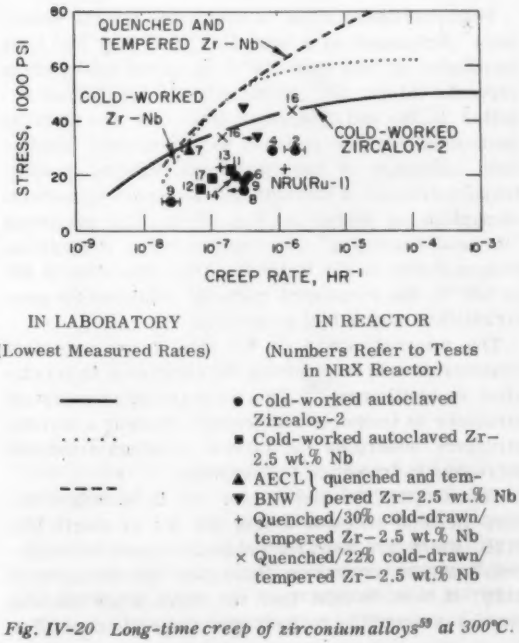

Fig. IV-20 Long-time creep of zirconium alloys[59] at 300°C.

Table IV-4 TENSILE PROPERTIES OF THE Zr–2.5 WT.% Nb ALLOY IN VARIOUS METALLURGICAL CONDITIONS[58]

Metallurgical condition	Irradiation history*	Test temp., °C	Yield stress (0.2% offset), 1000 psi	Fracture stress, 1000 psi	Elongation, %		Reduction of area, %
					Uniform	Total	
Slow cooled from ($\alpha + \beta$) phase	Unirradiated	RT	61	132	12		56
	Irradiated	RT	167	150	3		37
	Unirradiated	300	32	100	18	30	72
	Irradiated	300	80	120	2	11	60
Slow cooled from β phase	Unirradiated	RT	73	130	9		44
	Irradiated	RT	160	123	10		13
	Unirradiated	300	34	92	5	12	67
	Irradiated	300	68	120	4	9	40
Quenched from ($\alpha + \beta$) phase and aged 24 hr at 500 C	Unirradiated	RT	109	194	4		60
	Irradiated	RT	142	210	1		55
	Unirradiated	300	85	167	3	12	70
	Irradiated	300	116	175	<1	11	65
Quenched from β phase and aged 24 hr at 500 C	Unirradiated	RT	113	170	4	10	>25
	Irradiated	RT	153	160	<1	1	<5
	Unirradiated	300	81	133	3	12	56
	Irradiated	300	114	126	1.5	2	<20
Cold drawn 40% after slow cooling from ($\alpha + \beta$) phase	Unirradiated	RT	97	122	1		30
	Irradiated	RT	131	152	1		26
	Unirradiated	300	60	90	1		34
	Irradiated	300	101	116	1		26

*Specimens were at 250 to 325°C during irradiation to 3×10^{20} neutrons/cm^2.

These specimens had been irradiated at 500°F (260°C) to a fast-flux accumulation of 6.2×10^{20} neutrons/cm^2. Tests at room temperature and 550°F (288°C) indicated that the limiting criterion was the strength of Zircaloy-2. The failure in the Zircaloy-2 portion of the transition specimens was found to be a function of the degree of hydriding.

Pressure-Vessel Steels

Postirradiation room-temperature tensile tests[61] were performed on a low-alloy steel that had been irradiated at less than 100°C to a total fast-neutron exposure of 2×10^{19} neutrons/cm^2. Irradiation resulted in the usual strength increases and ductility decreases that are common to fast-neutron irradiation. Annealing of the specimens resulted in additional increases in strength and decreases in uniform elongation as shown in Fig. IV-21. The maximum "thermal hardening" was found to occur at annealing temperatures of 100 to 150°C. After annealing at 450 to 500°C, the irradiated material exhibited the preirradiation mechanical properties.

The microstructure of the steel is an important consideration in determining its resistance to irradiation embrittlement.[46e] The most radiation-resistant structure is tempered martensite, whereas a ferritic structure undergoes the largest irradiation-induced increases in transition temperature.

Catastrophic delayed failure due to hydrogen occurs in high-strength steels but not in steels like 212B, which are used for pressure-vessel construction.[30] Since irradiation increases the strength of 212B, it was thought that the steel would thereby become susceptible to hydrogen embrittlement after irradiation. Testing of irradiated material indicated that if the neutron-exposure levels remain low enough so that the nil-ductility-temperature (NDT) criteria are satisfied, no catastrophic delayed failure can be expected from hydrogen embrittlement.

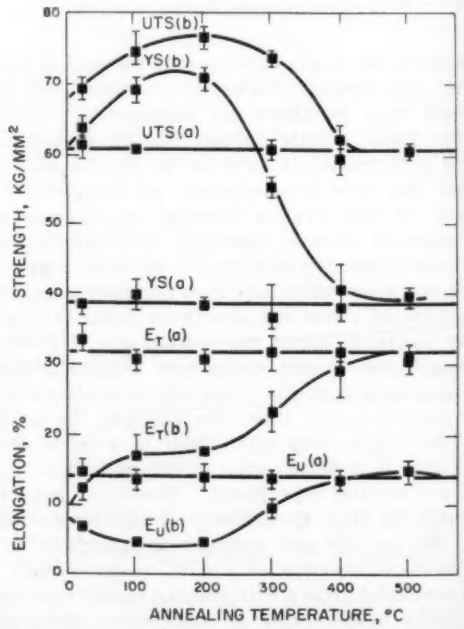

Fig. IV-21 Effect of postirradiation annealing on room-temperature mechanical properties of irradiated low-alloy steel.[61] (a) Unirradiated; (b) fast-neutron exposure of 2×10^{19} neutrons/cm^2.

Miscellaneous

Aluminum specimens[56] reinforced by silica fibers were irradiated to a total fast flux of 5×10^{19} neutrons/cm^2 at 50°C. Tensile tests on these specimens indicated a 30% increase in fracture strength.

Tensile tests[46f] have been performed on irradiated V–Ti alloys containing chromium, niobium, or molybdenum and irradiated to a total neutron exposure of 1.4×10^{21} neutrons/cm^2 (>0.1 Mev). These tests were performed at 20, 200, 400, 650, and 750°C. The tests show that (1) irradiation leads to drastic reductions in elongation at room temperature accompanied by significant increases in yield and ultimate strength; (2) increasing the testing temperature results in annealing out the irradiation-induced damage so that, at 650 and 750°C, the preirradiation mechanical properties are restored; and (3) increasing the titanium content in the alloys resulted in a more rapid recovery of preirradiation properties during annealing. Although the material contained significant quantities of boron, which was transmuted to helium by irradiation, no helium-bubble-induced intergranular fracture was observed at elevated temperatures.

Workers at Harwell[47] have irradiated molybdenum specimens at 490°C to a total fast exposure of about 1.5×10^{22} neutrons/cm^2. These specimens were tested in tension at 600, 700, and 800°C after irradiation, and the results are shown in Table IV-5. The increase in strength and decrease in ductility are attributed to the point-defect type of damage. The microhardness of the material showed complete recovery of preirradiation hardness after annealing at 1200°C.

The effect of irradiation on the mechanical properties of hafnium has been summarized.[62] Hafnium, in the form of control rods, was irradiated at three different levels of total neutron exposure, the maximum level being 6×10^{21} neutrons/cm^2. Tensile tests were performed at room temperature, 300°F (149°C), and 600°F (316°C). These results indicate increases in yield and tensile strength and decreases in ductility that are similar to irradiation effects for other materials. No saturation of irradiation-induced effects on mechanical properties was found up to exposures of 6×10^{21} neutrons/cm^2.

Basic Studies of Radiation Effects

Specimens[63] of iron containing 0.005 wt.% carbon were irradiated to fast-neutron exposures of 2×10^{18}, 1×10^{19}, and 2×10^{20} neutrons/cm^2 at 30 to 90°C. When these specimens were observed under an electron microscope, none of the lattice defects that cause changes in mechanical properties could be observed. Annealing for 2 hr at 250°C did not result in any changes in properties or microstructure as observed by electron microscopy. Further annealing at 350°C for 2 hr resulted in restoration of some mechanical properties and the appearance of small dislocation loops. With increasing annealing temperature, the size of the loops increased until a maximum was reached and then decreased with further increases in temperature. Small dislocation loops appeared in irradiated iron specimens containing 0.001 wt.% carbon only after a fast-neutron exposure of 2×10^{20} neutrons/cm^2. It was therefore concluded that carbon interstitials react with neutron-produced defects and prevent them from growing at room temperatures to an observable size. As the temperature is increased, these complex combinations of defects and carbon

Table IV-5 EFFECT OF IRRADIATION ON THE ELEVATED-TEMPERATURE TENSILE PROPERTIES OF MOLYBDENUM[47]

Grain size	Condition	Yield strength (0.2% offset), psi	Ultimate tensile strength, psi	Elongation, %	Test temp., °C
As received	Unirradiated	72,580	78,490	4.2	600
	Unirradiated	64,550	73,400	3.4	700
	Unirradiated	57,280	73,090	4.6	800
	Irradiated	Max. stress	101,800	0	600
	Irradiated	78,180	78,480	0.5	700
	Irradiated	70,910	73,640	2.9	800
50 μ	Unirradiated	11,820	41,210	30.4	600
	Unirradiated	11,520	31,520	21.9	700
	Unirradiated	12,310	30,150	25.9	800
	Irradiated	Max. stress	80,300	0	600
	Irradiated	Max. stress	54,550	1.2	700
	Irradiated	38,790	39,240	2.7	800
17 μ	Unirradiated	13,630	34,240	32.3	600
	Unirradiated	11,520	32,730	29.2	700
	Unirradiated	12,910	29,610	33.8	800
	Irradiated	Max. stress	71,220	0	600
	Irradiated	48,780	49,840	0.5	700
	Irradiated	43,940	44,540	1.8	800

atoms agglomerate to form visible dislocation loops. Somewhat similar results have been seen for irradiated gold, where loops are observed in pure annealed gold but are not observed in quenched gold containing stacking-fault tetrahedra.[64] These stacking faults probably play a role similar to that of the carbon atoms in solution by tying up the irradiation-produced defects and thereby preventing them from agglomerating into dislocation loops.

Free nitrogen in the presence of a fast-neutron environment contributes to the ductile–brittle transition-temperature shift in pure iron.[65] This was demonstrated by irradiating pure-iron specimens containing enough titanium (0.042 wt.%) to tie up the nitrogen and other specimens containing free nitrogen in solution. Both types of specimens had about the same grain size. A total exposure of 1.4×10^{19} neutrons/cm^2 increased the ductile–brittle transition temperature 60°C in the iron with the titanium addition and 160°C in the iron that contained free nitrogen.

The number of defect clusters in nickel was found to be independent of fast-neutron exposure, but the size of the clusters was found to increase with increasing fast-neutron exposure in the range 10^{18} to 10^{19} nvt (for energy >1 Mev).[24] The effect of neutron irradiation on the defect-cluster size in nickel and molybdenum is illustrated in Table IV-6.

Table IV-6 EFFECT OF FAST-NEUTRON EXPOSURE ON SIZE OF DEFECT CLUSTERS[24]

Material	Irradiation temp., °C	Total neutron exposure, neutrons/cm^2	Cluster size, A
Nickel	40	2.5×10^{18}	50
Nickel	40	5×10^{19}	70
Nickel	40	1×10^{19}	100
Molybdenum	500	2.5×10^{19}	330

It has been shown that better correlation in irradiation effects, based on transition-temperature shift as measured by Charpy V-notch specimens, can be obtained by using the total number of displacements rather than the number of fast neutrons as in the present practice.[66] These findings are based on irradiation of specimens in three different reactors that had large variations in neutron spectrum.

(M. Kangilaski)

Selected Mechanical Properties of Cladding and Structural Materials

Refractory Metals

The results of fatigue tests on TZM and TZC alloys are reported by TRW Inc.[67] Notched specimens (K_t = 1.75) of TZM alloy at 1800°F (982°C) and TZC alloy at 2000°F (1093°C) were studied. The fatigue curve was extremely sensitive to applied stress, and a decrease in peak dynamic-stress values from 20,000 psi to 15,600 psi produced a variation in failure time from 0.6 hr (4.1×10^7 cycles) to greater than 143 hr (>9.86×10^9 cycles). Tests conducted on smooth specimens of TZC bar stock defined the resonant wavelength at 2000°F (1093°C); however, no failure occurred in this material at a peak dynamic stress of 23,900 psi after 500 hr and 3.6×10^{10} cycles.

The effect of specimen size on the ductile-to-brittle transition of Nb–V alloys was studied at Knolls Atomic Power Laboratory.[68] Decreasing the number of grain boundaries across the gauge section of tensile specimens from 5 to 1 did not have a large effect on the tensile properties. The transition temperature was increased 55°C by increasing the vanadium content from 4 to 6 wt.%. The ductile-to-brittle transition temperature appears to be lowered by a decrease in specimen size. The data from this and an earlier study indicated that the strength of niobium alloys with 4 to 6 wt.% vanadium was not influenced by grain size in the range 35 to 1460 μ.

The creep-rupture properties of FS-85 (Nb–27 wt.% Ta–10 wt.% W–1 wt.% Zr) were studied at Oak Ridge[69] at temperatures between 982 and 1427°C. Pretest annealing temperatures were shown to have a pronounced effect in that the creep-rupture strength of the alloy was progressively increased by pretest anneals at increasing temperatures up to about 1600°C. Higher pretest annealing temperatures produced inferior strength and ductility. A fine precipitate in the grain boundaries was observed in the failed creep specimens. At longer times and higher temperatures, this precipitate was more evident and appeared to be related to an intergranular fracture with very little deformation of the matrix material. It was believed that pretest annealing placed more of this material in solution, allowing it to reprecipitate in a finely dispersed state at the test temperature and consequently produce the higher strength properties. This precipitate is believed to be ZrO_2.

The creep properties of Cb-753 (Nb–5 wt.% V–1.25 wt.% Zr) have been compared with those of a number of other niobium alloys by researchers at Oak Ridge.[70] These alloys were compared on the basis of the stress necessary to produce rupture in 1000 hr at various temperatures (Fig. IV-22). Several conclusions were reached during the course of the study. The Cb-753 alloy was shown to recrystallize during deformation after only 80 hr at 982°C. The vanadium-bearing alloys, B-66 and Cb-753, demonstrated different slopes from the other alloys, indicating that the allowable stress for small strains over a long time will be less than that for the Nb–1 wt.% Zr alloy.

Creep-rupture properties for the T-222 (Ta–9.5 wt.% W–2.5 wt.% Hf–0.01 wt.% C) alloy have also

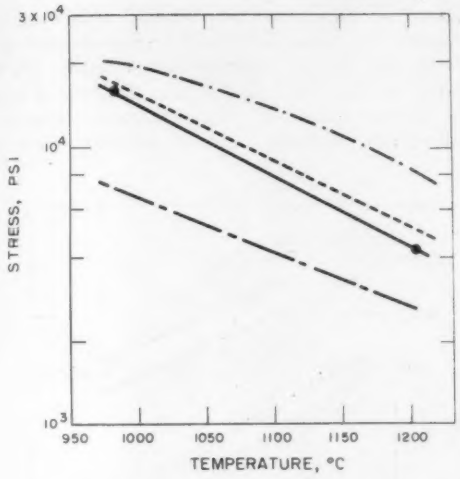

Fig. IV-22 Comparison of the stress to produce rupture in 1000 hr for Cb-753 with that for several other niobium-base alloys.[70] ——— D-43 (Nb–10 W–1 Zr–0.1 C); ---- B-66 (Nb–5 V–5 Mo–1 Zr); —·— Nb–1 Zr; ——— Cb–753 (Nb–5 V–1.25 Zr).

been reported by Oak Ridge.[71] The results of these tests are summarized in Fig. IV-23. The weld material appears to be slightly stronger than base material. Specimens were examined metallographically after testing at 982, 1093, and 1204°C and were found to be similar in appearance. The material was not recrystallized and was characterized by a small grain size and a fine precipitate (probably carbides). At 1427°C the material recrystallized during the test, whereas at 1649°C recrystallization and extensive grain growth occurred.

IIT Research Institute is conducting a program to develop vanadium-base alloys.[72] Titanium, silicon, and carbon were added to the base alloys of V–20 wt.% Nb and V–Nb–Ta, and the mechanical strength of the alloys was determined. The highly fabricable V–20 wt.% Nb–10 wt.% Ti alloy exhibited density-corrected strengths of up to 1,300,000 in. at –320°F (–196°C), 800,000 in. at 1200°F (649°C), and 250,000 in. at 1800°F (982°C). Alloys containing tantalum additions had density-corrected strengths above 400,000 in. at 1800°F and 160,000 in. at 2200°F (1204°C). Typical data for two vanadium alloys are shown in Fig. IV-24 and compared with those for a number of commercial alloys. Both these alloys retain their strength even up to 2400°F (1316°C).

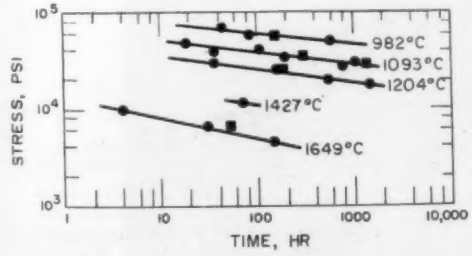

Fig. IV-23 Creep-rupture properties[71] of T-222. ●, base metal; ■, weld specimens.

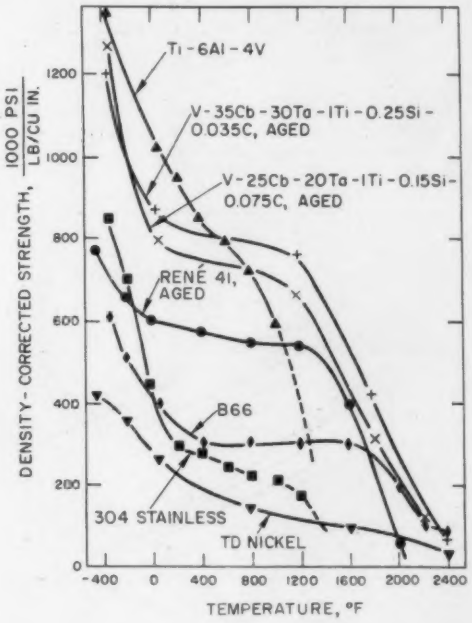

Fig. IV-24 Ultimate tensile-strength data for structural alloys.[72]

The creep-rupture properties of two types of unalloyed tungsten and two tungsten-base alloys were determined at Oak Ridge.[73] Base-line data for powder-metallurgy tungsten exhibited considerable scatter as shown in Fig. IV-25. Inhomogeneous deformation along the gauge length and temperature variation are considered contributing factors in the observed scatter. Creep-rupture data from this study are also compared with those of other experimenters in Fig. IV-26, where the agreement appears to be reasonably good. Results obtained at 1650 and 2200°C for powder-metallurgy tungsten, several heats of TCD tungsten, tungsten–2 wt.% thoria, and Sylvania A (W–0.5 wt.% Hf–0.2 wt.% C) are compared in Fig. IV-27. At 1650°C, tungsten–2 wt.% thoria is the strongest material up to rupture lives of 500 hr, where the Sylvania A material then offers the best strength. The powder-metallurgy and TCD tungsten were the weakest of the materials tested.

The chemical stability and the particulate stability of refractory oxides, nitrides, and carbides in tung-

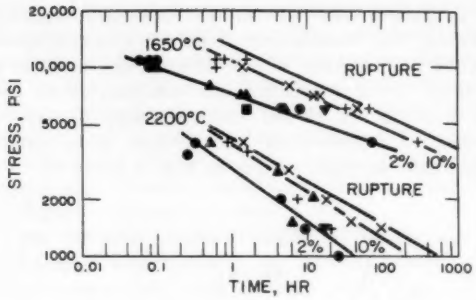

Fig. IV-25 Creep-rupture properties of powder-metallurgy tungsten.[73] 2%: ●, transverse; ▲, longitudinal; ■, 45°. 10%: +, transverse; ×, longitudinal; ▼, 45°.

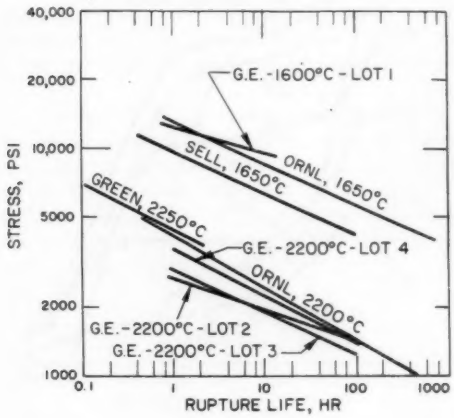

Fig. IV-26 A comparison of the creep-rupture properties of tungsten.[73]

sten were investigated at Westinghouse.[74] The refractory dispersoids were found to be chemically inert in pure tungsten to 2200°C, but none exhibited complete particulate stability under all processing and annealing conditions. Contaminants like tungsten oxides, oxygen, and carbon were found to be very effective, at relatively low temperatures, in changing the chemical composition of the dispersoids. The tensile properties of tungsten and W–ThO_2 alloys as a function of temperature are shown in Figs. IV-28 and IV-29. The W–ThO_2 alloys are stronger than unalloyed tungsten in the temperature range investigated; however, changes in relative ductilities occur at about 1400°C.

The ductile–brittle transition behavior of zone-refined tungsten single crystals was related to crystal orientation at Lewis Research Center, National Aeronautics and Space Administration (NASA).[75] Studies of tensile axis orientations ⟨100⟩, ⟨110⟩, and ⟨111⟩ demonstrated that the transition behavior was highly orientation dependent. The ⟨110⟩ crystals exhibited a sharp ductile–brittle transition, on the basis of a reduction-in-area measurements, and showed the lowest transition temperature, 205°K. Crystals of the ⟨100⟩ tensile axis exhibited a much more gradual transition with temperature from ductile-to-brittle behavior, with a transition tempera-

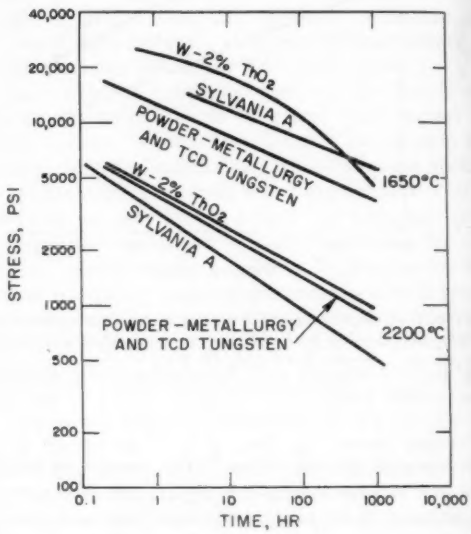

Fig. IV-27 Comparative creep-rupture properties of several tungsten-base alloys.[73]

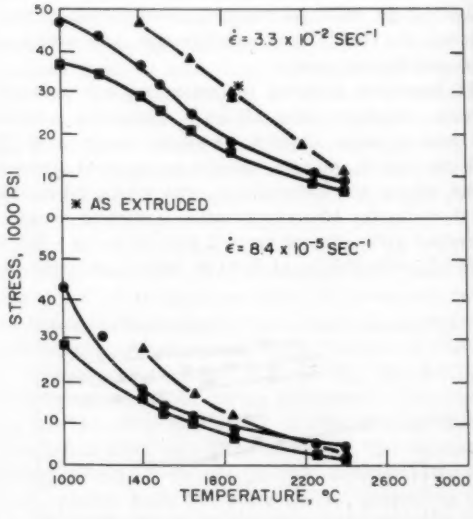

Fig. IV-28 Ultimate strength[74] of high-purity tungsten and W–ThO_2 alloys, annealed ½ hr, 2400°C. ▲, W–3.8 vol.% ThO_2, hot compacted, extruded; ●, W–1.9 vol.% ThO_2, hydrogen sintered, swaged; ■, high-purity tungsten, hydrogen sintered, swaged.

ture of about 380°K, on the basis of a 50% reduction in area. The transition temperature of the ⟨111⟩ crystals was intermediate between those of the other orientations. Specimens of all orientations showed measurable plastic deformation at temperatures far below their respective ductile–brittle transition temperature. The tensile flow characteristics were also found to be affected by orientation. The ⟨110⟩ oriented specimens exhibited a high yield strength and a yield-point drop, with necking almost immediately following yielding. In contrast, the ⟨100⟩ and ⟨111⟩ oriented crystals exhibited no yield point and, when tested above the transition temperature, showed considerable uniform elongation before necking.

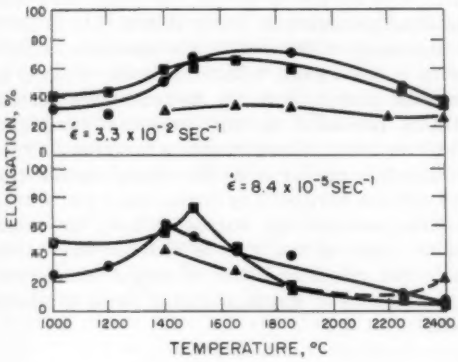

Fig. IV-29 Ductility[74] of high-purity tungsten and W–ThO_2 alloys, annealed ½ hr at 2400°C. ▲, W–3.8 vol.% ThO_2, hot compacted, extruded; ●, W–1.9 vol.% ThO_2, hydrogen sintered, swaged; ■, high-purity tungsten, hydrogen sintered, swaged.

Miscellaneous

A continuing program to study the metallurgical characteristics of high-strength structural materials is in progress at the Naval Research Laboratory.[76] The objectives of the program are to determine the performance characteristics of high-strength materials using standard and recently developed laboratory techniques and to establish the significance of the laboratory tests for predicting the service performance of the materials in large, complex structures. Quenched and tempered steels, maraging steels, titanium alloys, and aluminum alloys are being investigated, with most of the studies to date concerning fracture-toughness characteristics. The report on this program is an excellent reference on the fracture toughness of materials.

Atomics International has reported the results of biaxial-stress-rupture tests in helium on 304 and 316 stainless steels.[77] The data are summarized in Fig. IV-30 for 1250 and 1350°F (677 and 732°C). The effect of heat-to-heat variation in alloy chemistry on the rupture strength is shown in this plot.

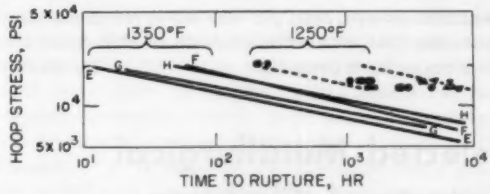

Fig. IV-30 Biaxial-stress-rupture properties[77] of stainless steel at 1250 and 1350°F. Data points for heats A, B, C, D fall between the lines for heats E and H. Heats A to D and G, 304 stainless steel; heats G and H, 316 stainless steel. ●, heats A to D and G; ■, heat E; ▲, heat F; ▼, heat H.

The Mechanical Properties Data Center at Belfour[78] has issued the seventh of a series of reports designed to acquaint users with the content and use of the center. This report covers data available on nickel- and chromium-base alloys.

The effect of nitrogen on the ductility of chromium has been reported by workers at Ames Laboratory.[79] Their results indicate that the brittle–ductile transition temperature of chromium increases with increasing nitrogen content above approximately 400 ppm, regardless of the heat-treatment, as shown in Fig. IV-31. Normally the ductility of a metal decreases with increasing interstitial-impurity content, as indicated with nitrogen contents of less than 400 ppm.

Lee, at the University of Arizona,[80] investigated the hardening mechanisms in cobalt-base superalloy AR 213 (Co–20 wt.% Cr–5 wt.% Al–4.5 wt.% W–2.3 wt.% Ta). The author presents a comprehensive review of present knowledge of hardening mechanisms in metal and discusses their applicability to the system of interest. A minimum solution temperature of 2200°F (1204°C) is required to obtain complete solutioning. The precipitate overages rapidly at temperatures above 1600°F (871°C). A hard phase

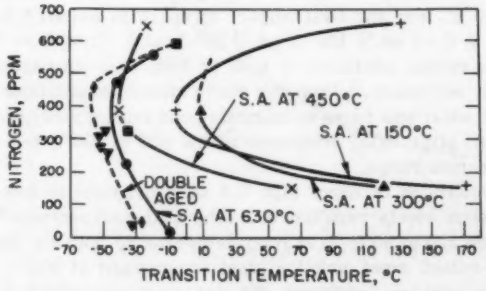

Fig. IV-31 Effect of nitrogen content and aging conditions on the brittle–ductile transition of chromium.[81] Single aging: +, aged at 150°C; ▲, aged at 300°C; ×, aged at 450°C; ●, aged at 630°C. Double aging: ♦, aged at 100 to 150°C and at 630°C; ▼, aged at 250 to 375°C and at 630°C; ■, aged at 450 to 475°C and at 630°C.

identified as (Ta,Zr)(C,N) was observed in the alloy, indicating that excessive amounts of zirconium and/or nitrogen were present. (J. A. De Mastry)

Selected Metallurgical Aspects of Cladding and Structural Materials

Pressure-Vessel Steels

The embrittlement[81] of both weld and base metal of HT 60, a Ni–Cr–Mo steel, takes place by heating at 550°C for times up to 5000 hr. No change in room-temperature elongation takes place, but both the strength and hardness are decreased by the aging process. A considerable decrease in impact strength occurs in the base metal, whereas the impact strength of the weld metal is increased by heating at this temperature for 1000 hr. Additional heating of the weld metal up to 5000 hr decreases the impact strength of the weld metal to the level of the base metal. The embrittling process is believed to operate as follows: (1) martensite is tempered and growth of spheroidal carbide occurs, (2) fine ferrite grains are formed, (3) ferrite grains grow and carbides migrate to grain boundaries.

In other studies on pressure-vessel steel, it has been found that fatigue of the steels into the plastic range results in considerable increase in the transition temperature of brittle-to-ductile fracture.[82] Fatigue in the plastic range at temperatures of 200 to 300°C appears to be more likely to cause embrittlement than fatigue at room temperature.[83] The mechanism of embrittlement was found to be an increase of effective surface energy, which makes crack propagation easier. For thick sections[84] of Mn–Mo pressure-vessel steels, it has been found that a cooling rate of 10°C/min from the austenitizing temperature is necessary to obtain a toughness of 30 ft-lb at −12°C. For the best impact strength in welded 0.18 wt.% C–1 wt.% Mn–1 wt.% Ni–1 wt.% Cr–0.5 wt.% Mo steels, additions of 0.02 to 0.05 wt.% aluminum are necessary.[85] With the above aluminum additions, the steel was found to maintain good impact strength, even after being tempered in the 625 to 650°C temperature range.

Additions of more than 0.3 wt.% uranium to low-carbon steels resulted in a drop in impact strength[86] from 220 to 80 ft-lb at room temperature both for the as-rolled steel and for steel normalized at 900°C. The uranium additions did not have any effect on the as-rolled tensile properties but increased the strength in the quenched and tempered conditions. The uranium additions prevent the growth of polygonal ferrite by retaining a fine acicular structure. This structure retards softening during tempering in the 370 to 730°C temperature range and prevents grain growth at higher tempering temperatures. Maximum solubility of zirconium in low-carbon steels was found to be 0.14 wt.% at room temperature.[87] Excess zirconium resulted in ZrC and alpha iron, with the amount of pearlite being reduced by the excess zirconium. A British patent has been issued for a low-alloy steel that has been found to have excellent properties for construction of massive pressure vessels from rolled and normalized plate.[88] The alloy steel has the following composition: 1.0 to 1.2 wt.% Mn, 1.4 to 1.7 wt.% Ni, 0.24 to 0.35 wt.% Mo, 0.25 to 0.55 wt.% Cr, 0.08 to 0.20 wt.% V, less than 0.15 wt.% C, and the balance Fe.

The following theory[89] has been developed in connection with failure of low-carbon-steel tubes operating at temperatures of 600 to 1000°F (316 to 538°C) and pressures of 450 to 2700 psi. Hydrogen, which is present in the steam, diffuses into the steel and reacts with carbon, forming methane. The methane exerts a pressure in microfissures along grain boundaries and causes their enlargement. These microfissures propagate to the inside surface, from where crevice corrosion by pitting takes place. These pits are enlarged by corrosion until the cross-sectional area of the tube is reduced and the tube fails by the combined effect of stress concentration at the pits and of the hoop stress owing to internal pressure.

Stainless Steels and Superalloys

Addition of titanium to Fe–Cr–Ni stainless steels raises the temperature[90] at which sigma phase is stable to above 960°C. Titanium additions promote the formation of ferrite and sigma phase at the expense of austenite. The solubility of titanium is decreased with decreasing iron content, the excess titanium being precipitated as Ni_3Ti. Additions of 5 to 8 wt.% molybdenum to a titanium-containing high-nickel precipitation-hardenable stainless steel (36 NKhTYu) resulted in increased strength.[91] The heat-treatment consisted of quenching from 950 to 1200°C and tempering at 600 to 850°C. The strength increase was found to be due to solid solution of molybdenum and reduced diffusion rates, which retarded overaging of the precipitates. Excess molybdenum (above the solubility of 4 wt.%) formed a Fe_2Mo phase that acted as a second hardening phase in addition to the Ni_3Ti.

The physical and mechanical metallurgy, along with the oxidation resistance of Fe–Cr–Al–Y alloys, has been summarized.[8] These alloys are very oxidation resistant because of the formation of a surface film of Al_2O_3. This film is further stabilized by yttrium, which prevents it from spalling. The low solubility of yttrium in iron (<0.1 wt.%) causes most of the yttrium to exist as YFe_9. This fine second phase strengthens the matrix, but, since the solubility of yttrium does not increase appreciably with temperature, the re-

distribution of the particles cannot be achieved by heat-treatment. Therefore the alloy has to be hot worked to break up the YFe_3 particles to obtain the desired structure. Recently it has been found that a very fine YFe_3 dispersion can be obtained by atomization of the alloy directly from the molten state in an inert atmosphere. The brittle-to-ductile transition temperature of the alloy is considerably increased with increasing yttrium content.

NASA has reviewed the effects of composition, mechanical working, and heat-treatment on the mechanical properties of nickel and nickel-base alloys.[92] The alloys discussed include nickel, Monel K-500, Inconel X-750, Inconel 718, René 41, Waspaloy, Udimet 500, Hastelloy C, Alloy 713C, Alloy 713LC, and IN-100.

The effect of molybdenum[93] and niobium[94] additions on Ni–Cr alloys has been related to strength properties. It was found that both of the alloying elements promoted strengthening by precipitation hardening and that aging further increased the strength. The maximum stress-rupture strength at 700 to 750°C was obtained for the Ni–20 wt.% Cr–7.2 wt.% Nb alloy.

Variations in silicon and iron content and their effects on the mechanical properties of L-605 or Haynes Stellite No. 25 (Co–Ni–W–Cr alloy) have been determined.[95] It was found that the reduction of silicon content from a level of 0.49 to 1.0 to one of 0.12 to 0.23 wt.% increased the room-temperature ductility from 2 to 13% after the alloy had been aged 1000 hr at 1600°F (871°C). No significant effects on mechanical properties were obtained by varying the iron content from 0.16 to 3.24 wt.%. The loss of ductility with the higher silicon alloys was attributed to more precipitate at the grain boundaries. The time to rupture at 1600°F (871°C) with a 17,500-psi load was somewhat reduced by increasing silicon and iron contents. Additions of 1 to 15 wt.% molybdenum to cobalt resulted in an alloy with improved strength and with sufficient ductility to be forgeable.[96] Additions of silicon, beryllium, or aluminum resulted in improved oxidation resistance. Strength and ductility of the alloy were improved by additions of tantalum, niobium, or aluminum.

A Co–Y phase diagram has been constructed.[97] Eight intermetallic Co–Y compounds have been identified. The lowest eutectic (715°C) is formed between Y_3Co and Y_3Co_2 at 37 wt.% cobalt.

Zirconium Alloys

The lattice parameters, atomic volume, nearest-neighbor interatomic distance, axial ratio, and coefficients of thermal expansion of zirconium have been determined[98] up to 1130°K. The occurrence of a yield point in polycrystalline zirconium has been found to be dependent on grain size and temperature.[99] It was found that the occurrence of the yield point could be correlated to the strain-hardening coefficient. The factors that promoted a yield point were small grain size and low strain-hardening coefficients. For low stresses it has been shown that diffusion-controlled creep may become important with most of the creep occurring by grain-boundary diffusion.[100] It is theoretically predicted that a grain size of 0.5×10^{-3} in. can limit the creep strain to 1% in 100,000 hr at 300°C with a load of about 16,000 to 30,000 psi.

In recent years the main concern with zirconium alloys in water-cooled reactors has been the formation of zirconium hydride platelets. These platelets cause a large reduction in ductility when they are oriented perpendicular to the direction of stress. A good summary of the recent research on hydrogen in zirconium alloys was presented by various investigators at the 128th Electrochemical Society Meeting in Buffalo, N. Y. These papers have been published in two issues of *Electrochemical Technology*.[101]

Better hydrogen impregnation of zirconium alloys can be obtained by using a hydrogen furnace instead of pressurized water at elevated temperatures.[102] At 400°C, introduction of CCl_4 into the furnace is very effective in removing the thin ZrO_2 film that usually is present on the surface of zirconium alloys. Removal of the ZrO_2 film results in a rapid rate of ingress of hydrogen into the sample. The terminal solubility[103] of hydrogen in Zircaloy-2 has been determined and is given in Fig. IV-32. These results

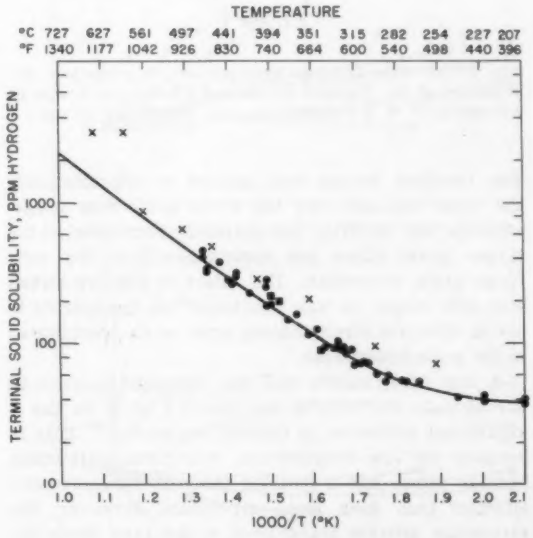

Fig. IV-32 Terminal solid solubility of hydrogen in Zircaloy-2 as a function of temperature.[103] ●, *General Electric (Ontario);* ×, *A. Sawatzky, diffusion and solubility of hydrogen in the alpha phase of Zircaloy-2,* Journal of Nuclear Materials, *2(1): (1960);* ■, *A. Sawatzky, Atomic Energy of Canada Ltd., 1965.*

are somewhat lower than those reported by earlier investigators. It has been shown that addition of 100 ppm hydrogen to alpha zirconium results in considerable loss of ductility for large-grained material.

The tensile properties[104] of hydrided and nonhydrided zirconium as a function of grain size, as determined at Chalk River, are illustrated in Fig. IV-33. Samples containing 100 ppm hydrogen were vacuum annealed for various periods of time at 700°C to produce complete recrystallization and various amounts of grain growth. The samples then were slowly cooled to produce grain-boundary hydrides.

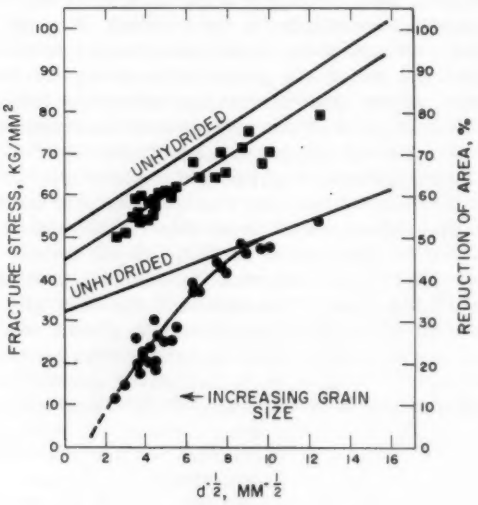

Fig. IV-33 The effect of hydrogen on the grain-size dependence of the fracture stress and % reduction in area of zirconium.[104] ●, % reduction in area; ■, fracture stress.

The fracture stress was reduced by approximately the same amount over the whole grain-size range, whereas the ductility was markedly decreased at the larger grain sizes and approached zero for very large grain diameters. The effect on the flow stress was only slight. It was concluded that the hydride is not an effective strengthening agent when precipitated in the grain boundaries.

It has been shown that the hydrogen content in Zircaloy-2, Zircaloy-4, and Zr–2.5 wt.% Nb has a significant influence on thermal expansion.[105] This is because the low-temperature, tetragonal, zirconium hydride phase has a smaller thermal-expansion coefficient than does alpha zirconium. However, the zirconium hydride transforms to the less dense fcc phase, which has a considerably higher thermal-expansivity than does the alpha-zirconium phase. No specific temperature of the transformation was reported by the investigators. The abrupt change in the thermal expansion of hydrided Zircaloy is shown in Fig. IV-34. Figure IV-35 shows that the impact strength of hydrided Zircaloy increases rapidly and approximates the impact strength of nonhydrided Zircaloy at 200°C. Although the temperatures where the thermal expansion undergoes an abrupt change and the impact strength of hydrided Zircaloy increases are not exactly the same, there is a possibility that both of these phenomena are related to the phase change in zirconium hydride. Recent microindentation tests[108] of hydrided zirconium indicate that zirconium hydrides can deform plastically up to at least 8% at 50°C. These hardness tests also indicate much higher tensile strengths for zirconium hydrides than the results derived by tensile testing.

The prior beta grain size has no significant effect on room-temperature strength of alpha-Zr–2.5 wt.% Nb alloys.[107] However, the elongation is reduced from 20 to 8% as the prior beta grain size is increased from 2 to 100 mils.

The effect of stress on the orientation of hydride platelets in zirconium was investigated by Walters[106]

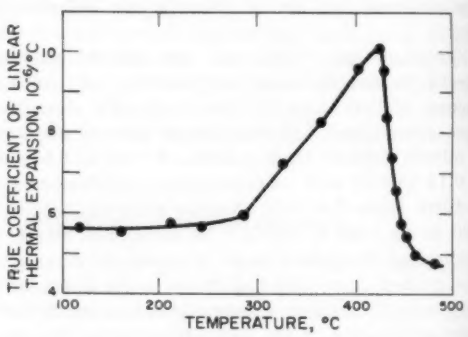

Fig. IV-34 Variation of thermal expansivity with temperature for Zircaloy-4 containing 260 ppm hydrogen by weight.[105]

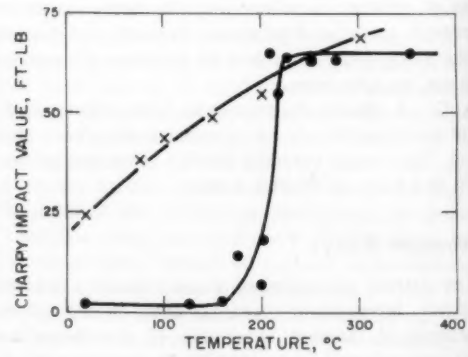

Fig. IV-35 Impact transition curve for hydrided Zircaloy specimens containing ~60 ppm hydrogen by weight.[105] ×, nonhydrided; ●, hydrided.

by means of transmission electron microscopy. Specimens were hydrogenated by steam treatment at 400°C, and the hydrides were precipitated by cooling under different applied tensile stresses. Precipitation was found to occur only on $10\bar{1}0$ planes, and a stress-orientation effect was observed when the stress axis was normal to both $10\bar{1}0$ and $11\bar{2}0$ planes. In addition, the effect of a constant density of hydride platelets on the tensile properties of zirconium was studied as a function of specimen thickness. Hydriding of these specimens produced slight increases in the 0.1% proof stress and ultimate tensile strength compared with those of heat-treated control specimens. Thin specimens were hardened slightly more than thick specimens. The decrease in elongation to fracture on hydriding was much greater in the thinner specimens, however. The hydrides were found mainly at the grain boundaries in all specimens, and fracture occurred across hydride platelets and at hydride–matrix interfaces. Electron-microscope-replica studies revealed that thin specimens failed in a brittle manner whereas the thicker specimens showed typical ductile fracture by void growth and agglomeration.

The fracture of zirconium-containing hydride precipitates has been examined by Beevers.[109] The fracture process was found to occur in three stages: (1) crack propagation within the hydride precipitates, (2) propagation of the hydride cracks into the zirconium, and (3) propagation of the zirconium cracks.

Niobium and Tantalum Alloys

The effects of various alloying elements on the strength and ductility of niobium alloys at room temperature and 1100°C have been determined by the Russians.[110] These effects are illustrated in Figs. IV-36 to IV-38. There is considerable difference in the relative strengthening effect of the various elements on niobium when compared with the results[111] discussed in the previous issue of *Reactor Materials*. In the United States considerable effort has been directed toward development of niobium- and tantalum-base alloys having good elevated-temperature strength, weldability, and ductility at low temperatures which make for ease of fabrication. Some of the elements which have been added are W, Zr, Mo, V, Hf, Y, Ti, and C. In a recent Bureau of Mines study, the mechanical properties of 23 different alloys were determined.[112] The best properties were exhibited by Nb–20 wt.% Hf–5 wt.% W–10 wt.% Ti. A recrystallized sample of this material was fabricable at room temperature and had a strength of 44,000 psi at 1200°C. The material had excellent oxidation resistance, the oxidation rate being 7.7 mg/(cm)(hr) at 1000°C. U. S. patents have been issued to General Electric for niobium- and tantalum-base alloys[113,114] and to General Telephone and Electronics Laboratory, Inc., for a tantalum-base alloy.[115] These refractory-

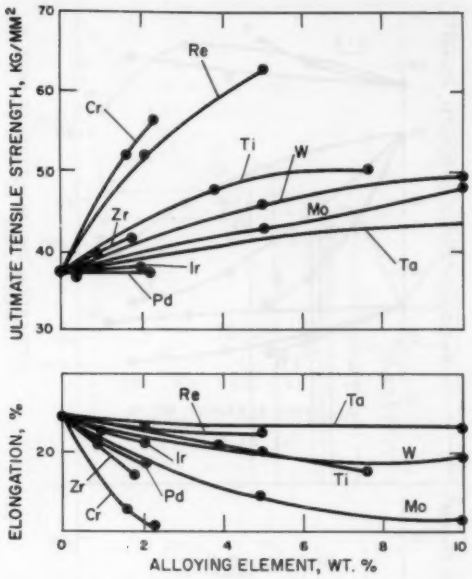

Fig. IV-36 Effect of concentration of alloying elements on room-temperature strength and ductility of niobium.[110]

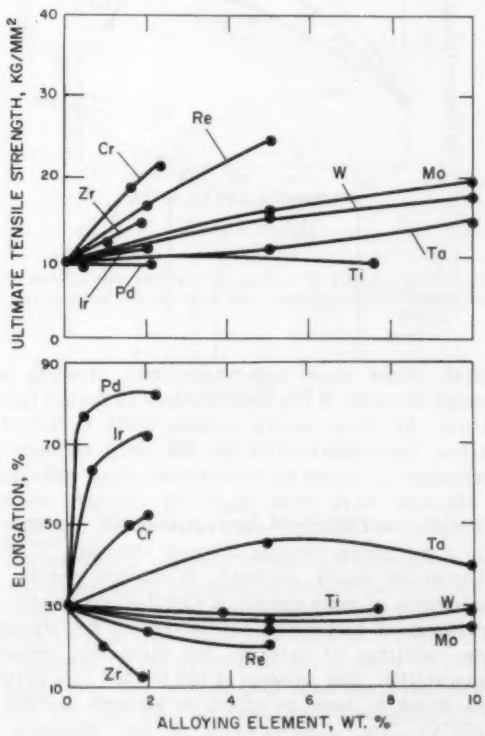

Fig. IV-37 Effect of composition on the tensile properties of niobium alloys at 1100°C.[110]

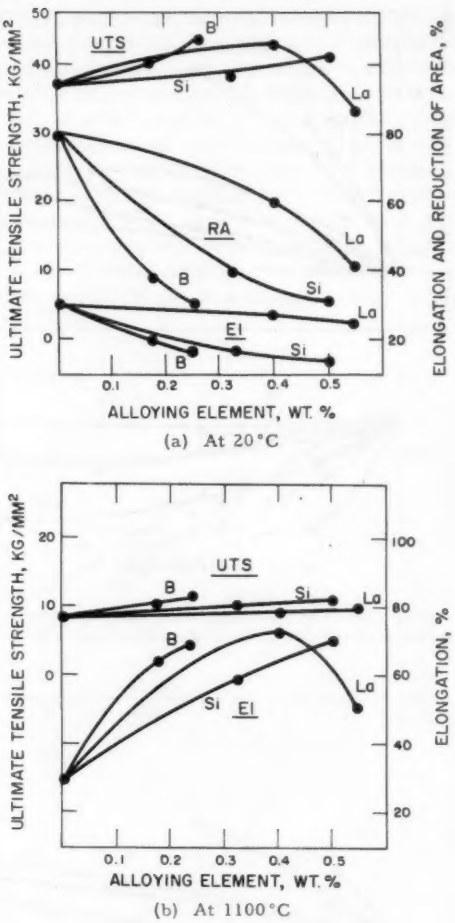

Fig. IV-38 Effect of boron, lanthanum, and silicon concentration in niobium alloys on their tensile properties.[110]

metal alloys have high-temperature strength and enough ductility at low temperatures to permit fabrication. All these alloys contain 0.004 to 0.2 wt.% carbon and either 0.01 to 3.0 wt.% hafnium or zirconium to impart elevated-temperature strength.

Attempts have been made to improve the hot strength, weldability, and fabricability of Ta–W alloys by adding various alloying elements,[116a] The addition of small amounts of yttrium results in restriction of grain growth at elevated temperatures. Additions of zirconium are better for hot strength than additions of hafnium, but zirconium reduces fabricability. The addition of 400 to 1500 ppm carbon was found to have no effect on strength at 3500°F (1928°C). The dispersion of fine carbides in tantalum-base alloys, which have been solid-solution strengthened by additions of tungsten, rhenium, and hafnium, results in improved strength at 3500°F (1928°C) with good low-temperature ductility.[116b] For optimum elevated-temperature properties, the carbon content should be more than 0.05 wt.%. The alloys do not age harden, and they have high recrystallization temperatures. The elevated-temperature ductility is somewhat impaired by hot shortness that results from strain-induced precipitation and grain coarsening.

The physical and mechanical properties of Cb-753 (Nb–10 wt.% W–2.5 wt.% Zr) have been summarized.[116c] This alloy has excellent short-time elevated-temperature strength, fabricability, and weldability. The strength in the alloy is derived from fine ZrO_2 particles dispersed in a matrix of Nb–V–Zr solid solution. The alloy has excellent bend ductility, and its weldments show good ductility at liquid-nitrogen temperatures.

The Nb–Hf–N alloys appear to follow a classical precipitation hardening on heat-treatment.[117] The Nb–5 wt.% Hf–0.2 wt.% N alloy hardens because of precipitation of HfN until overaging occurs at 800 to 900°C. A rapid decrease in hot hardness occurs at 980°C, but at 1300°C the hot hardness is still considerably higher than that of a Nb–5 wt.% Hf. This alloy exhibits an elevated-temperature strength after aging at 1200°C which is superior to that of commercially available niobium alloys. However, engineering applications of the alloy are severely limited by its low ductility at low and high temperatures. This low ductility is associated with the HfN precipitation at the grain boundary.

It has been demonstrated that optimum thermal-mechanical processes are available that can result in the best room-temperature or elevated-temperature properties of the precipitation-hardenable dispersion-hardened niobium alloy Cb-132 (Nb–20 wt.% Ta–15 wt.% W–5 wt.% Mo modified with various zirconium and carbon additions).[116d] Time was observed to be an important parameter in thermal–mechanical processes since it determined whether strain-induced precipitation and overaging or accelerated spheroidization would predominate.

The stress to rupture[118] of D-43 (Nb–10 wt.% W–1 wt.% Zr–0.1 wt.% C) can be increased by annealing the material at 1538°C for 1 hr. Further improvements in stress-rupture properties can be obtained for ½ hr at 1649°C, cold working 25%, and then annealing at 1427°C for 1 hr. The cold working in the second heat-treatment is believed to furnish dislocations for the carbide particles to precipitate, which results in a finer and more dispersed precipitate. Aging of the heat-treated alloy at 982°C for 500 hr results in short-time stress-rupture properties that are lower than those exhibited by the as-received material.

The creep mechanism[119] of Nb–20 wt.% Ta–15 wt.% W–5 wt.% Mo was studied between 980 and 1370°C. It was found that nondiffusion-controlled mechanisms such as crystallographic slip were pre-

dominant below about 1050°C. Above this temperature, diffusion-controlled creep mechanisms such as grain-boundary sliding and substructure formation become predominant. Recrystallization in niobium single crystals was found to originate at the intersection of twins.[120]

The bcc beta phase in Nb–Zr alloys decomposes into two bcc phases by a spinoidal transformation, with one phase rich in niobium and the other rich in zirconium.[121] These two phases are stable only between 600 and 950°C and decompose, on further cooling, to another bcc niobium phase and a hcp zirconium phase, respectively. The rate of the spinoidal transformation was found to vary little with zirconium content. Cold-working the material 90% speeds up the decomposition by a factor of 10 to 15. However, the decomposition is slowed down by a factor of 10 to 20 by increasing the grain size 200-fold.

Recent research has resulted in the completion of several binary and ternary phase diagrams. The two tentative Nb–Co diagrams[122,123] are shown in Figs. IV-39 and IV-40. Figure IV-41 shows the Nb–Al

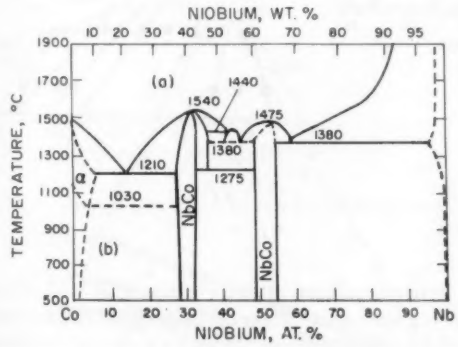

Fig. IV-39 The Nb–Co phase diagram.[122] (a) Liquid; (b) magnetic transformation.

phase diagram.[124] Equilibrium diagrams of the ternary systems Nb–Hf–C, Nb–Zr–C, and Nb–Ti–C were determined by X-ray diffraction and metallography.[125] These systems, shown in Fig. IV-42, illustrate the continuous solid solutions of the monocarbides. Only limited solubility of hafnium, zirconium, and titanium was found in Nb_2C.

The isothermal cross section of the Ta–Hf–C system at 2050°C has been determined[126] and is shown in Fig. IV-43. No phases other than those appearing in the three binary systems were observed. A liquid phase was found in the hafnium-rich corner of the ternary section. The evaporation rates of mixed Ta–Hf carbides with carbon contents varying from 41 to 50 wt.% have been determined[127] at temperatures of 2200 to 3000°K.

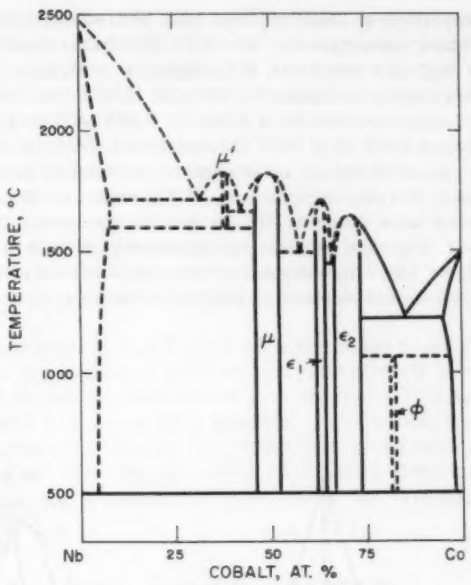

Fig. IV-40 Possible equilibrium diagram of the Nb–Co system.[123]

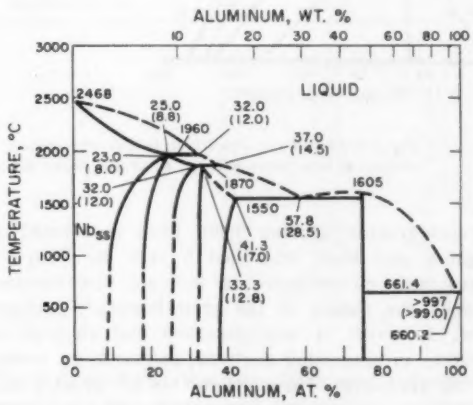

Fig. IV-41 The Nb–Al phase diagram.[124]

Tungsten, Rhenium, and Molybdenum Alloys

The effects of carbon, oxygen, and nitrogen on the room-temperature mechanical properties of single-crystal tungsten were determined.[128] Increasing the carbon content from 0.0012 to 0.054 wt.% resulted in an increase in the yield strength of from 48,300 to 104,000 psi. The reduction of area decreased from 100 to 40%, and the NDT temperature increased from −196 to 0°C. No changes in microhardness were detected. The changes in mechanical properties were due to the straining of the cubic lattice by hexagonal

W_2C particles. These findings have been substantiated by other investigators, who have found that Fe_3W_3C and W_2C are the cause of brittleness in tungsten.[129] Impregnation by oxygen for 48 hr at 1200°C (increasing oxygen content from 0.001 to 0.002 wt.%) and by nitrogen for 5 hr at 2300°C (content not analyzed) did not result in significant changes in mechanical properties at room temperature.[128] No oxide or nitride phases were detected. These results concerning the effect of oxygen and nitrogen disagree somewhat with data by other investigators, who report considerable dependence of mechanical properties on impurities.

elevated-temperature strengths on the order of 3 to 5 times that of unalloyed tungsten can be obtained. A U. S. patent has been issued to the AEC on an easily sinterable and machinable tungsten alloy that contains 0.3 to 0.5 wt.% nickel and 0.8 to 1.1 wt.% iron.[132]

Recently considerable interest has been shown in rhenium technology. The effects of various elements on mechanical and physical properties of rhenium have been determined.[133] The recrystallization temperature[134] for high-purity rhenium was found to be between 1000 and 1500°C, and the recrystallization temperature of cast rhenium was 1200 to 1750°C.

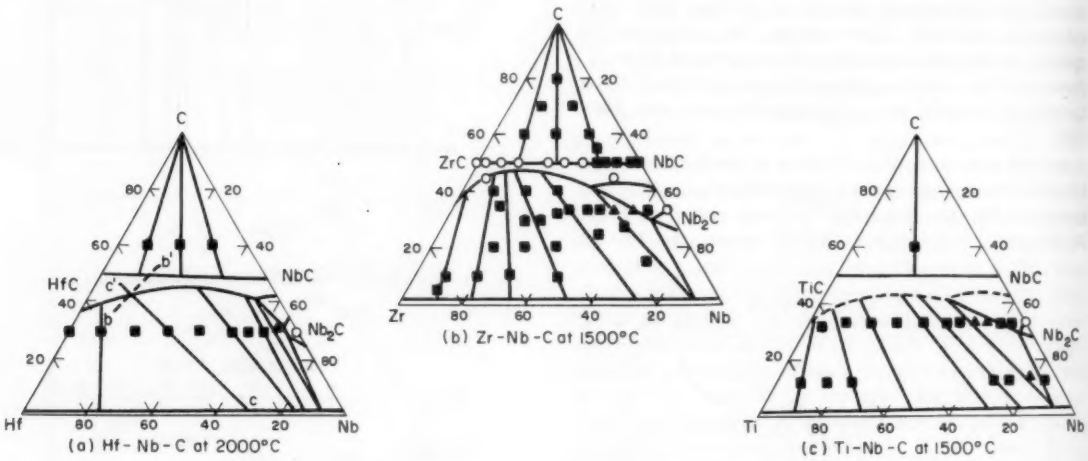

Fig. IV-42 Phase equilibria in various ternary systems.[125] Concentrations are in at.%. ○, single-phase alloys; ■, two-phase alloys; ▲, three-phase alloys.

Fractographic studies have been performed on tungsten and W–3 wt.% and 5 wt.% Re alloys.[130] There was no evidence to indicate that rhenium changes the nature of the grain-boundary precipitates; however, it was observed that rhenium is effective in promoting ductility, primarily by reducing the grain size. The ductility[131] of W–30 wt.% Re–30 wt.% Mo can be restored by stress relieving above 1575°C. There were numerous cracks in the sigma-phase particles at stress-relieving temperatures below 1625°C. Therefore it is recommended that a temperature of above 1650°C be used for best results. In investigating[116e] the effect of ThO_2 dispersions on W–5 wt.% Re, the ThO_2 content was varied from 1.1 to 4.4 wt.%. The optimum strength at 1600°C and low-temperature ductility were obtained with 2.2 wt.% ThO_2.

Tungsten alloys containing niobium, hafnium, or zirconium, along with varying carbon contents, can be obtained by vacuum-arc-melting procedures.[116f] These alloys can be fabricated after encapsulation in molybdenum. The recrystallization temperature range is 3400 to 4800°F (1870 to 2650°C), and

The critical amount of deformation that was necessary for the start of recrystallization was between 3 and 5%. Figure IV-44 shows a Re–Cr–C isotherm at 1300°C developed by the Russians.[135]

Hot workability of electron-beam-melted molybdenum was studied as a function of alloying additions.[136] Additions of boron, zirconium, and silicon resulted in a reduction in grain size. Hardness was decreased by the addition of zirconium, rhenium, and carbon, and, consequently, the hot workability was improved by eliminating cracking at grain boundaries. All the additions were found to increase the recrystallization temperature of molybdenum, with the postrecrystallization hardness being considerably increased.

A high-ductility molybdenum sheet has been developed by workers at the Bureau of Mines.[137] The sheet is obtained by high-temperature, high-vacuum sintering treatments and by the use of metal deoxidizers instead of carbon. The sheet has exceptionally good room-temperature ductility (31% elongation) after recrystallization. The elevated-temperature embrittlement of molybdenum is believed to be caused

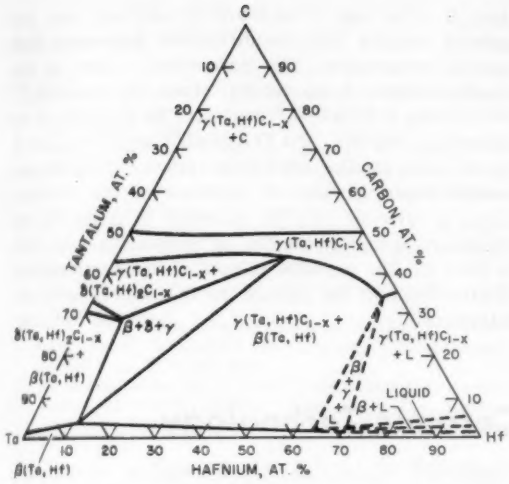

Fig. IV-43 Proposed isothermal cross section[126] of Ta–Hf–C system at 2050°C. Phase determined by X-ray diffraction.

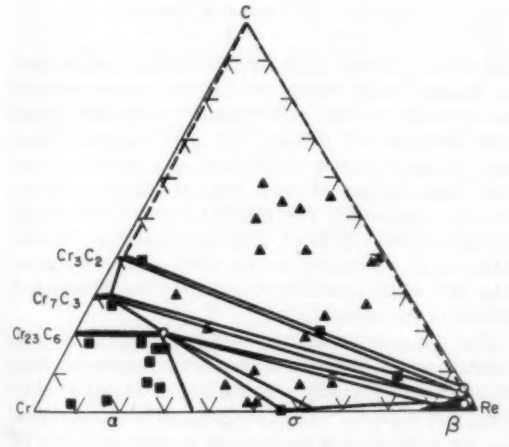

Fig. IV-44 The 1300°C isotherm of the Re–Cr–C phase diagram.[135] ○, single-phase; ■, two phase; ▲, three phase.

by different mechanisms at different temperatures.[138] At 800°C the cause of embrittlement is interaction with interstitial impurities. At 1300°C the embrittlement is attributed to a weakness in grain boundaries, which is due to void formation by vacancy diffusion.

Miscellaneous

Magnesium alloys containing 8.2 to 10.6 wt.% yttrium, which are oxidation resistant up to 510°C, have been developed.[139] These alloys are age hardenable and have yield strengths of up to 55,000 psi, with elongations of about 10%.

Recrystallization studies[140] have been performed on Magnox AL80 (Mg–0.73 wt.% Al with minor beryllium and zinc additions) that had been deformed at 200°C. Results of the recrystallization study (Table IV-7) indicate that secondary recrystallization occurs at 400°C, centered on about 30% deformation. The secondary recrystallization is believed to be caused by segregation of beryllium at the grain boundaries, which restricts grain growth at lower temperatures. As the temperature is increased, diffusion of beryllium becomes significant; this unpins the grain boundaries, allowing grain growth at about 400°C.

Additions of 0.35 to 0.95 wt.% zirconium to aluminum were found to increase the yield strength fourfold to sixfold above that of pure aluminum.[141] With a sixfold increase in yield strength, the total elongation decreased to 13%, and the reduction in area remained at about 81%. The electrical conductivity of the material was considerably reduced by the zirconium additions.

Table IV-7 GRAIN SIZE[140] IN MAGNOX AL80 DEFORMED AT 200°C AND ANNEALED AT VARIOUS TEMPERATURES FOR 1 HR

Deformation, %	Grain size, 10^{-3} in., at indicated annealing temperature		
	200°C	300°C	400°C
0.0			3.29
1.4	2.80	4.34	8.27
2.0	2.96	4.05	5.07
2.7	2.96	4.29	4.76
4.1	2.64	3.87	4.64
4.7	2.70	3.44	
5.4	2.67	3.12	3.78
6.1	2.81	2.52	3.88
7.1	2.40		
7.4			3.58
8.1			3.00
10.1	2.55	1.89	3.50
20.0	1.77	1.38	4.48
30.0	1.31	1.18	4.54
40.0	0.67	1.10	4.39
50.0			3.94

The effect of material removal by electrochemical methods on the mechanical properties of various metals and alloys has been reviewed by the DMIC.[142] The processes discussed are electrochemical machining, electrolytic grinding, electrochemical milling, and electropolishing. Generally, these processes result in a smoother surface than that obtained by mechanical means. The mechanical properties of materials that are easily worked mechanically are not affected. However, the mechanical properties of materials that are difficult to form, such as tungsten and beryllium, are considerably improved since a better surface is obtained. In some instances the fatigue strength is reduced by electrochemically working the surface. This is attributed to removal of surface material containing residual stresses that improve the fatigue properties. (M. Kangilaski)

Diffusion Studies

A bibliography by Askill on tracer diffusion in metals was noted in *Reactor Materials*, Summer 1966. A supplement[143] has been published to Parts I and II of the bibliography which concerned self-diffusion and impurity diffusion, respectively. The supplement contains additional data from diffusion literature reported in 1965. A bibliography and tabulation of self-diffusion data in metal oxides has also been compiled at Harwell.[144] This document surveys the literature from 1946 to 1965 and contains 117 references from which self-diffusion coefficients in simple metal oxides were extracted. The oxides reported include those of Al, Be, Hf, Mg, Ni, Si, and Ti and rare-earth oxides of Ce, Pr, and Tb, and extensive self-diffusion data on UO_2 and ZnO.

Fission-product diffusion in nonfuel materials has been reviewed in a publication from General Atomic.[145] The authors discuss theoretical aspects concerned with radiation damage and its effects on diffusion, the derivation of diffusion equations, and the effects of gas-bubble formation and swelling on diffusion. Also included are reviews of fission-product migration in metals, agglomeration of inert gases in metals, and fission-product diffusion in ceramics and carbon materials. The fission products reviewed included noble gases and relatively volatile nonmetallic elements, such as Se, Te, Br, and I, and metallic products that involve some 28 elements. The report is supplemented with 243 references. Additional work at General Atomic[146] involved studies of diffusion phenomena of UO_2 and UC–ZrC materials clad with refractory metals and alloys at temperatures between 1400 and 2000°C. The refractory metals W, Mo, Ta, Nb, Ir, Re, and W–25 wt.% Re, and two alloys of W–Mo were studied. Interactions at the interface were examined, as were the effects of composition, stoichiometry, and temperature on electron-emission properties of the clad materials in vacuum.

Lawrence Radiation Laboratory[147] has investigated the diffusion of ^{59}Fe in Fe–5.7 at.% Al to determine the effects of substitutional solutes on the self-diffusion of iron. The data obtained fit the equation $D = 3.67 \exp(-58{,}700/RT)$ cm^2/sec in the temperature range 850 to 1185°C. The values for the activation energy are slightly lower than the current values for ^{59}Fe diffusion in iron, and the frequency factor is slightly higher. These changes in self-diffusion parameters are attributed to the aluminum content in the iron solvent; no anomalous or other changes from the iron self-diffusion pattern were noted.

Carbon diffusion in NbC was examined by Brizes, Cadott, and Tobin[148] over a range of temperature 1700 to 2300°C. The same growth-rate behavior as in TaC discussed above was observed. In NbC, carbon diffuses according to an Arrhenius-type equation, $D = 7.6 \exp(-88{,}200/RT)$ cm^2/sec, and the authors suggest that the diffusivity decreases with carbon composition. The parametric values in the equation differ from values given by Resnick,[149] $D = 1.2 \exp(-79{,}000/RT)$ cm^2/sec. An experiment by Bornstein, Hirokis, and Friedrich[150] used Nb–1 wt.% Zr to make similar studies of carbon diffusivity and carbide-layer growth on surfaces of the niobium alloy. A value of −72,700 cal/mole is given for the activation energy in the NbC at temperatures of 1200 to 1815°C. The possible effects of the small amount of zirconium in the carbide surface layers were not determined. (A. N. Ashurst)

Ceramic Technology

Buford[151] investigated the mechanism of diffusion of helium through single-crystal and polycrystalline alumina in the temperature range 25 to 900°C. In the range from 200 to 700°C, the equation for the coefficient of diffusion along the c-axis was found to be:

$$D = 6.2 \times 10^{-6} \exp(-0.32\text{ev}/KT)$$

The most probable diffusion mechanism, as indicated by the activation energy of 0.32 ev, was considered to be atom-vacancy interchange occurring around edge dislocations. It also was found that the magnitude of the diffusion coefficient was density dependent, and decreased with repeated heating for the samples examined. The estimated activation energy for this process, 0.13 ev, indicated that atom-vacancy interchange, occurring mostly along grain boundaries, was the most probable mechanism for diffusion of helium in this material.

The dependence of the Young's modulus of polycrystalline dysprosium and erbium oxides on temperature and porosity was studied by Manning, Marlowe, and Wilder.[152] The extrapolated modulus values, E_D, for materials of theoretical density were 24×10^6 psi for Dy_2O_3 and 27×10^6 psi for Er_2O_3. The porosity dependence was found to be represented by an equation of the form

$$\frac{E}{E_D} = 1 - AP$$

where A is a constant and P is volumetric void fraction. The constant, which probably is dependent on pore structure, was found to be 2.44 for the Dy_2O_3 and 2.36 for the Er_2O_3. Young's modulus of Er_2O_3 decreased by 13% when the specimens were heated from room temperature to 1000°C. The Young's modulus of Dy_2O_3 decreased at the same rate to 837°C, then dropped more rapidly on heating to 1000°C, reaching a value of 83% of that at room temperature. (H. D. Sheets)

References

1. Norman Hackerman (Ed.), Zirconium Symposium, *Electrochem. Technol.*, 4(3-4): 81-162 (March–April 1966); *ibid.*, 4(5-6): 231-249 (May–June 1966).
2. P. L. Allen, D. A. Moore, and F. W. Trowse, The Relation of Proof Testing to Long-Term Corrosion Behavior of Zirconium Alloys, British Report TRG-Report-1134 (S), May 12, 1966.
3. G. Östberg (Comp.), Progress Report on Reactor Materials and Fuel Elements Other than for Superheaters, Swedish Report S-352, July 1966.
4. Oak Ridge National Laboratory, unpublished, September 1966.
5. N. J. M. Wilkins, Measurement of Anodic and Corrosion Films by Optical Interference, British Report AERE-R-5175, March 1966.
6. F. H. Haynie and W. K. Boyd, Stress-Corrosion Cracking of Aluminum Alloys, Report DMIC-228, Battelle Memorial Institute, Defense Metals Information Center, July 1, 1966.
7. Mcl. R. Louthan, Jr., The Role of Dislocations in Transgranular Stress-Corrosion Cracking of Austenitic Stainless Steel, USAEC Report DP-1008, Savannah River Laboratory, March 1966.
8. C. S. Wukusick, The Physical Metallurgy and Oxidation Behavior of Fe-Cr-Al-Y Alloys, USAEC Report GEMP-414, General Electric Company, Nuclear Materials and Propulsion Operation, June 1, 1966.
9. Société d'Etudes, de Recherches et d'Applications pour l'Industrie, Studies of Steel Corrosion in High-Temperature Water and Steam, Quarterly Report No. 14, USAEC–Euratom Report EURAEC-1625, Apr. 29, 1966.
10. J. M. Francis and W. H. Whitlow, The Morphology of Oxide Film Growth on AISI Type 304 Stainless Steel in High-Temperature Water at 300 and 350 C, *J. Nucl. Mater.*, 20(1): 1-10 (July 1966).
11. D. L. Keller, Progress Relating to Civilian Applications During May 1966, USAEC Report BMI-1774, Battelle Memorial Institute, June 1, 1966.
12. N. D. Greene and F. G. Hodge, Oxidation Characteristics of the Lanthanide Metals, *Corrosion*, 22(7): 206-213 (July 1966).
13. J. M. McKibben, Performance of Mild Steel in D_2O Moderator-Coolant in the HWCTR, *Nucl. Appl.*, 2: 21-26 (January–February 1966).
14. N. D. Tomashov and T. V. Matveeva, Corrosion and Electrochemical Behavior of Rhenium, *Zashch. Metal.*, 2: 57-62 (January–February 1966).
15. B. W. Marshall, An Experimental Study of the Effects of Oxygen on Tantalum Ablation in a Hyperthermal Plasma Tunnel, USAEC Report SC-RR-65-615, Sandia Corp., April 1966.
16. P. F. Campbell, K. A. Gebler, and M. H. Ortner, Development of Oxidation-Resistant Coatings for Use Above 3500°F, Report NASA-CR-65285 (N-66-21018), Vitro Laboratories, September 1965.
17. L. Sama and B. Reznik, Development of Production Methods for High-Temperature Coating of Tantalum Parts, Report AFML-TR-66-217, Sylcor Division, Sylvania Electric Products Inc., August 1966.
18. R. T. Wimper and A. R. Stetson, Development of Coatings for Tantalum Alloy Nozzle Vanes, Report RDR-1396-2, Solar, Division of International Harvester Co., May 13, 1966.
19. J. C. Wurst, J. A. Cherry, and D. A. Gerdeman, Evaluation of Materials Systems for High Temperature Aerospace Applications. Part I. Report AFML-TR-65-339 (Pt. I), University of Dayton Research Institute, July 1966.
20. F. A. Comprelli, F. J. Hetzler, and T. A. Lauritzen, Clad Compatibility with Mixed Oxide Fuel and Sodium, in Proceedings of the Conference on Safety, Fuels, and Core Design in Large Fast Power Reactors, October 11–14, 1965, USAEC Report ANL-7120, pp. 355-373, General Electric Company, Advanced Products Operation.
21. R. C. Andrews, R. H. Hiltz, L. H. Kirschler, S. J. Rodgers, and F. Tepper, Topical Report No. 4. Results of Mechanical Properties Tests of 316 SS Specimens in 1200°F Sodium Contaminated with Carbon, USAEC Report MSAR-65-194, MSA Research Corp., December 1965.
22. R. H. Hiltz, Topical Report No. 6, Effect of Carburization on the Phases in Austenitic Stainless Steel, USAEC Report MSAR-66-119, MSA Research Corp., June 1966.
23. R. C. Andrews, R. H. Hiltz, L. H. Kirschler, S. J. Rodgers, and F. Tepper, Topical Report No. 5, Results of Mechanical Properties Tests of 316 SS Specimens in 1200°F Sodium Contaminated with Oxygen (~300 ppm), USAEC Report MSAR-66-78, MSA Research Corp., May 1966.
24. F. W. Albaugh, S. H. Bush, J. J. Cadwell, D. R. deHalas, and D. C. Worlton, Reactor Fuels and Materials Development Programs for Fuels and Materials Branch of USAEC Division of Reactor Development and Technology, Quarterly Progress Report, January–March 1966, USAEC Report BNWL-CC-694, Battelle–Northwest, May 1966.
25. C. Wohlberg, Estimates of Possibility of Hydrogen Embrittlement of Tantalum in the FRCTF, USAEC Report LA-3508, Los Alamos Scientific Laboratory, Aug. 18, 1965.
26. F. W. Knight, W. A. Hendricksen, G. L. O'Neill, and W. L. Lyon, Compatibility of Oxide Fuels [UO_{2+x} and $(Pu,U)O_{2+x}$] with Sodium and NaK, *Trans. Amer. Nucl. Soc.*, 9(1): 37-39 (June 1966), paper presented at 1966 Annual Meeting of the American Nuclear Society, Denver, Colo., June 20–28, 1966.
27. Oak Ridge National Laboratory, unpublished, July 7, 1966.
28. Allison Division, General Motors Corp., Investigation of Bimetallic Liquid Metal Systems, Progress Report, February 1–May 31, 1966, USAEC Report GMAD-3643-5 (EDR-4719), June 20, 1966.
29. G. P. Benedictova, G. N. Dubinin, M. G. Kapman, and G. V. Shcherbedinskii, Potassium Diffusion into Mono- and Polycrystalline Molybdenum (in Russian), *Metalloved. Term. Obrabotka Metal.*, No. 5: 55-57 (May 1966).
30. Argonne National Laboratory, Reactor Development Program Progress Report, May 1966, USAEC Report ANL-7219, June 30, 1966.
31. Argonne National Laboratory, Reactor Development Program Progress Report, July 1966, USAEC Report ANL-7245, Aug. 26, 1966.
32. M. Bagouin, D. Guerard, and A. Herold, The Action of Lithium Vapor on Graphite, USAEC Report BNL-tr-78, translated by S. J. Amoretty from *Compt. Rend., Ser. C. Chim. Sci.*, 262: 557-559 (Feb. 14, 1966).
33. Atomic Energy of Canada Ltd., unpublished, 1966.
34. R. Garcia and F. G. Hammitt, Ultrasonic-Induced Cavitation Studies in Pb-Bi Alloy 500-1500 F, *Corrosion*, 22(6): 157-167 (June 1966).
35. R. Garcia, F. G. Hammitt, and R. E. Nystrom, Comprehensive Cavitation Damage Data for Water, Mercury, and Lead–Bismuth Alloy Including Correlations with Material and Fluid Properties, Technical Report No. 4, Report NP-16048, University of Michigan, May 1966.
36. R. F. S. Robertson, Fuel, Materials, and Coolants for WR-1, Paper 66-CNA-311 presented at Annual Conference on Organic and Heavy Water Reactors, Winnipeg, May 30–June 1, 1966, Canadian Report AECL-2553, August 1966.
37. Los Alamos Scientific Laboratory, Quarterly Status Report on Advanced Reactor Technology (ART) for Period Ending April 30, 1966, USAEC Report La-3524, May 1966.
38. B. J. Thamer, Corrosion Tests of Hastelloy N, Inconel 600, and HYMU-80 Exposed to UCl_3–KCl at 900°C,

USAEC Report LA-3476, Los Alamos Scientific Laboratory, Feb. 4, 1966.
39. J. H. Stang, E. M. Simons, J. A. DeMastry, and J. M. Genco, Compatibility of Liquid and Vapor Alkali Metals with Construction Materials, Report DMIC-227, Battelle Memorial Institute, Defense Metals Information Center, Apr. 15, 1966.
40. S. H. Fenney, Bibliography on Liquid Metals, 1958–1963, British Report TRG-Inf. Ser.-312 (R).
41. C. J. Kubit, R. N. Stanutz, D. N. Fultonberg, and W. S. Hazelton, A Study of the Zircaloy-Steam Reaction, *Trans. Amer. Nucl. Soc.*, 9(1): 299-300 (June 1966).
42. J. M. Genco and G. E. Raines, Metal-Water Reactions During a Loss-of-Coolant Accident: The Zirconium Steam Reaction, *Trans. Amer. Nucl. Soc.*, 9(2): 555 (October–November 1966).
43. L. Baker and R. O. Ivins, Analyzing the Effects of a Zirconium-Water Reaction, *Nucleonics*, 23(7): 70-74 (July 1965).
44. W. Dienst, H. J. Hauck, and H. J. Laue, Anderung der Mechanischen Eigenschaften von Chrom-Nickel-Stahlen und Nickellegierungen Durch Neutronenbestrahlung, *J. Nucl. Mater.*, 18: 337-347 (1966).
45. H. Böhm, W. Dienst, and H. J. Hauck, Untersuchungen Uber Die Hochtemperatur-Versprodung Von Austenitischen Chrom-Nickel-Stahlen Und Nickellegierungen Durch Neutronenbestrahlung., *J. Nucl. Mater.*, 19: 59-69 (1966).
46. Papers presented at the 69th Annual Meeting of ASTM, Atlantic City, N. J., June 27–July 1, 1966.
    a. I. P. Bell, J. Standring, P. C. L. Pfeil, G. H. Broomfield, K. Q. Bagley, and A. F. Fraser, The Effects of Irradiation on the High-Temperature Properties of Austenitic Steels and on Precipitation-Hardened Nickel Alloy.
    b. W. R. Martin and J. R. Weir, Solutions to the Problems of High-Temperature Irradiation Embrittlement.
    c. A. C. Roberts and D. R. Harries, Effects of Irradiation and Heat Treatment on the High-Temperature Properties of Austenitic Stainless Steel.
    d. A. F. Rowcliffe, G. J. C. Carpenter, H. F. Merrick, and R. B. Nicholson, An Electron Microscope Investigation of the High-Temperature Embrittlement of Irradiated Stainless Steels.
    e. J. R. Hawthorne and L. E. Steele, Metallurgical Variables as Possible Factors Controlling Irradiation Response of Structural Steels.
    f. H. Böhm, W. Dienst, H. J. Hauck, and H. J. Laue, Irradiation Effects on the Mechanical Properties of Vanadium-Base Alloys.
47. United Kingdom Atomic Energy Authority, Atomic Energy Research Establishment, Metallurgy Division, unpublished.
48. H. Böhm, W. Dienst, and H. Hauck, High-Temperature Embrittlement of Austenitic Steels and Nickel Alloys by (n,α) Reactions (in German), *Z. Metallk.*, 57: 352-357 (May 1966).
49. E. E. Bloom, J. O. Steigler, W. R. Martin, and J. R. Weir, Jr., Comparison of Displacement Damage and Strength for Stainless Steel Irradiated at Intermediate Temperatures, USAEC Report ORNL-TM-1535, Oak Ridge National Laboratory, June 1966.
50. W. R. Martin and J. R. Weir, Jr., Irradiation Embrittlement of Low- and High-Carbon Stainless Steels at 700, 800, and 900°C, USAEC Report ORNL-TM-1516, Oak Ridge National Laboratory, June 1966.
51. I. S. Levy and K. R. Wheeler, Improved Postirradiation Tensile Properties of Hastelloy X-280, USAEC Report BNWL-202, Battelle–Northwest, March 1966.
52. I. S. Levy, Improved Postirradiation Stress-Rupture Properties of Hastelloy X-280, USAEC Report BNWL-231, Battelle–Northwest, July 1966.
53. J. E. Irvin, Effects of Irradiation and Environment on the Mechanical Properties and Hydrogen Pickup of Zircaloy, *Electrochem. Technol.*, 4: 240-249 (May–June 1966).
54. C. J. Baroch, J. P. Hoffmann, H. E. Williamson, and T. J. Pashos, Comparative Performance at Zircaloy and Stainless Steel Clad Fuel Rods Operated to 10,000 MWD/T in the VBWR, USAEC Report GEAP-4849, General Electric Company, Nuclear Technology Department, April 1966.
55. M. R. Piggott, Radiation Behavior of Al–SiO_2 Composites, presented at Conference of Metallurgists (CIMM), University of Toronto, August 1966.
56. V. Fidleris and C. D. Williams, Influence of Neutron Irradiation on the Creep of Zircaloy-2 at 300°C, *Electrochem. Technol.*, 4: 258-267 (May–June 1966).
57. D. S. Wood, J. Winton, and B. Watkins, Effect of Irradiation on the Impact Properties of Hydrided Zircaloy-2 and Zirconium-Niobium Alloy, *Electrochem. Technol.*, 4: 250-258 (May–June 1966).
58. C. E. Ells and V. Fidleris, Effect of Neutron Irradiation on Tensile Properties of the Zirconium-25 Niobium Alloy, *Electrochem. Technol.*, 4: 268-274 (May–June 1966).
59. Atomic Energy of Canada Ltd., unpublished, 1966.
60. J. E. Irvin and T. T. Claudson, The Effects of Irradiation and Environment on the Mechanical Properties of Inconel-Zircaloy Transition Joints, USAEC Report BNWL-190, Battelle–Northwest, February 1966.
61. N. Milasin, Contribution a l'Etude du Durcissement par Irradiation d'un Acier Faiblement Allie Destine au Caisson de Reacteurs, *J. Nucl. Mater.*, 19: 301-311 (1966).
62. C. V. Taylor and J. G. Goodwin, A Compilation of the Properties of Hafnium, USAEC Report WAPD-TM-528, Westinghouse Electric Corporation, Bettis Atomic Power Laboratory, August 1966.
63. J. S. Bryner, A Study of Neutron Irradiation Damage in Iron by Electron Transmission Microscopy, *Acta Met.*, 14: 323-336 (March 1966).
64. R. M. J. Cotterill, A Comparison Between Neutron Damage in Annealed Gold and in Quenched Gold, *Appl. Phys. Lett.*, 9: 29-31 (July 1, 1966).
65. R. L. Colombo, F. S. Rossi, and J. Sebille, The Effect of Nitrogen on the Radiation Embrittlement of Iron, *Solid State Commun.*, 4: 55-58 (January 1966).
66. A. Cowan, G. D. Fearnehough, J. Gillies, and G. M. Lees, Irradiation Damage in Mild Steel: A Comparison of Crack Arrest Test and Charpy Criteria and the Influence of Neutron Spectrum, British Report TRG-Report-1069, Feb. 10, 1966.
67. C. R. Honeycutt and J. C. Sawyer, Determination of Elevated-Temperature Fatigue Data on Refractory Alloys in Ultra-High Vacuum, Report NASA-CR-54916, TRW Inc., Jan. 15, 1966.
68. C. D. Calhoun, Ductile-to-Brittle Transition of Niobium-Vanadium Alloys with Small Ratios of Specimen Diameter to Grain Diameter, USAEC Report KAPL-3146, Knolls Atomic Power Laboratory, August 1965.
69. R. L. Stephenson, Creep-Rupture Properties of FS-85 Alloy and Their Response to Heat Treatment, USAEC Report ORNL-TM-1456, Oak Ridge National Laboratory, July 1966.
70. H. E. McCoy, Jr., An Evaluation of the Creep Properties of Cb-753 and a Comparison of This Alloy with Several Other Niobium-Base Alloys, USAEC Report ORNL-TM-1347, Oak Ridge National Laboratory, January 1966.
71. H. E. McCoy, Jr., Creep-Rupture Properties of the Tantalum-Base Alloy T-222, USAEC Report ORNL-TM-1576, Oak Ridge National Laboratory, September 1966.
72. Illinois Institute of Technology Research Institute, Vanadium Alloy Studies, Final Report, March 1, 1965–May 31, 1966, USAEC Report IITRI-B6042-5, June 29, 1966.
73. H. E. McCoy, Jr., Creep-Rupture Properties of Tung-

sten and Tungsten-Base Alloys, USAEC Report ORNL-3992, Oak Ridge National Laboratory, August 1966.
74. H. G. Sell, W. R. Morcom, G. W. King, and N. F. Cerulli, Development of Dispersion-Strengthened Tungsten-Base Alloys, Report AFML-TR-65-407 (Pt. 1), Westinghouse Electric Corp., October 1965.
75. R. G. Garlick, Effect of Orientation on Ductile-to-Brittle Transition of Tungsten Single Crystals, Report NASA-TMX-1252, National Aeronautics and Space Administration, Lewis Research Center, July 1966.
76. R. J. Goode, R. W. Huber, D. G. Howe, R. W. Judy, Jr., P. P. Puzak, K. B. Lloyd, T. W. Crooker, R. E. Morey, E. A. Lange, and C. N. Freed, Metallurgical Characteristics of High-Strength Structural Materials, Report AD-634094 (NRL-6405), Naval Research Laboratory, November 1965.
77. Atomics International, Annual Technical Progress Report, AEC Unclassified Programs, Fiscal Year 1966, USAEC Report NAA-SR-12010, Aug. 31, 1966.
78. Mechanical Properties Data Center, Nickel- and Chromium-Base Alloys, May 1, 1966.
79. Ames Laboratory, Annual Summary Research Report of Chemistry, Engineering, Metallurgy, Physics, and Reactor Divisions, July 1, 1965–June 30, 1966, USAEC Report IS-1500, July 1966.
80. C. S. Lee, Hardening Mechanisms in a Cobalt-Base Superalloy, Report AD-635249, University of Arizona, May 1966.
81. M. Inagaki, I. Okane, and H. Suzuki, Effect of Exposed Time at Elevated Temperature on the Embrittlement of Welded Joints of HT 60 Steel for Nuclear Pressure Vessels, Japanese Report NSJ-tr-60, translated from *Yosetu Gakkaishi*, 33: 1010-1019 (1964).
82. Centre National de Recherches Metallurgiques, A Study of Plastic Fatigue Embrittlement of Reactor Pressure Vessel Steels, Quarterly Report No. 8, October 1–December 31, 1965, USAEC–Euratom Report EURAEC-1547.
83. M. Weisz and M. Erard, Contribution to the Study of the Embrittlement, by Alternating Plastic Deformations of Steel for Nuclear Reactor Vessel (in French), *Mem. Sci. Rev. Met.*, 63: 180-188 (February 1966).
84. T. Ando and H. Susukida, Heat Treatment for Improving the Notch Toughness for Heavy Section Mn–Mo Steel for Nuclear Reactor Vessels, *Mitsubishi Juko Giho (Mitsubishi Heavy Industries Technical Review)*, 3: 36-42 (January 1966).
85. Société des Forges et Ateliers du Creuset, Basic Study on a Few Embrittlement Forms Affecting Joints Welded on High Resistance Steel; and on Means of Improving Their Mechanical Properties, USAEC–Euratom Report EURAEC-1419, May 1965.
86. G. P. Contractor and D. A. Munro, Some Observations of the Tempering Response of Low-Carbon Uranium-Bearing Steels, *Trans. Met. Soc. AIME*, 236: 447-454 (April 1966).
87. N. P. Kuleshova and V. G. Lutsyak, Solubility of Zirconium in the Ferrite of Low-Carbon Steel, *Metalloved. Term. Obrabotka Metal.*, No. 12: 43-44 (1964).
88. R. W. Nichols, T. F. Pearson, and A. G. Haynes, Improvements Relating to Low Alloy Steels, British Patent No. 1,020,572, Feb. 23, 1966.
89. R. A. Winborne, Brittle Failures of Carbon Steel Tubes, USAEC Report NAA-SR-Memo-11707, Atomics International, Nov. 15, 1965.
90. B. Hattersley and W. Hume-Rothery, Constitution of Certain Austenitic Steels, *J. Iron Steel Inst. (London)*, 204 (7): 683-701 (July 1966).
91. A. V. Smirnova and V. A. Sol'ts, Structural Transformation in 36 NKhTYu Alloys with Molybdenum, *Metalloved. Term. Obrabotka Metal.*, No. 2: 2-6 (1965).
92. C. J. Slunder and A. M. Hall, Thermal and Mechanical Treatments for Nickel and Selected Nickel-Base Alloys and Their Effect on Mechanical Properties, Report NASA-TMX-53443 (N66-23858), Battelle Memorial Institute, Apr. 20, 1966.
93. I. E. Kontorovich, Effects of Molybdenum on the Properties of Nickel-15 Chromium Alloy, *Metalloved. Term. Obrabotka Metal.*, 1: 19-21 (January 1966).
94. G. A. Sbeshnikova, Nickel-Chromium Alloys with Niobium, *Metalloved. Term. Obrabotka Metal.*, 1: 29-34 (January 1966).
95. G. D. Sandrock, R. L. Ashbrook, and J. C. Freche, Effect of Variations in Silicon and Iron Content on Embrittlement of L-605(HS-25), Report NASA-TMX-52099 (N66-18360), National Aeronautics and Space Administration, Lewis Research Center, October 1965.
96. J. J. Rausch and J. B. McAndrew, Cobalt-Base Alloys Containing Molybdenum, U. S. Patent No. 3,243,289, to U. S. Navy, Mar. 29, 1966.
97. K. J. Struat, The Yttrium-Cobalt Alloy System, paper presented at Fifth Rare-Earth Research Conference held at Wright-Patterson Air Force Base, Ohio, August 30–September 1, 1965.
98. J. Goldak, Lattice Parameters, Thermal Expansion, and Grueneisen Coefficients of Zirconium at 4.2 to 1130°K, *Phys. Rev.*, 144: 478-484 (Apr. 15, 1966).
99. Illinois Institute of Technology Research Institute, Yield Phenomena and Fracture of Hydrided Zirconium, Quarterly Report, January 1–March 31, 1966, USAEC Report IITRI-578P27-17, May 4, 1966.
100. R. B. Jones, Diffusion Creep in Zirconium Alloys, *J. Nucl. Mater.*, 19: 204-207 (May 1966).
101. Papers presented at 128th Electrochemical Society Meeting, Buffalo, New York, October 10–14, 1965, *Electrochem. Technol.*, 4(5-6) (May–June 1966); *ibid.* (7-8) (July–August 1966).
102. J. Winton, A Method for Gas-Hydriding Zirconium Alloys at 400°C, British Report TRG-Report-1255, May 20, 1966.
103. A. R. Daniel, Terminal Solid Solubility of Hydrogen in Zircaloy-2, Canadian Report AECL-2453 (DF65CAP-31), June 6, 1965.
104. C. E. Coleman and D. Hardie, The Influence of Grain Size on the Tensile Properties of Hydrided Alpha Zirconium, *J. Nucl. Mater.*, 19: 201-203 (May 1966).
105. G. F. Slattery, Effect of Hydride on the Thermal Expansivity of Zirconium Alloys, *J. Less-Common Metals*, 11: 89-98 (August 1966).
106. J. F. R. Ambler, Effect of Temperature on the Micro-Indentation Properties of Zirconium Hydride, Canadian Report AECL-2538, March 1966.
107. L. G. Bell and T. S. Dicks, The Effect of Prior Beta Grain Size on the Ductility of Zirconium–2.5 Wt.% Niobium Alloy, *Can Met. Quart.*, 4: 259-68 (October–December 1966).
108. G. P. Walters, Hydride Morphology in Stressed Zirconium and the Influence of Specimen Size on Ductility, *Electrochem. Technol.*, 4: 216-221 (May–June 1966).
109. C. J. Beevers, Fracture of Zirconium Containing Zirconium Hydride Precipitates, *Electrochem. Technol.*, 4: 222-225 (May–June 1966).
110. N. D. Tarsov, R. A. Ulyanov, and Y. D. Mikhalylov, Effect of Alloying on the Physicomechanical Properties of Niobium, *Fiz. Metal. Metalloved.*, 18: 740-745 (1964).
111. G. D. McAdam, Substitutional Niobium Alloys of High Creep Strength, *J. Inst. Metals*, 93: 559-564 (1965).
112. H. R. Babitzke, R. Siemens, and H. Kato, High-Temperature Columbium and Tantalum Alloys, Report BM-RI-6777, Bureau of Mines, 1966.
113. J. W. Clark, Columbium-Base Alloy of Improved Fabricability, U. S. Patent No. 3,236,638, to General Electric Company, Feb. 22, 1966.
114. J. W. Clark, Tantalum-Base Alloy, U. S. Patent No. 3,243,290, to General Electric Company, Mar. 29, 1966.
115. D. C. Dickinson and S. Friedman, High-Temperature Alloy, U. S. Patent No. 3,243,291, to General Telephone and Electronics Laboratory, Inc., Mar. 29, 1966.

116. Papers presented at Symposium on Physical Metallurgy of Refractory Metals, French Lick, Ind., Oct. 3–5, 1965 (to be published in 1967 by Gordon and Breach, Science Publishers, Inc.).
   a. M. L. Torti, Strength, Weldability, and Heat Treatment of Ta-W-Hf and Ta-W-Zr Alloys.
   b. W. H. Chang, Effect of Carbide Dispersion in Tantalum-Base Alloys.
   c. M. Schussler, Properties of Haynes Alloy Cb-753.
   d. A. L. Hoffmanner, Thermal-Mechanical Processing of a Precipitation-Hardenable, Dispersion Hardened Columbium Alloy.
   e. D. J. Maykuth, H. R. Ogden, and R. I. Jaffee, W-5Re-2.2ThO_2, A Ductile Tungsten Sheet Alloy.
   f. M. Semchyshen and E. Kalus, Tungsten-Base Alloy Development.
117. R. T. Begly, J. L. Godshall, and R. Stickler, Precipitation-Hardening Niobium-Hafnium-Nitrogen Alloys, in *Metals for the Space Age, Plansee Proceedings, 1964*, pp. 401-420, Chase Brass & Copper Co., 1965.
118. R. L. Stephenson, Effect of Heat Treatment on the Creep-Rupture Properties of D-43 Alloy, USAEC Report ORNL-TM-1587, Oak Ridge National Laboratory, September 1966.
119. B. Harris, Structural Changes During Creep of a Solution-Hardened Niobium Alloy, *J. Less-Common Metals*, 9: 244-257 (1965).
120. J. C. Ogle and C. J. McHargue, Annealing of Deformation Twins in Columbium, *Trans. Met. Soc. AIME*, 236: 686-694 (May 1966).
121. A. R. Love and M. L. Picklesimer, The Kinetics of Beta-Phase Decomposition in Niobium-Zirconium, *Trans. Met. Soc. AIME*, 236: 430-435 (April 1966).
122. A. K. Shurin and G. P. Dmitrieva, Niobium-Cobalt Phase Diagram, USAEC Report IS-Trans-36, translated from *Sb. Nauch. Rabot Inst. Metallofiz., Akad. Nauk Ukr. SSR*, (Russian) No. 18: 175-177 (1964).
123. A. Raman, X-Ray Investigation in the Niobium-Cobalt System, *Trans. Met. Soc. AIME*, 236: 561-565 (April 1966).
124. C. E. Lundin and A. S. Yamamoto, The Equilibrium Phase Diagram, Niobium-Aluminum, *Trans. Met. Soc. AIME*, 236: 863-872 (June 1966).
125. T. F. Fedorov, N. M. Popova, and Y. I. Gladyshevskiy, Ternary Hf-Nb-C, Zr-Nb-C, and Ti-Nb-C Systems, *Izv. Akad. Nauk SSSR, Metal.*, No. 3: 158-163 (May–June 1965).
126. D. L. Deadmore and I. Zaplatynsky, The Ternary System Tantalum-Hafnium-Carbon at 2050°C, Report N65-21739 (NASA-TN-D-2768), National Aeronautics and Space Administration, Lewis Research Center, April 1965.
127. L. Kaufman and G. Stepakoff, Computational Methods for Calculation of Rates of Evaporation in the Ta-Hf-C System, Report NASA-CR-458, ManLabs, Inc., April 1966.
128. E. M. Savitskii, and G. L. Tsarov, Investigation of the Effect of Interstitial Impurities on the Structure and Properties of Tungsten Single Crystals, *Vestsi Akad. Navuk BSSR, Ser. Fiz.-Tekh. Navuk*, No. 2: 84-91 (1965).
129. Z. Cochnar, Cause of Brittle Fracture in Tungsten Wire, *Z. Metallk.*, 57: 225-227 (March 1966).
130. A. Gilbert, Fractographic Study of Tungsten and Dilute Tungsten-Rhenium Alloys, *J. Less-Common Metals*, 10: 328-343 (May 1966).
131. General Electric Company, Nuclear Materials and Propulsion Operation, High Temperature Materials Program Progress Report No. 59, Part A, USAEC Report GEMP-59A, May 31, 1966.
132. A. C. Neeley, Highly Densified and Machinable Tungsten-Iron-Nickel Alloy, U. S. Patent No. 3,241,955, to USAEC, Mar. 22, 1966.
133. J. H. Port, Recent Developments in Rhenium and Rhenium Alloy Technology, in *Metals for the Space Age, Plansee Proceedings, 1964*, pp. 613-635, Chase Brass & Copper Co. 1965.
134. E. M. Savitskii and G. E. Chuprikov, Recrystallization Diagram for Rhenium of High Purity, *Izv. Vyssh. Ucheb. Zaved. Tsvetn. Met.*, 1: 112-115 (1966).
135. L. V. Gorshkova, T. F. Fedorov, and Y. B. Kuzma, Rhenium-Chromium-Carbon System, *Porosh. Met. Akad. Nauk Ukr. SSR*, 3: 75-77 (March 1966).
136. H. J. Boors, J. Gerlach, and H. J. Hamel, The Influence of Additions on Hot Deformation of Molybdenum Melted by Electron Beam, *Metall.*, 20: 123-126 (February 1966).
137. E. A. Loria and J. M. Kees, Consolidation and Mechanical Properties of Electrowon Molybdenum, Report BM-RI-6771, Bureau of Mines, Reno Metallurgy Research Center, April 1965.
138. E. Pink, Embrittlement of Molybdenum at Average and Elevated Temperatures, *Planseeber. Pulvermet.*, 14: 15-22 (April 1966).
139. R. V. London, R. E. Edelman, and H. Markus, Development of a Wrought High-Strength Magnesium-Yttrium Alloy, *Amer. Soc. Met. Trans. Quart.*, 59: 250-261 (June 1966).
140. A. K. Bhattacharjya and T. B. Vaughan, The Recrystallization Characteristics of Magnox AL80, *J. Nucl. Mater.*, 19: 187-189 (May 1966).
141. I. N. Ageeva, N. A. Grekov, and M. I. Zamotorin, Effect of Zirconium on the Mechanical and Electrical Properties of Aluminum, *Tr. Leningr. Politekh. Inst.*, 234: 69-74 (1964).
142. J. A. Gurklis, Metal Removal of Electrochemical Methods and Its Effects on Mechanical Properties of Metals, Report DMIC-213, Battelle Memorial Institute, Defense Metals Information Center, Jan. 7, 1965.
143. J. Askill (Comp.), A Bibliography on Tracer Diffusion in Metals: Part I. Self-Diffusion in Pure Metals. Part II. Impurity Diffusion in Pure Metals, USAEC Report ORNL-3795 (Parts I and II)(Suppl.), Oak Ridge National Laboratory, June 1966.
144. P. A. Cumming and P. J. Harrop, Bibliographic Review of Self-Diffusion in Metal Oxides, British Report AERE-Bib-143, October 1965.
145. M. T. Simnad and L. R. Zumwalt, Diffusion of Fission Products (and Transmutation Products) in Nonfuel Materials. A Review, USAEC Report GA-6542, General Atomic Division, General Dynamics Corp., Dec. 15, 1965.
146. L. Yang, R. G. Hudson, and F. D. Carpenter, Some High Temperature Diffusion Studies on Materials of Thermionic Interest, USAEC Report GA-6472, General Atomic Division, General Dynamics Corp., June 28, 1965.
147. D. Y. F. Lai and R. J. Borg, Diffusion of Iron in an Iron-Aluminum Alloy, USAEC Report UCRL-14752, University of California, Lawrence Radiation Laboratory, Mar. 24, 1966.
148. W. F. Brizes, L. H. Cadott, and J. M. Tobin, Carbon Diffusion in the Carbides of Niobium, *J. Nucl. Mater.*, 20: 57-67 (1966).
149. R. Resnick, R. Steinity, and L. Seigle, Determination of Diffusivity of Carbon in Tantalum and Columbium Carbides by Layer Growth Measurements, *Trans. Met. Soc. AIME*, 233: 1915-1918 (October 1965).
150. N. S. Bornstein, E. C. Hirokis, and L. A. Friedrich, Diffusivity Data on the Formation of Niobium Carbide Surface Films, *J. Less-Common Metals*, 10: 200-205 (1966).
151. W. B. Buford, Jr., Diffusion Rate and Activation Energy of Helium Through Single Crystal and Polycrystalline Alumina (Thesis), USAEC Report TID-22828, Georgia Institute of Technology, May 1966.
152. W. R. Manning, M. O. Marlowe, and D. R. Wilder, Temperature and Porosity Dependence of Young's Modulus of Polycrystalline Dysprosium Oxide and Erbium Oxide, *J. Amer. Ceram. Soc.*, 49(4): 227-228 (April 1966).

Section V

Reactor Materials

Special Fabrication Techniques

Melting and Casting

Researchers at the Bureau of Mines[1] have been preparing and evaluating small centrifugal castings of HfC + C, NbC + C, and ZrC + C alloys. Samples taken from castings have been evaluated in hot-hardness and air-reactivity tests. The hot hardness of cast single-phase HfC at 600°C was 600 DPH; at 1500°C it was 190 DPH. Hot-hardness values for HfC containing graphite flakes were 350 and 150 DPH at 600 and 1500°C, respectively. Linear oxidation rates were noted on specimens of NbC + C, HfC + C, ZrC + C, and TaC + C exposed in static air oxidation tests in the temperature range 450 to 800°C. Oxidation rates were obtained by measurement of changes in weight during 6- to 7-hr tests. The results of tests showed that: (1) oxidation resistance of the castings was not significantly affected by differences in free-carbon content and (2) there was only a slight difference in oxidation resistance among the four carbide materials TaC + C, HfC + C, ZrC + C, and NbC + C (given in order of decreasing oxidation resistance).

A three-electrode arc-melting furnace was designed and assembled by Stanford Research Institute[2] for use in a study of growth parameters in refractory-carbide single crystals. Experiments were performed on TaC. Excessive supersaturation caused uncontrolled nucleation and led to rapid precipitation of many small crystals rather than the growth of large crystals. When excess free tantalum and carbon were absent from the melt system and another TaC sample was used as the nutrient, the chemical activities of carbon and tantalum in the solution in equilibrium with the nutrient were diminished. Solvents with low activity coefficients were required to compensate for low activities and keep the carbon and tantalum concentration at an adequate level.

Two furnaces for float-zone melting are described briefly, and data on zone melting of UC are presented in a report issued by Atomics International.[3] The report states that induction-zone melting of UC in a helium atmosphere does not cause much loss of uranium by preferential vaporization, and it was therefore possible to make use of the compositional changes along the length of the zone-melted rod to calculate distribution coefficients that indicated the shape of the U–C phase diagram in the neighborhood of the melting point of UC. Electron-beam zone melting in vacuum produced single crystals of UC that normally contained UC_2 as a second phase; but, at a fast transverse rate, the evaporation of uranium was minimized, and single-phase UC single crystals were produced.

An industrial technique for the preparation of uranium carbide bars from the dioxide has been described by the French.[4] The carbide is first produced by carbon reduction of the oxide, and then melting and casting are performed in an arc furnace. The results of these experiments showed that it is possible to develop, on an industrial scale, a method of carbothermy which is applicable to uranium dioxides of different characteristics and which leads to a high reaction rate of the oxide with carbon.

A process for preparing rare-earth nitrides of high purity, free of oxygen, in an unreactive consolidated form by reactive arc melting is described by International Business Machines Corporation.[5] In their process the rare-earth metal is arc melted in a high-purity nitrogen atmosphere. A steep temperature gradient in the melt caused the nitride to precipitate to the bottom of the melt. The dissociation of nitrogen gas in the arc plasma and the rapid stirring of the melt by the arc current probably contributed to a high reaction rate. The product was in the form of a dense ingot suitable for fabricating specimens for physical-property measurements and was more resistant to reaction than fine powder obtained by other methods.

New melting techniques for improving the ductility of molybdenum are being examined by Climax.[6] Vacuum-arc-cast ingots were prepared in a program designed to show the effects of various deoxidizing agents on the ductility of molybdenum. Castings were made from powder that had been treated in palladium-diffused hydrogen and then directly transferred to the melting furnace without exposure to air. Unnotched Charpy-impact specimens of bars that had been deoxidized by thorium or neodymium sustained 30 ft-lb (41.5×10^3 g-cm) of energy without fracture at temperature below −80°C; the best carbon-deoxidized bar subjected to similar test conditions absorbed 30 ft-lb without fracturing at a temperature of −60°C. A series of ingots with small additions of aluminum, chromium, or nickel was also evaluated. Rolled-bar stock from an ingot to which chromium had been added yielded unnotched Charpy-impact specimens

that absorbed 30 ft-lb of energy without fracturing at a temperature of −129 °C.

The Japanese[7] have been studying the electron-beam melting of refractory metals. They found that the electron-beam melting of molybdenum ingots with alloying-element additions was quite different from that of pure molybdenum ingots. That is, for example, melting of a molybdenum ingot with a 1.8 wt.% zirconium addition resulted in an increased frictional force between the ingot and the inner surface of the mold, which caused ingot rotation and pronounced roughness of the melted ingot's surface. Such an occurrence was probably due to the coexistence of liquid and solid phases in the ingot during the melting, and it was verified that, within a wide temperature range, it was difficult to make a good ingot. Their results also showed that the level of carbon decreased to about the same as that in pure molybdenum. On the other hand the amount of titanium and zirconium lost during the melting was about 99.8% and about 95.5 to 96.9%, respectively.

The deoxidation of molybdenum during arc melting was also studied by the Japanese,[8] who investigated the effect of carbon, boron, and TiH as deoxidizers. Emphasis was placed on the effects of boron on the workability of molybdenum. Their results can be summarized as follows: The deoxidation reaction by carbon can be based on the reaction C + O → CO. The overaddition of carbon is not completely used for deoxidation, but instead results in the precipitation of intergranular carbides. The TiH is effective as a deoxidizer. The intergranular precipitates that are made by the addition of TiH are fine and dispersed. The TiH + carbon is even more effective as a deoxidizer. Boron is useful as a deoxidizer and also is very effective in grain refinement. Molybdenum containing boron possesses two kinds of intergranular precipitates. One is granulelike and results from small additions of boron; the other is stripelike and results from large additions of boron. Both precipitates appear to assist in strengthening grain boundaries. Molybdenum containing boron is very ductile and, even when it contains a high oxygen content (100 ppm), can be worked at a relatively low temperature (800 °C). (S. G. Nelson)

Hot and Cold Working

The Defense Metals Information Center[9] has issued a publication entitled "Metal Deformation Processing, Volume II." This report surveys information on deformation characteristics of metals and their effect on processing operations. Specific topics covered in the report include: the theory of plasticity; high-velocity forming; work-hardening mechanisms in metals; shear forming and spinning of metals; friction and wear in metal-deformation processes; rod, wire, and tube drawing; and applications of static high pressure to the forming of metals—hydrostatic extrusion.

The Materials Advisory Board[10] has also issued a report on metalworking. This report describes the state of knowledge in the following aspects of metal processing: lubrication in metalworking, application of deformation theory to practice, limitations of extrusion processes, and thin sheet rolling.

With the rapid advances in growing large single crystals from commercial-purity tungsten powder using the arc-Verneuil technique, fabrication of single-crystal sheet becomes more of a reality.[11] Considerable progress in the understanding of the associated anisotropic substructural changes that occur during rolling has been made. Starting single-crystal billet sizes of 1½ by ⅜ by 12 in. already have been produced, with the potential final size unlimited because of the unique method of traversing the hot-plasma source both reciprocally and vertically from the seed. Compared with polycrystalline material, tungsten sheet fabricated from single crystals has immediate advantages because of the absence of grain boundaries. Single-crystal sheet can be rolled at temperatures between 700 and 1000 °C, is free of delamination, and possesses strength levels comparable to those of polycrystalline tungsten sheet and yet still has as much as 14% elongation at room temperature. This material has a ductile-to-brittle transition temperature in bending that is below room temperature and can be welded without affecting the monocrystalline nature of the crystal. Because of the anisotropic nature of single crystals, mechanical properties of the sheet are directional and might be disadvantageous for some applications. Although still on a laboratory scale, the possibility of advancing the technology to produce large-size sheet looks promising.

Comparisons of pressed, sintered, and arc-cast tungsten and molybdenum billets for forging were made by Aerojet-General.[12a] It was concluded that pressed-and-sintered and arc-cast molybdenum forgings can be used interchangeably for engineering applications, provided that the impurity levels are comparable and the forging techniques employed for each type of material are similar. It was also concluded that only pressed-and-sintered tungsten is suitable for forgings. All the molybdenum forgings investigated displayed anisotropy in mechanical properties; the anisotropy was most pronounced in the pressed-and-sintered material. In applications requiring directional uniformity of properties, therefore, the forging procedures should be carefully selected and controlled.

Extrusion and drawing techniques were developed by Nuclear Metals[13] for seamless tubing of unalloyed tungsten and W−25 wt.% Re with diameters below about 0.4 in. Billets filled with molybdenum were used for both compositions. Four warm-drawing techniques were found to be feasible for both mate-

rials. Significant progress in drawing resulted from the establishment of swaging as a practical method of pointing. (S. G. Nelson)

Powder Processing

Various equations proposed in the past relating the pressure applied on a powder to its resulting volume were tested by the French.[14] Data obtained by pressing spherical particles of alumina (less than 1 μ in diameter) were used. The equation proposed by Kawakita is the only one that correctly fits the experimental results obtained by the French.

Los Alamos[15] has proposed two mixing theorems to provide greater packing densities of powders. These theorems are also useful for predicting which of several powders or binary combinations of powders gives the highest density and for calculating the weight-mixing ratio to give maximum packing density for particular combinations. Calculations are based on the proper use of particle-size data obtained from typical commercial particle-size measuring devices, on proper definitions of mixing and the fraction of powder occurring in size intervals, and on functional or nonfunctional description of the data.

Several studies were conducted at Union Carbide[16] to determine ways of producing satisfactory pellets of uranium monocarbide. It was found that densification by cold pressing is dependent upon the powder particle size, oxygen content, and the lubricant used in pressing. Certain sintering aids were also investigated. The addition of approximately 0.5% nickel was found to enhance densification, and an average density of 97% of theoretical was obtained after sintering when 2 wt.% uranium disilicide was used under the proper conditions.

An Austrian paper[17] describes the production of large quantities of high-purity carbides and solid solutions of carbides. Processing is accomplished in an auxiliary metal bath contained in a carbon tube furnace with a protective atmosphere or vacuum. Chemical analyses of carbides produced by solid-state reactions of the components and those produced in liquid-metal baths are compared in this paper.

The compacting and sintering behavior of tungsten carbide–cobalt powder mixtures has been investigated by the Germans.[18] The compacting behavior was found to be dependent on the particle size, the particle-size distribution of the carbides, and the type of cobalt additions. The compacting density could be increased by the use of powder mixtures that show various agglomerate sizes as a result of different milling treatments. The final density of the sintered alloy was found to be independent of the compacting density and to increase with the intensity of the milling treatment and the degree of decarbonizing of the initial powder.

The results of isothermal sintering studies on tungsten carbide–cobalt powder compacts were not in agreement with present sintering theories. The initial stages of sintering indicated a time-independent sintering velocity and an activation energy of 59 kcal/mole for temperatures over and above the eutectic temperatures. With a continuous temperature increase, the sintering began at 800°C and proceeded very rapidly up to 1100°C, where, before melting of the W–C–Co eutectic occurred, a large amount of porosity appeared. At temperatures above the eutectic temperatures, densities of 99% of theoretical were obtained in powders that were initially milled together. Hand-mixed powders were sintered almost as fast, but the final density was under 98%. Decreasing the particle size increased the sintering velocity.

A survey of the published literature on the hot pressing of metallic carbides was presented in a Swedish[19] article. On the basis of information in the literature, a hot-pressing apparatus utilizing resistance heating was designed and constructed. Nine metallic carbides from Groups IV, V, and VI of the periodic table were hot pressed to high densities. Mixed carbides and carbides of varying carbon content were also prepared. Compacting details, together with data on lattice parameters and microhardnesses, are presented.

A furnace designed and built for the sintering of uranium dioxide in a flow of hydrogen at 1800°C has been described by researchers in Hungary.[20] The combustion chamber which measured 40 mm in diameter and 120 mm long was also used in sintering other materials in vacuum, in hydrogen, or in a neutral gas flow. The principles of design and some experimental results obtained during the development of the laboratory furnaces are discussed.

Oak Ridge[21] reports that sintered-aluminum-product (SAP) material is the prime candidate construction material for the fuel rods and pressure tubes of the Heavy Water Organic Cooled Reactor (HWOCR). Previously available SAP alloys exhibited erratic behavior in the form of poor process yield, structural inhomogeneity, gas fissuring and blistering, anisotropic properties, premature fracture, and low creep ductility. Because most of the erratic behavior is believed to be either process or material related, a detailed study is being conducted to determine the material and processing parameters necessary to produce a desired end product consistently and economically.

The Russians[22] have studied the structure of SAP material by an ionic bombardment method. They point out the practical value of the ionic bombardment method for the investigation of all types of materials prepared by powder metallurgy. Photomicrographs prepared by this method showed that the basic SAP structure is a cellular lattice con-

sisting of oxide particles bounded by aluminum pseudograins.

A method for slip casting of parts made of finely ground molybdenum disilicide powder using distilled water as a suspending medium has also been described by the Russians.[23] They show the effects of *p*H of the slip medium, the solid–liquid ratio, and the temperature on the properties of the slip and the castings. It is pointed out that slips have two casting intervals at *p*H levels of 4 to 5 and 9 to 11, the second of which provides better casting properties and higher densities. The final density of samples sintered for 2 hr at 1650°C was 5.5 g/cm^3.

Lewis Research Center[24] has investigated the feasibility of high-energy-rate compaction as a means of consolidating powder blends used in the preparation of dispersion-strengthened alloys. The techniques produced samples of sufficient density (greater than 85% of theoretical) that they could subsequently be examined with an electron microscope. An advantage of the methods studied is that consolidation was accomplished without application of high temperature, and thus agglomeration that might result through diffusion or chemical reaction may be avoided. A cartridge-actuated compaction press proved to be a practical laboratory apparatus that readily consolidated nickel-base blends. Particles as fine as 0.01 μ were discernible in the microstructures. This particle size is within the range considered desirable for dispersion strengthening. A tungsten-base blend was also compacted with a slight modification of the cartridge-actuated compaction press. In a limited number of tests, the Dynapak and the direct-contact sheet explosive methods also proved to be effective means of consolidating powder blends. (S. G. Nelson)

Pressure Bonding

Bettis workers[25] have examined a series of 45 PWR production elements manufactured by their qualified reference production process. Ten failures were experienced in the bonding operation owing to weld failures in the bonding cans. Runout tabs are currently being used at the arc-initiation and -extinguishing areas of the can welds to avoid thermal-shock effects related to such failures. Evaluation of the 35 remaining elements showed that design criteria were maintained, with the exception of cladding thickness. The variation in cladding thickness was a result of the pickling operation prior to assembly. Twelve of the 35 elements required a flattening anneal of 4 hr at 1000°F (538°C) to meet the flatness specification. After the elements were vacuum annealed 6 hr at 1450°F (788°C) to remove residual hydrogen from the bonding operation and subsequent beta treatment, hydrogen contents of test coupons were found to range between 6 and 9 ppm, well within specifications.

Experimental work at Bettis[26] concerning the theory and mechanism of Zircaloy pressure bonding has been summarized. It was generally concluded that the basic bonding mechanism was nucleation and growth rather than diffusion. Bonding surfaces consisting of fractured or partial grains and having a high degree of cleanliness were necessary for good bonding. Several successful cleaning procedures were developed which left no films on the surfaces other than fragile films that were readily pierced or broken in subsequent bonding. Heating into the solid–solid transformation region was found to promote nucleation at the bonding surfaces and to markedly improve the quality of the resultant pressure bonds. Surface roughness was not considered necessary for good bonds but was believed helpful in achieving rupture of the initial surface films. The simultaneous application of pressure and temperature during the bonding cycle was found to provide the required intimate contact of surfaces at the point where nucleation and growth occurred. (S. W. Porembka)

Plating

Nonelectrolytic Chemical Plating

A continuously regenerated, electroless nickel-plating facility has been operated on an experimental basis by Douglas United Nuclear.[27] Stainless-steel equipment was used, with electrolytic passivation employed to prevent plating on the stainless steel. Chemical composition of the bath, an acid type with sodium hypophosphite as the reducing agent and lactate buffering, was monitored by *p*H measurement. Makeup consisted of nickel sulfate, sodium hypophosphite, and sodium hydroxide. Deposition rate was controlled to within 0.5 ± 0.05 mil/hr. Good-quality plate was deposited up to a bath age of 1.4 sq ft-mils of nickel deposited per gallon of bath.

Work by the British[28] has been reported on the metallizing of silicon nitride whiskers. Electroless coatings of nickel, silver, and copper were found to exhibit poor adhesion with this material and were considered totally unsatisfactory. Vapor deposition of nickel carbonyl gave coatings showing more uniformity and reasonable adherence. Phillips Petroleum[29] studied electroless nickel coating of 6061 aluminum as a means of preventing the buildup of thermally insulating aluminum oxide corrosion films on fuel plates. Various types of heat-treatment were employed subsequent to the nickel-plating operation. Corrosion tests in pressurized water indicated that a nondiffusion heat-treatment (54 hr at 410°C) offered the best corrosion resistance.

Proceedings of the 1964 Plansee[12] conference includes a report[12b] of research on the fluidized-bed

deposition of protective coatings on refractory metals. The work involved deposition of silicon onto a Mo–0.5 wt.% Ti alloy and a D-14 alloy (Nb–5 wt.% Zr). Diffusion coatings of the corresponding silicide on the molybdenum alloy gave useful protection against oxidation for 1.5 hr at 3050°F (1670°C). The oxidation resistance of coatings on the D-14 alloy was not as well defined.

In the same publication, chemical vapor-deposition techniques for the application of tungsten and molybdenum coatings[12c] to nonmetallic powders, including oxides, carbides, and borides, were described. Hydrogen reduction of the chlorides of tungsten or molybdenum was used to deposit metal on finely divided oxide powder in a fluidized bed. Another method was also used in which hydrogen reduced an oxide coating on the refractory powder. The coated products could be pressed and sintered satisfactorily.

A kinetic analysis of steel chromizing by Taub et al.[30] includes three series of experiments in which there existed dissimilar chromium-supply fluxes. These fluxes were obtained from pure chromium metal or ferrochromium alloy with and without different chlorine-compound activators. Equations are presented which permit calculation of any time–temperature combination for formation of a predetermined thickness of a high-chromium layer.

A recent report from Battelle–Geneva[31] describes the use of a $NbSi_2$ layer impregnated with tin and aluminum to provide oxidation protection for niobium. In high-temperature service the $NbSi_2$ supports the Sn–Al phase, a mobile liquid, which acts as a barrier against oxygen by forming an Al_2O_3 film at the surface of the coating. The mobility of the liquid phase accounts for a highly important self-healing property. The coating is applied by reaction of the niobium part with a Sn–Al–Si bath.

General Atomic[32] studied the tungsten cladding of uranium–zirconium carbides by vapor deposition (WF_6 + hydrogen). The carbides reacted rapidly with impurities in the reactant gas mixture and with product HF. Satisfactory cladding was accomplished by using high-purity reactants and by conducting the initial plating at the lowest possible temperature (350 to 400°C), thus producing a seal coat. The temperature could then be increased during the rest of the coating procedure.

Workers at Oak Ridge[33] have published a report that outlines desirable procedures for using thermochemical calculations to guide chemical vapor-deposition experiments. Although not a substitute for experimentation, such calculations can rule out unfavorable reaction schemes and point out logical starting conditions for favorable reactions. The procedures are illustrated through the use of examples of vapor plating UC and UO_2.

A review of nonconventional ceramic-forming methods, including vapor deposition, electrodeposition, high-energy-rate forming, reaction sintering, and hot isostatic pressing, prepared by Battelle–Columbus authors,[34] is included in a recent book published by the American Nuclear Society. Areas of potential applicability of each of the techniques were identified. A comprehensive book on the subject of vapor deposition has also been published.[35] Both physical and chemical vapor-deposition processes are treated in detail from the standpoint of fundamentals, techniques, and applications. This book should be helpful to both those experienced in vapor deposition and those initiating work in this area.

(E. H. Hall)

Electroplating

A report based on research at Autonetics discusses a method for plating pore-free coatings on beryllium powder compacts.[36] Substrate surface defects such as pores and inclusions induce pores in the coating when conventional cycles including chemical polishing, zincating, and copper-strike plating are adopted. Such pores can be minimized by outgassing both before and after zincating, employing an alkaline pyrophosphate zincating bath, and using ultrasonic agitation during copper-strike plating. Overlay deposits such as electroless nickel were free of pores and pits when the improved cycle was adopted for plating.

Particles of diamond dust, zirconia, or thoria have been dispersed in chromium electroplate.[37] Dispersions of 1% did not improve resistance to wear; however, improved resistance was observed for chromium containing a greater amount of dispersoids, which was electrodeposited at higher than normal current densities.

A procedure for the electrolytic precipitation of plutonium reduction products on a stainless-steel cathode is based on the regulation of hydrogen-ion concentration, current, and time.[38] Other factors had a lesser influence on this quantitative precipitation. Successful results also were obtained with uranium, neptunium, and several other metal-ion solutions exhibiting at least two valency states. The mechanism appears analogous to the precipitation of hydrated chromic oxide films on cathode surfaces as used on tin-plated steel for promoting the adherence of paint.

A similar electrolytic procedure for precipitating uranium from ammonium oxalate solutions has been reported by another source.[39] With electrolysis at 4 amp, approximately 5 mg of uranium was quantitatively deposited on a 35-mm-diameter copper-cathode disk in 15 min. The *p*H of the 10 to 15 ml solutions was adjusted to 9.0.

Although pressure bonding was pursued in place of diffusion bonding for cladding fuel elements at Bettis, the diffusion-bonding studies developed potentially useful chemical-displacement coating procedures for Zircaloy.[40] Displacement coatings of copper as thick as 0.0003 in. were deposited in only 10 min when Zircaloy specimens were rotated at high speed. High-

speed agitation not only accelerated the coating rate but also improved the appearance of the coatings. Increasing the agitation improved the density of the coating but did not eliminate discontinuities (pits). Displacement coatings of iron on Zircaloy were nonadherent. (W. H. Safranek)

High-Energy-Rate Processes

Westinghouse–Astronuclear[41] is evaluating the bond integrity and thermal stability of a series of 16 explosively bonded bimetal combinations. These systems include refractory-alloy sheets of Nb–Ta, Nb–1 wt.% Zr, FS-85, and T-222 (Ta–10 wt.% W–2.5 wt.% Hf–0.01 wt.% C) bonded to Inconel 600 and to AISI 347 and 321 stainless steels. This study includes tensile tests, hardness traverses, cold rolling of the bonded sheets, metallographic analyses, nondestructive testing, thermal cycling, stress-rupture testing, and isothermal anneals at 1400, 1500, and 1600°F (760, 816, and 871°C) for 1600 hr to determine thermal stability. Hardness and strength increases were observed for all materials, and all bimetal combinations except the FS-85–AISI 321 combination could be cold rolled. The test program has now progressed through the nondestructive-testing phase.

A study of explosive spot welding has been initiated by Aerojet-General.[42] Metals to be joined include aluminum, titanium, and high-strength steel alloys in the 0.011- to 0.375-in. thickness range. The program is designed to investigate the effects of process parameters on weld quality and to develop and build a spot-welding machine. (H. S. Gurev)

Nondestructive Testing

Ultrasonic Techniques

An ultrasonic micrometer has been developed by the British for measuring the thickness of stainless-steel tubing.[43] The micrometer makes use of the effects of a resonant member on an incident ultrasonic pulse of long duration (approximately 300 cycles). The coupling medium is a column of water that touches only one side of the material to be measured. When the carrier frequency is adjusted so that the electrical output signal of the transducer exhibits a null in the center of the pulse, the material (metal sheet) is very nearly in half-wave dilatational resonance or in one of the harmonic resonances. The necessary conditions for producing the null are (1) that there be a high mismatch between the characteristic acoustic impedances of the metal and of the water, (2) that the beam width be narrow, and (3) that the frequency be properly chosen. It is claimed that the micrometer can measure the thickness of a 0.010-in. steel sheet with "a reading error of the order of 0.1%."

The onset of vaporous cavitation in an ultrasonic field depends upon the vapor pressure of the liquid. Aeroprojects has made use of this fact in their development of an incipient boiling detector installed in a molten potassium loop at Oak Ridge.[44] Detection of incipient boiling is accomplished by monitoring the ultrasonic power required to produce cavitation in the liquid phase. The instrument has produced cavitation at temperatures ranging from 300 to 1200°F and at power levels of 0.6 to 60 watts; however, it has not been accurately calibrated to date.

Argonne has conducted interesting studies on the correlation of heat-transfer properties and ultrasonic transmission properties of bonds.[45] Both copper braze-bonded specimens and roll-bonded specimens in the form of BORAX fuel-plate sections were investigated by use of a thermal-pulse method for measuring the thermal diffusivity and thermal conductivity. The front surface of the specimen was uniformly irradiated by a very short pulse (≤500 μsec) of radiant energy from a xenon flash tube. The temperature history of the back surface was continuously monitored by feeding the output from the thermocouple in contact with the back surface into a differential amplifying system and then into an oscilloscope. The oscilloscope trace was then photographed. The estimated accuracy of this technique was ±10%.

Experiments with the copper braze-bonded specimens showed that, for a decrease in transmitted ultrasonic energy, there was a corresponding decrease in heat-transfer properties, i.e., thermal diffusivity and thermal conductivity, and that this relation is strongly frequency dependent. It is also true that there is a correlation between the amplitude of the reflected ultrasonic echo from the back surface and the tensile strength of braze-bonded copper plates. Therefore testing brazed bonds ultrasonically is justified whether the concern is strength or thermal properties of the bond. In some cases a decrease in ultrasonic transmission through roll-bonded specimens occurred with a decrease in thermal conductivity. These changes were generally so small that it would be unlikely that they would be detected at all, if the ultrasonic test were made at a normal scanning speed. There were also a number of points where a decrease in thermal conductivity was not accompanied by an change in ultrasonic transmission. Argonne's general conclusion was "that a decrease in the amplitude of the transmitted pulse always signified a loss in thermal conductivity for both the braze and the roll bonds, but that, depending upon the resolution and sensitivity of the ultrasonic system, there will be small areas of poorer thermal properties that cannot be detected by an ultrasonic through-transmission method." (D. Ensminger)

NDT Techniques Other Than Ultrasonic

A new nondestructive method for measuring homogeneity of uranium and/or thorium in nuclear fuels has been applied to mixed oxide fuels by investigators at Knolls.[46] The method is based on examination of damage trails made by neutrons in glass microscope slides. The initial trails or tracks on the slides cannot be seen by an optical microscope but can be seen after enlargement by etching. Useful details as to procedure and limitations are presented with references. Limited study of the use of other materials in which damage trails occur for other particles is mentioned.

The feasibility of using the measurement of thermal-neutron-capture gamma rays as a nondestructive technique for determination of concentrations and distributions of burnable poisons in reactor fuel materials has been reported by investigators at Illinois Institute of Technology.[47] Data were obtained using specimens simulating fully enriched-uranium fuel elements containing B, Cd, Sm, Eu, Gd, Dy, and Hf and using fuel pellets from a core loading of an EBW reactor. These pellets represented a 6% enrichment and contained europium and samarium as a mixed burnable poison. The fuel-poison samples were irradiated with a thermal-neutron beam from the reactor, and the prompt gamma rays were detected in a 3- by 3-in. NaI(Tl) scintillation detector. The data show that variations in burnable-poison content smaller than 2% of the total macroscopic absorption cross section of the fuel element can be detected and that significant improvements in this sensitivity can be anticipated with improved systems design.

Argonne[48] has continued investigation of the television-type neutron imaging system. It was determined that the addition of a "gamma control amplifier" successfully extended the range of the neutron presentation and thus permitted five steps of a plastic stepwedge to be easily observed, whereas only four steps could be seen formerly. In other experiments the light yield of the output phosphor of the neutron-intensifier tube after an estimated 50 hr of neutron irradiation was still in excess of 100 foot-lumens for a tube acceleration voltage of 28 kv and an incident neutron intensity of 2×10^7 neutrons/(cm^2)(sec). The incurred decrease in light yield, if any, was determined to be $< 2\%$. Other experiments have shown superiority of the neutron image method in comparison with X-ray television for the observation of water-bubble phenomena in the presence of metal shielding. A water column width of 2.5 mm was used, with metal shielding of up to 1.9 cm of aluminum and 0.31 cm of steel placed in the neutron imaging beam. The metal filters made essentially no difference in the neutron method, and motion and bubble patterns could easily be followed. With X-ray television the bubble patterns could be observed when no metal filter was used, but the image was more difficult to observe as aluminum and steel filters were added in the X-ray field. As a result of the developments, a neutron test facility will be installed by investigators at Princeton University for use in the study of heat-transfer characteristics as affected by fluid flow and bubble action. An unsuccessful attempt to observe Laue neutron diffraction patterns from an MgO single crystal indicates that, for visual detection of a 3-mm-diameter neutron-irradiated area, the neutron intensity would have to be approximately 5×10^3 neutrons/(cm^2)(sec) or higher.[49]

Investigators at Oak Ridge[21] have continued their empirical and analytical studies of eddy-current test-coil phenomena. Factors such as coil dimensions, frequency, specimen conductivity and permeability, and coil-to-specimen spacing (lift-off) are of interest. A composite plot of probe–coil impedance for various frequencies and lift-off is presented for a family of four coils of the same shape but different sizes. The data appear to complement and perhaps extend the familiar classic results obtained by Foerster.

Improvements have been reported in development of the multiparameter eddy-current tubing tester by investigators at Battelle–Northwest.[50] The addition of sampling circuits to perform the functions of timing, sampling, and pulse elongation have provided an increase in parameter-separating ability. These modifications permit the use of the maximum value of the defect signal in each channel of a four-channel unit. It is now possible to cancel out indications due to a drilled hole of a given depth; this was not possible in a system in which a sampling circuit was not incorporated. A prototype eddy-current tubing tester also is being designed which utilizes the multiparameter concepts developed to date. The new tester will have a two-channel readout, and it is intended that probe wobble effects will be reduced in both output channels. Laboratory tests at two frequencies show that a large reduction in probe wobble-signal effects can be obtained. Results of development of a phase-sensitive detector for use with eddy-current instruments are also considered. The detector provides amplitude accuracy within 1% and phase accuracy within 1° over the frequency range of 25 to 500 kHz. (A. F. Leatherman)

References

1. Bureau of Mines, Albany Metallurgy Research Center, Quarterly Progress Report No. 31, April 1–June 30, 1966, USAEC Report USBM-RC-1249.
2. R. W. Bartlett, W. E. Nelson, E. Carr, and F. A. Halden, Study of Growth Parameters for Refractory Carbide Single Crystals, Quarterly Status Report No. 5, March 1–June 1, 1965, Report N65-31950 (NASA-CR-64323), Stanford Research Institute, July 6, 1965.
3. G. Ervin, Jr., and A. K. Smalley, Zone Melting of Uranium Monocarbide, USAEC Report NAA-SR-11813, Atomics International, May 25, 1966.
4. A. Porneuf, Preparation of Uranium Carbides Starting with the Dioxide, Melting in Arc Furnace, and Casting,

Rev. Hautes Temp. Refract., 2: 333-365 (October–December 1965).

5. R. J. Gambino and J. J. Cuomo, Preparation of Rare-Earth Nitrides by Reactive Arc Melting, *J. Electrochem. Soc.*, 113: 401-403 (April 1966).
6. M. Semchyshen and R. Q. Barr, Research on New Methods for Improving the Ductility of Molybdenum, *J. Less-Common Metals*, 11: 1-13 (July 1966).
7. T. Takaai, The Electron-Beam Melting of Refractory Metals. IV. The Electron-Beam Melting of Molybdenum Minor Alloys, *Nippon Kinzoku Gakkaishi*, 29: 918-923 (1965).
8. T. Hosoda and T. Matoba, The Deoxidation of Molybdenum During Arc Melting and the Effect of Boron on the Workability, *Nippon Kinzoku Gakkaishi*, 30: 231-237 (1966).
9. F. W. Boulger, A. F. Gerds, and W. A. Glaeser, Metal Deformation Processing, Volume II, DMIC-226, Battelle Memorial Institute, Defense Metals Information Center, July 7, 1966.
10. Materials Advisory Board, National Academy of Sciences–National Research Council, Metalworking Processes and Equipment, Progress Report No. 3, March–October 1965, Report MAB-206-M(3), Oct. 31, 1965.
11. L. Raymond and F. R. Chavat, Tungsten Single Crystal Sheet, *Amer. Inst. Aeron. Astronaut. J.*, 4: 895-899 (May 1966).
12. F. Benovsky (Ed.), *Metals for the Space Age, Plansee Proceedings, 1964*, Metallwerke Plansee A. G., Reutte/Tyrol, 1965.
    a. J. J. Warga, F. D. Evans, and R. J. Kotfila, Comparison of Pressed and Sintered and Arc-Cast Billets for Refractory Metal Forging, pp. 184-198.
    b. P. J. Chao, Fluidized-Bed Deposition of Protective Coatings on Refractory Metals, pp. 301-315.
    c. A. H. Roberson, A. Landsberg, and F. E. Block, Nonmetallic Powders Coated with Tungsten and Molybdenum, pp. 316-324.
13. S. Isserow, J. G. Hunt, R. G. Jenkins, and A. L. Geary, Fundamental and Applied Research and Development in Metallurgy. II. Fabrication of Seamless Tungsten and Tungsten-Rhenium Tubing, USAEC Report NMI-1264, Nuclear Metals Division of Textron Inc., June 15, 1965.
14. P. Vergnon, Pressing of Powders, French Report CEA-Bib-70, May 1966.
15. H. D. Lewis and A. Goldman, Theorems for Calculation of Weight Ratios To Produce Maximum Packing Density of Powder Mixtures, *J. Amer. Ceram. Soc.*, 49: 323-327 (June 21, 1966).
16. C. R. Schmitt, Powder Metallurgy of Uranium Monocarbide, USAEC Report Y-1510, Union Carbide Corporation, Y-12 Plant, Apr. 13, 1966.
17. R. Kieffer and H. Rassaerts, The Use of an Auxiliary Metal Bath for the Production of High-Purity Carbide Powders of the IVa-VIa Group of Elements, *Inst. J. Powder Met.*, 2(2): 15-22 (April 1966).
18. H. E. Exner, Experimental Investigation of Compacting and Sintering Behavior of a Tungsten Carbide-Cobalt Alloy, *Metall.*, 20: 448-454 (May 1966).
19. L. Ramquist, Hot-Pressing of Metallic Carbides, *Power Met.*, 2(7): 26-46 (Spring 1966).
20. L. Mizsnay, I. Bencze, and V. Probald, Furnace of UO_2 Sintering, *Magyar Tud. Akad. Kozp. Fiz. Kut. Int. Kozlemem.*, 13: 413-430 (1965).
21. S. Peterson (Comp. and Ed.), Metals and Ceramics Division Annual Progress Report for Period Ending June 30, 1966, USAEC Report ORNL-3970, Oak Ridge National Laboratory, October 1966.
22. L. I. Gladneva, N. I. Efremenkova, L. S. Lebedeva, G. V. Spivak, V. A. Shelamov, and Yurosova, Determining the Structure of Sintered Materials of the Me-MeO System by Ionic Bombardment, *Porosh. Met., Akad. Nauk. Ukr. SSR*, No. 5, 67-73 (May 1966).
23. A. G. Dobrovalskii and N. V. Nazarchuk, Slip Casting of Molybdenum Disilicide, *Porosh. Met. Akad. Nauk. Ukr. SSR*, No. 5: 1-8 (May 1966).
24. G. Reinhardt, W. S. Cremens, and J. W. Weeton, Cold Consolidation of Metal Plus Dispersoid Blends for Examination by Electron Microscopy, Report NASA-TN-D-3511, National Aeronautics and Space Administration, Lewis Research Center, July 1966.
25. Westinghouse Electric Corporation, Bettis Atomic Power Laboratory, Pressurized Water Reactor (PWR) Project, Technical Progress Report, April 23–July 22, 1966, USAEC Report WAPD-MRP-117.
26. J. Weber and W. L. Frankhouser, Theory and Mechanism of Zircaloy Pressure Bonding, USAEC Report WAPD-305, Westinghouse Electric Corporation, Bettis Atomic Power Laboratory, July 1966.
27. G. F. Jacky, An Experimental, Continuously Regenerated, Electroless Nickel-Plating Facility, USAEC Report DUN-800, Douglas United Nuclear, Inc., Feb. 15, 1966.
28. R. Barclay and C. A. Calow, The Metallizing of Ceramic Whiskers, British Report AWRE-O-18/66, February 1966.
29. Phillips Petroleum Company, Nuclear Technology Branches Quarterly Report, January 1–March 31, 1966, USAEC Report IDO-17192, August 1966.
30. A. Taub, E. Aladag, Z. Cak Mak, and M. Timucin, Kinetic Analysis of the Mechanism of the Chromizing Process in Steel, *Appl. Mater. Res.*, 5(3): 138-42 (July 1966).
31. B. Lux, P. Stecher, and N. Perlhefter, Oxidation Protection of Niobium by a $NbSi_2$ Layer Impregnated with SnAl, Report N66-28584, (NASA-TT-F-10183), Battelle Memorial Institute, Geneva Laboratories, Jan. 15, 1966.
32. J. R. Lindgren, Tungsten Cladding of Uranium-Zirconium Carbides by Vapor Deposition, Report N66-24970 (NASA-CR-74685), General Atomic Division, General Dynamics Corp., Mar. 8, 1963.
33. J. D. Fleming, W. C. Robinson, and C. F. Leitten, Jr., Thermochemical Analysis of Vapor-Plating Processes, USAEC Report ORNL-TM-1454, Oak Ridge National Laboratory, July 1966.
34. A. Boltax and J. Handwerk (Eds.), Nonconventional Ceramic-Forming Methods, in *Nuclear Applications of Nonfissionable Materials*, pp. 305-327, American Nuclear Society, 1966.
35. C. Powell, J. Oxley, and J. Blocher, Jr. (Eds.), *Vapor Deposition*, John Wiley & Sons, Inc., New York, 1966.
36. B. F. Rothschild and R. G. Nabors, Plating of Beryllium, *Metal Finishing*, 63(7): 49 (July 1965).
37. F. X. Hassion and J. Szanto, Occlusion of Various Refractory Materials in Chromium Plate on Steel Substrates, Report SA-TR-18-1091 (AD-621920), Springfield Armory, Aug. 16, 1965.
38. N. E. Baerring, Electrodeposition of Actinide and Lanthanide Elements, Swedish Report AE-217, February 1966.
39. V. S. Roslyakov and M. P. Yezhova, Electrolytic Deposition of Small Quantities of Uranium from Solutions, *Radiokhimiya*, 7(5): 625-627 (1965).
40. C. R. Woods and T. R. Padden, Chemical Replacement Plating of Zircaloy, USAEC Report WAPD-238, Westinghouse Electric Corporation, Bettis Atomic Power Laboratory, May 1961.
41. J. L. Godshall and R. W. Buckman, Jr., Evaluation of Refractory/Austenitic Bimetal Combinations, Quarterly Progress Report No. 2, September 22–December 22, 1965, Report WANL-PR(EE)-002, Westinghouse Electric Corporation, Astronuclear Laboratory.
42. A. E. Doherty, H. G. Westerfield, L. H. Knop, E. K. Henrikson, and R. E. Pesante, Develop Manufacturing Methods To Utilize Explosives as a High Energy Source To Spot Weld Metals, Interim Engineering Progress Report, July 1–September 31, 1966, Report IR-9-802(Vol. I), Aerojet-General Corporation.
43. E. E. Aldridge, A Numerical Study of the Mode of Working of the Ultrasonic Micrometer Used in Thickness Measurements of Stainless Steel Tubing, British Report AERE-M-1742, April 1966.

44. Aeroprojects, Inc., Applications of Ultrasonic Energy: Ultrasonic Instrumentation for Nuclear Applications, USAEC Report NYO-3622-3, June 1966.
45. R. A. di Novi, Correlation of the Heat Transfer Properties and Ultrasonic Transmission Properties of Bonds, USAEC Report ANL-7074, Argonne National Laboratory, February 1966.
46. A. S. Covert and W. W. Shultz, Assessment of Inhomogeneity of Solid Reactor Fuels by Fission Track Counting, USAEC Report KAPL-M-6556, Knolls Atomic Power Laboratory, April 1966.
47. R. C. Greenwood and J. Spalek, Evaluation of Thermal Neutron Capture Gamma Ray Techniques for Nondestructive Analysis of Reactor Burnable Poisons, USAEC Report IITRI-578P11-54, Illinois Institute of Technology Research Institute, Oct. 27, 1965.
48. Argonne National Laboratory, Reactor Development Program Progress Report, July 1966, USAEC Report ANL-7245, Aug. 26, 1966.
49. Argonne National Laboratory, Reactor Development Program Progress Report, June 1966, USAEC Report ANL-7230, June 1966.
50. F. W. Albaugh, S. H. Bush, J. J. Cadwell, D. R. de Halas, and D. C. Worlton, Battelle Memorial Institute, Pacific Northwest Laboratory, unpublished, August 1966.

LEGAL NOTICE

This journal was prepared under the sponsorship of the U. S. Atomic Energy Commission. Neither the United States, nor the Commission, nor any person acting on behalf of the Commission:

A. Makes any warranty or representation, expressed or implied, with respect to the accuracy, completeness, or usefulness of the information contained in this journal, or that the use of any information, apparatus, method, or process disclosed in this journal may not infringe privately owned rights; or

B. Assumes any liabilities with respect to the use of, or for damages resulting from the use of any information, apparatus, method, or process disclosed in this journal.

As used in the above, "person acting on behalf of the Commission" includes any employee or contractor of the Commission, or employee of such contractor, to the extent that such employee or contractor of the Commission, or employee of such contractor prepares, disseminates, or provides access to, any information pursuant to his employment or contract with the Commission, or his employment with such contractor.